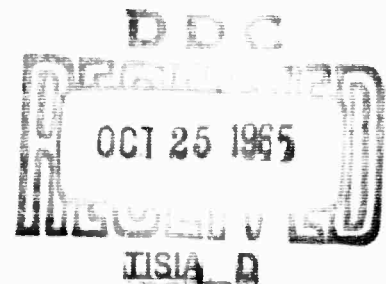# Preparation and Characterization of Ultra-Pure Solids

Annual Report
July 1, 1964 - June 30, 1965
on
ARPA Order 418

J. H. SCHULMAN, G. T. RADO,
A. R. ACHTER, AND A. I. SCHINDLER

August, 1965

U.S. NAVAL RESEARCH LABORATORY
Washington, D.C.

MISSING PAGE
NUMBERS ARE BLANK
AND WERE NOT
FILMED

CONTENTS

i

PREFACE

The Naval Research Laboratory is conducting a broad investigation on the preparation and characteristics of ultra-pure imperfection-free solids in an effort to improve our understanding of the relationships between the behavior of materials and their fundamental physico-chemical make-up.

The specific efforts emphasized during this general investigation encompass theoretical studies of crystal growth kinetics, metallic behavior and alloy formation, the nature of the interactions responsible for the magnetic properties of spin-ordered materials, effects of high temperature on materials, and optical and radiation-sensitive properties of non-metallic materials. The scope of properties being investigated to elucidate the behavior and characteristics of ultra-pure and imperfection-free solids is wide, and includes electrical, mechanical, galvano-magnetic, magneto-electric, luminescence, and crystal morphology. Similarly, materials chosen for study represent a broad selection which includes refractory and transition metals and alloys, intermetallic compounds, alkali halides, glasses, and certain spin-ordered substances.

Four areas of investigation showing considerable progress during the year starting July 1964 are discussed herein. These investigations, each under the cognizance of a separate research group at the Laboratory, cover accomplishments on alkali halide crystals, refractory metal crystals, transition metal single crystals, and magnetic materials.

The research program on the preparation of ultra-pure alkali halide single crystals incorporates three interrelated steps: purification, single crystal growth, and characterization and analysis. Both physical and chemical purification methods are in use, and Kyropoulos techniques as well as zone-refining have been under study for single crystal production. Several other groups working on alkali halide purification are already devoting most of their efforts to KCl. KBr, on which much of our earliest work was done, is a material whose optical and physical properties are of great interest to solid-state physicists at NRL and at many other laboratories in this country and abroad. Since experience with solid state mass spectrometry here has emphasized the seriousness of cross-contamination which can result when the same apparatus is used for the processing or analysis of different alkali halides, efforts at NRL are being concentrated exclusively on KBr for the present. Results obtained in the purification, crystal growth, and analysis of KBr and other alkali halides are presented and some proposed lines of further investigation are discussed.

In the preparation and study of highly perfect specimens of refractory metals, accomplishments have been made in four areas: (a) procedures have been developed for the growth of single crystals of niobium by the strain-anneal technique and for the study of their structure by x-ray and metallographic methods, (b) measurements have been made of the rate of sintering of porosity in the grain boundaries of niobium bicrystals, (c) bicrystals have been prepared for the study of the interfacial energy as a function of misorientation, (d) techniques have been developed for the measurement of intergranular diffusion in the bicrystals of niobium.

Studies on transition metal and intermetallic compound single crystals have been concentrated in four main areas: (a) crystal growth kinetics, (b) transition metal crystal preparation, (c) crystal perfection, and (d) purity evaluation. These efforts constitute a broad approach toward growing and evaluating transition metal and intermetallic compound single crystals in states of extreme purity and perfection, and toward formulating and verifying improvements to current theories governing such crystal formation. Significant achievements in these areas are discussed in detail. It is anticipated that, in the coming year, each of the four areas outlined above will be further developed. Interactions between these areas will also be emphasized.

The work on the preparation and characterization of magnetic materials has been primarily directed toward the improvement of the quality and size of flux-grown $Ga_{2-x}Fe_xO_3$ single crystals and toward the characterization of flux-grown Al_2O_3 and ▉-Ga_2O_3 single crystals by resonance (ESR and ENDOR) techniques. A considerable improvement was obtained in the size of $Ga_{2-x}Fe_xO_3$ single crystals. The high quality of the Al_2O_3 and ▉-Ga_2O_3 single crystals was confirmed by the practicability of successful ENDOR and applied electric field ESR measurements on Al_2O_3 and forbidden hyperfine ESR measurements on ▉-Ga_2O_3.

AUTHORIZATION

PROBLEM STATUS

This is an interim annual report; work on the problems continues.

ALKALI HALIDE CRYSTALS

Personnel Engaged in Program

Principal Investigator: James H. Schulman
         M. Krulfeld
         C. Marquardt
         J. Allard
         R. Black

Report Prepared by M. Krulfeld

ALKALI HALIDE CRYSTALS

A. INTRODUCTION

The Naval Research Laboratory program on the preparation of ultra-pure alkali halide single crystals suitable for solid-state research involves three interrelated steps: purification, single crystal growth, and adequate characterization and analysis. A combination of physical and chemical purification methods is almost always necessary for materials of very high purity, and both have been under study here. The growth of sizeable, pure single crystals of the alkali halides has in the past been almost exclusively by Kyropoulos or Stockbarger techniques or by zone-refining which combines purification with single crystal production. Factors involved in Kyropoulos growth and in zone-refining, as well as in deposition from the vapor phase, have been examined in the alkali halide program, with particular attention to contamination problems during these processes. Adequate chemical analysis for specific impurities in the low ppm and ppb range is an absolute necessity if progress in purification is to be measured. Many impurities at these low concentrations are known to affect some of the physical properties of alkali halides very significantly. Because analysis at these low concentrations is difficult, tedious, and requires highly specialized techniques, analysis has been the most neglected area in the field of very high purity alkali halide research. The work of Butler and Russell[1] on KCl at the Oak Ridge National Laboratory has perhaps been the most extensive effort on analysis to date. The characterization and analysis work of the alkali halide purification program at NRL has included ionic conductivity measurements, emission spectrography, atomic absorption and flame emission spectrophotometry, and solid-state spark-source mass spectrography.

A large part of the work in the past year, particularly in analysis, has been the setting up of necessary apparatus and facilities. Exploratory work in purification, crystal growth and analysis with the available apparatus has led to improved techniques and the design and fabrication of better apparatus. The foundation thus established should lead to a significant acceleration of progress in our future work.

It is obvious that in analysis, in purification, and in crystal growth alike the use of the same apparatus for processing different materials can lead

1

to very undesirable contamination effects. This has been disagreeably confirmed in connection with the stubborn persistence of memory effects from previous runs in mass spectrography, a ' a resultant interference with later analyses. With new zone-refining apparatus almost complete, with a new Kyropoulos growth apparatus being designed and with the need for recalibrating every analytical procedure each time a new matrix is used, it has been decided temporarily to concentrate al' efforts on purification, crystal growth, and analysis on one single alkali halide. This will minimize cross-contamination, will supply a wide spectrum of experience in all areas on one material, and will minimize the amount of pre-calibration necessary to obtain meaningful analytical data. In view of the amount of work already expended on it in several different areas the material chosen has been KBr.

Work during the past year in purification, crystal growth, and characterization of alkali halides is reported below.

B. PHYSICAL METHODS OF PURIFICATION

I. Zone Refining

One of the most successful purification methods to be applied to alkali halides is zone refining.[2] The original design of the apparatus presently used in this laboratory was influenced in part by an oral description by R. W. Warren of apparatus used at Westinghouse, a more complete description of which has recently appeared in the literature.[3]

In our apparatus a movable 200-watt platinum-wound zone heater is driven by a lead screw which can produce a range of forward zone speeds from 1.3 mm/hr to 100 cm/hr and a rapid reverse of 200 cm/hr. The molten zone is approximately 2 cm. wide. The boat is a 16 mm O.D. fused silica tube sealed at one end. This boat lies in an outer tube of fused silica, sealed at one end and provided with an O-ring flange at the other. The outer tube is connected by means of a Viton O-ring seal to the rest of the system, which consists of a cold trap and glass-teflon vacuum valves. The latter allow the system to be either evacuated or flushed and filled with gas.

In a typical procedure for KBr the pre-cleaned boat, loaded with powdered KBr starting material[*] is inserted in the outer tube. The system is assembled and connected to a vacuum pump which attains pressures less than μ, measured on a thermocouple gauge. After several hours of pumping at room

---

* 100 pound stocks of reagent grade KBr, KCl and NaCl have been purchased to provide reproducible starting material for all our work.

temperature a portable tube-furnace is placed around the outer tube and the temperature is raised at intervals in 50°C steps. After an eight-hour period, a final temperature of 300°C is reached, at which temperature the system is maintained for a full day. The vacuum system is then valved off and the system is allowed to cool to room temperature. HBr gas, purified by passing through a molecular sieve column (Linde, type 5-A) at 0°C, is then admitted to the system and allowed to flow through it at a rate of 300 cm^3/min for three hours. The system is then valved off and the tube furnace is heated to 700°C at a rate of 100°C/hr. The cold trap Dewar is filled with dry-ice in acetone, in order to trap the water formed by the reaction of HBr with OH^-, and the system is left to bake for sixteen hours or more. The portable tube furnace is then removed, and the zone heater is used to make thirty horizontal passes at a speed of 72 mm/hr followed by a final pass at a speed of 2.6 mm/hr.

In refining KCl, using HCl gas, the above procedure is modified by elimination of the molecular sieve, with which HCl reacts strongly; the HCl gas is prepurified by passage through glass wool and a dry-ice cold trap. In refining KBr, Br_2 has been used in place of HBr, and purges with purified argon have been used in conjunction with the vacuum heating. At present there are no analytical data to indicate the relative merits of these variations.

Ingots produced by the procedure described are approximately 30 cm long and of semicircular cross-section, 14 mm in diameter. Early attempts produced ingots which were extremely polycrystalline and contained large bubbles. These difficulties were largely eliminated by the very slow final pass. The ingots do not stick to the silica boats.

Emission spectrographic analyses of samples from the bow portions of typical KBr and KCl ingots, zone-refined from reagent-grade starting material, are shown in Table I. Qualitatively, these data indicate a significant reduction in all detected impurities, as compared to the starting material. The high Si concentration seen in some of the analyses may be due to contamination from the silica boat. In Table II samples from the tail portion of a typical KBr ingot and the residue deposited on the wall of the outer tube during the zone refining operation are compared with the starting material. All detectable impurities are highly concentrated in the tail portion. Some of these are volatile and condense on the cool tube walls ahead of the molten zone, causing the high concentrations in the residue. A semi-quantitative analysis of the bow portion of one KCl ingot showed that it contained less than 1 ppm Rb and Al and 2 ppm Ca.

Future zone refining experiments are planned to test the effectiveness of certain modifications of the technique: various gas atmospheres (flowing as well as static), various boat materials, cropping of ingots, and chemical treatment of starting material. Analyses of the gases will also be performed since they are a possible source of contamination.

TABLE I

Estimates of impurity concentration in zone refined KBr and KCl based on emission spectrography.

	KBr		KCl	
Impurity	Starting Material	NRL Zone Refined*	Starting Material	NRL Zone Refined**
Na	100-1000	N.D.	10-100	N.D.
Rb	+	+	10**	<1**
Mg	10-100	1-10	1-10	<1 - 1
Ca	+	+	10-100	2**
Al	10-100	1-10	10-100	<1**
Si	1-10	100-1000	1-10	1-10
Pb	N.D.	N.D.	N.D.	N.D.
Mn	N.D.	N.D.	N.D.	N.D.
Fe	N.D.	N.D.	1-10	<1-1
Ni	1-10	<1-1	N.D.	N.D.
Cu	<1-1	N.D.	<1-1	N.D.

Concentrations are given in ppm. N.D. indicates "not detected".

*Sample taken from 1" to 2" from bow end of ingot.

+ Test used not sensitive for this element.

**Semi-quantitative determination by step sector method.

4

TABLE II

Estimates of impurity concentration in the tail portion of a typical KBr ingot and in the residue deposited on the wall of the outer tube during the zone refining operation, based on emission spectrography.

Impurity	Starting Material	Tail Portion	Wall Residue
Na	100-1000	10,000-100,000	1000-10,000
Rb	100-1000	1000-10,000	+
Li	N.D.	1000-10,000	+
Cs	N.D.	N.D.	+
Mg	1-10	1000-10,000	100-1000
Ca	10-100	100-1000	10-100
Sr	N.D.	N.D.	N.D.
Ba	N.D.	100-1000	10-100
Al	10-100	10-100	1000
Si	10-100	10-100	1000-10,000
Pb	N.D.	N.D.	100-1000
Cr	N.D.	<1-1	1000
Mn	<1-1	1-10	100-1000
Fe	<1-1	1-10	1000-10,000
Ni	<1-1	10-100	1000-10,000
Cu	<1-1	100-1000	1000-10,000
Ag	N.D.	1-10	<1-1

Concentrations are given in ppm. N.D. indicates "not detected".

+ Insufficient sample available for sensitive test.

II. Sublimation

In connection with the vapor deposition studies described in a later portion of this report, a single experiment was run to determine qualitatively the possible purification obtained by subliming KBr in an inert atmosphere at temperatures somewhat below the melting point (730°C).

The apparatus consisted of a horizontal silica tube 27 mm in diameter and three feet long, closed by rubber stoppers at both ends, with about 12 inches of the middle section of the tube heated in a furnace. A thin (3 mm) silica tube was positioned at the larger tube center through holes in the stoppers and a moveable thermocouple in this thin tube provided temperature

measurement at any point along the tube length. A 4 inch length of silica tubing slightly smaller in diameter than the outer tube was placed at the hottest portion in the central section of the latter and served as boat for a charge of reagent-grade KBr. Fourteen 1/2 inch lengths of the same smaller quartz tubing, stacked horizontally together to form a 7-inch length of separable tube, were placed at one side of the boat. Additional holes in the end stoppers provided an inlet and an outlet, respectively, for prepurified nitrogen (Southern Oxygen Co.) flowing slowly through the system, first through the hot boat and then through the segmented tube, where KBr vapor deposited on the walls. A flowmeter on the outlet side permitted measurement of flow velocity of the nitrogen.

A run was made with a KBr charge temperature of about 716-719°C, a flow rate of nitrogen fluctuating about a value of approximately 200 cm^3 per minute, and with the segmented deposition surface on a dropping temperature gradient from a maximum of 694°C at segment 14 to a minimum of 71°C at segment 1. The slow sublimation and deposition process was allowed to continue for 142 hours. Appreciable deposits of KBr of about 0.1 to 0.3 grams were found only on segments 9 to 14, where deposition temperatures ranged from 694°C to 554°C, with maximum deposition at the 676° to 631° temperatures. Emission spectroscopic analysis of the deposits showed (a) a higher impurity content of calcium, copper, sodium and silicon in the cooler segments at 486° and 554°, compared with their content in the original KBr, and (b) a definite lowering in concentration of aluminum, magnesium, copper, sodium, silicon and iron impurities in the deposits made at 670° to 680°. Calcium showed only little reduction in the higher temperature deposits. The results indicated that vapor deposition crystal growth could provide some degree of purification during the growth process.

C. CHEMICAL METHODS OF PURIFICATION

I. Ion-exchange

Ion-exchange is one of the most effective methods of separating chemical species both in purification and in analytical chemistry. Some application to analysis will be discussed further in the "Characterization and Analysis" portion of this report. With regard to purification of alkali halides, Fredericks and Hatchett have employed ion-exchange techniques for pre-purification of alkali halides down to low ppm impurity levels.[4] In other work certain inorganic ion-exchangers have been found particularly efficient

6

for the separation of alkalis from other cations and for the separation of the different alkalis from each other.[5,6] Several of these inorganic exchangers have been purchased (ZP-1, ZT-1, ZM-1, and AMP-1 cation exchangers, Bio-Rad Laboratories, Richmond, California). ZP-1 (a dehydrated zirconium phosphate synthetic ion-exchanger) has been used in preliminary studies on reagent-grade NaCl and on KBr.

Because of the low impurity levels aimed for, some initially available chromatographic columns designed for easy assembly and cleaning had to be discarded, either because the method of assembly involved probabilities of trace contamination or because there was a very slight leakage of "fines" from the ion-exchange bed via insufficiently sealed edges of porous support material. We are now using a simple chromatographic column fabricated from 20 mm diameter Pyrex tubing with a sealed-in porous Pyrex frit at the bottom to act as support for the ion-exchange bed, provided with a combine stopcock and needle valve in which only glass and teflon are exposed to the solution.

First attempts in the ion-exchange work were on NaCl by the preliminary absorption of NaCl on the column followed by elution, a procedure for alkali separation from alkaline earths developed by Kraus and coworkers.[7] Approximately 50 ml. of 0.1 molar NaCl were absorbed on a ZP-1 column pre-treated with NH_4Cl to provide the NH_4^+ form of the ion-exchanger. The NaCl was then eluted with 0.5 molar NH_4Cl solution. Eluted fractions of about 18 ml. each were collected on a simple fraction collector in pre-cleaned polyehtylene vials provided with tight-fitting polyethylene caps for storage. Attempts to evaporate the fractions to dryness by vacuum evaporation with the solutions still in the original collector vials resulted in boiling and then freezing of the solution, followed by minimal evaporation of water from the frozen mass. An attempt to freeze-dry using a liquid nitrogen cold trap in a closed but unevacuated dessicator also gave slow freezing of the solution, although it was not in contact with the cold trap. 16 hours of exposure to the cold-trap treatment resulted in very little further evaporation of water from the frozen solution. Drying in a conventional drying oven at about 125°C, using a clean 50 ml Pyrex beaker for each fraction, the beaker being covered by an inverted, cleaned crystallizing dish to minimize contamination from particulate matter in the air was then adopted. Analysis of the solids indicated that there was so high a proportion of NH_4Cl in the solids that analysis of the NaCl for trace impurities was difficult.

Although the NH_4Cl could be driven off by raising the temperature above 335°C, it was felt that probabilities of contamination were too great and the amounts of eluted NaCl per fraction too small to make the NH_4Cl elution technique promising for purification purposes.

In more recent experiments the ZP-1 ion exchanger, pre-treated with 2 molar HBr to put the exchanger into the H^+ form, was used to treat 0.5 molar KBr. The solution, prepared from our reagent-grade KBr and distilled water, was passed through the column at a flow rate of about 0.4 ml per minute, with fractions of about 20 ml. each of the solution collected at 50 minute intervals in clean polyethylene vials after passage through the ion-exchange bed. Drying (using covered beakers once more) was again done in a drying oven at 125°C on every third fraction to obtain ion-exchanged KBr solids for analysis. No visible solids were obtained in the first few fractions, but solid KBr to the extent of 0.25 grams was found in fraction 15, with 0.7 to 0.85 grams in fraction 18, 21, 24, 27 and 30, in slowly increasing amounts. Portions of each of these solid fractions were analyzed by emission spectrography for comparison with the reagent-grade starting material. The results are shown in Table III. Not detected in either starting or ion-exchanged material were the elements: lithium, cesium, strontium, barium, lead, silver, zirconium or phosphorus. The data in the table indicates that rubidium was very effectively removed, traces of manganese were removed, and the calcium content reduced. Sodium, aluminum, silicon and nickel concentrations were approximately unchanged and the magnesium content was increased. The results from fraction to fraction for chromium, molybdenium, iron, copper, and possibly nickel appear erratic, and this suggests that for these elements the differences were due to contamination during storage, drying, or handling the dried samples, rather than the ion-exchange process. One possibility is that the cleaned stainless steel spatulas used in handling the dried KBr samples contributed to trace contamination. Tantalum spatulas have been fabricated and will be used in further work. The absence of Zr and P indicates no contamination from the ion-exchanger. Since the last fraction taken was among the purer KBr samples found, longer runs will be made taking many more fractions to determine if any further degree of purification is obtainable. These runs will also determine the total amount of purified salt which can be obtained for a column of given size before breakthrough occurs of the impurities held back by the ion-exchanger. The effects of pH variation and other

8

pertinent variables will also be investigated, as well as additional work with other ion-exchange materials.

TABLE III

Impurity contents estimated in ppm from emission spectrographic data on original KBr and on ion-exchanged fractions. N.D. indicates not detected.

Impurities	Baker and Adamson Reagent KBr (starting material)	SAMPLES Fraction 15	Fraction 18	Fraction 21	Fraction 24	Fraction 27	Fraction 30
Na	100-1000	1000-10,000	100-1000	100-1000	100-1000	100-1000	100
Rb	100-1000	N.D.	N.D.	N.D.	N.D.	N.D.	N.D.
Mg	1-10	100-1000	10-100	10-100	10-100	10-100	10-100
Ca	10-100	1-10	1-10	1-10	1-10	1-10	1-10
Al	10-100	1000-10,000	100-1000	100-1000	10-100	10-100	10-100
Si	10-100	100-1000	10-100	10-100	10-100	10-100	10-100
Cr	N.D.	1-10	<1-1	<1-1	N.D.	<1-1	<1-1
Mo	N.D.	100-1000	10-100	N.D.	1-10	N.D.	N.D.
Mn	<1-1	<1-1	N.D.	N.D.	N.D.	N.D.	N.D.
Fe	<1-1	10-100	1-10	<1-1	1-10	10-100	<1-1
Ni	<1-1	10-100	1-10	1-10	1-10	1-10	<1-1
Cu	<1-1	1-10	<1-1	<1-1	<1-1	1-10	<1-1
Zr	N.D.	N.D.	N.D.	N.D.	N.D.	N.D.	N.D.
P	N.D.	N.D.	N.D.	N.D.	N.D.	N.D.	N.D.

II. Solvent Extraction

Solvent extraction is a very sensitive method for the chemical separation of impurities from aqueous solutions. Two wide-range extracting agents applicable to the removal of many cations are dithizone (diphenylthiocarbazone) and TTA (thenoyltrifluoroacetone).[8] Some work has been done at this Laboratory using dithizone extraction on KBr solution at a pH of 9 as a pre-purification step prior to zone refining and crystal growth. Preliminary analysis indicates the removal of trace amounts of copper and some reduction in sodium content. TTA has been used by Quincy and Lavalle[9] as an essential extraction step in the preparation of high purity KCl. TTA and hexone (4-methyl-2-pentanone), the latter used by Quincy and Lavalle as the organic solvent in their extraction step, have been purchased. Further work is planned with both dithizone and TTA for the removal of specific impurities revealed by trace analysis.

D. CRYSTAL GROWTH

L. Kyropoulos Growth from the Melt

Single crystals of "pure" KBr and KCl have been grown using a Kyropoulos apparatus, previously described by Patterson[10] of this Laboratory. Reagent grade starting material was melted in a platinum crucible under a pure argon atmosphere. The argon was purified by passing it through a molecular sieve column (Linde, type 5-A) at room temperature and then through a Mickel gas purifier (John P. Mickel, Detroit). In Table IV a typical KBr crystal grown by this method is compared with two commercial crystals and the reagent-grade starting material.

Dithizone-extracted KBr has also been used as a starting material for crystal growth, but no analytical results are available at present. Future crystal growing will be performed in a much improved apparatus, currently being designed. It will provide more effective protection from contamination by ambient atmosphere and will be used exclusively for KBr to prevent cross-contamination from prior presence of other materials.

TABLE IV

Estimates of impurity concentrations in KBr crystals based on emission spectrography.

Impurity	Starting Material	Kyropoulos Crystal (NRL)	Harshaw	Optovac
Na	100-1000	10-100	N.D.	100-1000
Mg	10-100	10-100	10-100	100-1000
Al	10-100	1-10	10-100	10-100
Si	1-10	1-10	1-10	10-100
Pb	N.D.	N.D.	N.D.	N.D.
Mn	N.D.	N.D.	N.D.	10-100
Fe	N.D.	N.D.	N.D.	N.D.
Ni	1-10	$<$1-1	1-10	1-10
Cu	$<$1-1	N.D.	N.D.	$<$1-1

Concentrations are given in ppm. N.D. indicates "not detected".

II. Vapor Deposition

A major difficulty encountered in the production of single crystals by any process involving growth from the melt is that of contamination from the boat or crucible holding the material. A possible way of avoiding or minimizing this is by deposition from the vapor phase directly on a solid seed. In such a process only volatile impurities can act as contaminants, and a proper choice of deposition temperatures should serve to reject most of these.

The apparatus shown in Fig. 1 was designed and built for vapor deposition studies using hot, solid KBr as the charge. The solid was used because it sublimes readily and its use does not involve the cracking of quartz apparatus which frequently follows minor accidents with the molten material. The heated portion of the apparatus, which fits into a vertical nichrome resistance furnace was fabricated from quartz. The seed, cleaved from a single-crystal of Harshaw KBr 5 mm x 5 mm. in cross-section, is drilled vertically to accept the chromel-alumel thermocouple tip and transversely to accept a short length of platinum wire serving to pin the seed in place on the thermocouple tip. The closures and connections in the upper unheated sections consist of a large rubber stopper and rubber tubing. They serve the dual purpose of providing gas-tight seals and permitting the vertical positions of

the seed holder and of the inner quartz tube around the seed to be adjusted independently. Not shown in the figure are two additional chromel-alumel thermocouples, protected by quartz tubes, which are inserted into the charge bed of reagent-grade KBr in order to permit measurement and control of the charge bed temperature. The temperature of the seed can be varied by adjusting its vertical position in the apparatus. An inert gas carrier (argon) flowing down through the hot charge bed becomes saturated with KBr vapor, then flows up to the seed, where the KBr vapor is deposited on the seed and the walls of the apparatus, the inert gas continuing out of the apparatus to a flowmeter with which the rate of gas flow can be determined.

The variables investigated in this work were temperatures of charge bed and seed, rate of carrier gas flow, geometry and relative spacing of the inner quartz tube and the seed, and the quality and amount of the deposited KBr on the seed.

The temperature of the charge bed in this apparatus could not exceed the melting point of KBr (730°C) without clogging the apparatus and cracking the quartz upon cooling. Charge temperatures from 650°C to about 715°C have been used, with somewhat lower growth rates at the lower charge temperatures. The size of the opening in the inner quartz tube surrounding the seed, the distance between the opening and the seed face, and the velocity of flow of the hot, KBr-charged gas interact in a complex fashion to visibly affect the uniformity of the KBr deposit on the seed, spreading it with more or less uniformity on the face or bunching the growth at the seed center or edges. However, the major influence on the nature of the seed growth has been found to be the seed temperature. At seed temperatures below approximately 570°C the growth has the appearance of fine needles projecting from the seed face. Under the microscope it can be seen that the "needles" consist mostly of square crystalline platelets in different arrays, some overlapped at the corners, others at the edges like a long deck of thinly or thickly stacked cards. At seed temperatures from about 580°C to 640°C the growth of the seed face has been macroscopically flat and unifc   with little tendency for "needle" growth. Microscopic examination (50X) show that such seed growth faces consist almost entirely of thin, straight-edged and right-angled growth steps. Seed temperatures of about 650°C and higher tend to give spotty, irregular growth, and at 680°C and above, weight loss rather than weight gain of the seed has sometimes resulted. In general, with the charge temperature limited to less than 730°C, only low growth rates of the order of 0.1 to 0.2 milligrams per hour have been obtained

with growth faces of good appearance on a 5x5 mm seed face.

Single crystals of chemical compounds of some size have been grown by a wide variety of techniques from the vapor phase in recent years. In general, appreciable vapor pressures have been used, higher than the low vapor pressure of solid KBr at 715°C (vapor pressure of liquid KBr at 795°C is 1 mm Hg). Pizzarelo[11] produced "large ingots" of PbS from a PbS charge at a vapor pressure of 30 mm Hg. Reynolds and Greene[12] mention large single crystal grains of CdS weighing in excess of 50 grams as not unusual products of a vapor deposition process with the charge of CdS at 1250°C and the substrate at 1150°C. Fochs[13] used a gas flow system to transport CdS and obtain "plate-type crystals" estimated from a photograph to be about 1.5 square centimeters in area and about 0.5 mm thick, with a growth time of 1-2 days. The epitaxial growth of semi-conductors such as GaAs by vapor transport is presently an active field of investigation. In a recent paper Leonhardt[14] reported GaAs growth rates varying from 10 to 18 mg per hour, two orders of magnitude higher than our growth rates of KBr obtained using solid KBr as the charge at 715°C. We have designed and fabricated a new apparatus which will permit liquid KBr at much higher temperatures and vapor pressures to be used as the charge, with provisions for air cooling the seed-holder. With this apparatus we plan to determine if vapor deposition can be used to grow good single crystal KBr at a more useful rate.

E. CHARACTERIZATION AND ANALYSIS

1. Ionic Conductivity

Measurements of electrical conductivity as a function of temperature have been made on samples of zone-refined KBr and KCl, on commercial crystals, and on crystals grown by the Kyropoulos technique. From these measurements "knee temperatures" are obtained, at which the transition from the intrinsic region to the impurity-determined region of conductivity occurs. Because of numerous complications, some of which are discussed briefly in Reference (3), very small heterovalent cation concentrations determined from knee temperatures are known to be unreliable. Nevertheless, knee temperature can be used as a figure of merit in comparing two crystals differing only in heterovalent impurity content, a lower knee temperature indicating lower impurity concentration.

For these measurements crystals (0.2" x 0.2" x 0.02") are cleaved from the ingot, and electrodes are painted on the crystal faces with "Dag" graphite in alcohol dispersion No. 154. This sample is then held inside a thyratron-controlled furnace between spring-loaded platinum contacts; the

furnace chamber is filled with dry nitrogen. For frequencies in the range 100 cps to 1000 cps, conductivity is measured using a General Radio capacitance bridge, type 716C. A separate bridge circuit with a vibrating reed electrometer as a null detector is used for d.c. measurements. The apparatus is so constructed as to facilitate switching from a.c. bridge to d.c. bridge, and quasi-simultaneous measurements are made. Temperature is measured with a Pt-Pt:10% Rh, thermocouple using a Leeds and Northrup "Azar" recorder and is controlled within $\pm 1/2°C$. When the logarithm of the conductivity is plotted against the reciprocal of the absolute temperature the intrinsic region is shown by a straight line and the impurity region by a more or less straight line of different slope. The intersection of the two lines is the "knee".

Generally the a.c. measurement is more accurate at higher temperatures, whereas the d.c. measurement is more accurate at lower temperatures. Between 400°C and 600°C (approximate range) the a.c. and d.c. values of conductivity are the same within experimental error. This is in agreement with the finding of Gründig.[15]

Estimated knee temperatures from some of the above measurements are presented in Table V. Knee temperatures estimated from Gründig's[15] plots of conductivity as a function of temperature are included for comparison, and indicate that, on this basis at least, our crystals are lower in purity than those recently obtained by Gründig.

TABLE V

Estimated knee temperature for samples of KBr and KCl.

	KBr	KCl
Harshaw	700°K	675°K
Optovac	635°K	669°K
Kyropoulos (NRL)	658°K	---
Zone Refined (NRL)*	594°K	588°K
Zone Refined (Grundig)+	570°K	540°K
* Sample taken from 1" to 2" from bow end of ingot.		
+ Estimated from conductivity plots in Reference 15.		

II. X-ray Topography

The macroscopic and microscopic appearance of vapor-deposited KBr is quite different from that of the seed face, obtained by cleaving from single-crystal KBr. The qualitative crystal perfection of the original seed face and of the vapor-deposited layer of KBr produced upon it has been examined by X-ray topography. C. L. Vold of the Metallurgy Division and L. S. Birks of the Optics Division of NRL made comparative studies before and after KBr deposition, using two different modifications[16] of the Schulz X-ray micrograph technique. Both methods indicated relatively poor crystal quality in the seeds cleaved from the Harshaw single-crystal KBr, with similar poor quality in the vapor-deposited layers. There was a slight indication of possible improvement in quality of the vapor deposit as compared to the seed face, at least in some of the deposits. This work indicates the desirability of using improved seed material in order to obtain better deposits from the vapor phase.

III. Chemical Analysis

a. General Considerations on Analysis

The chemical analysis phase of the alkali halide purification program has thus far been limited to three salts, the sodium and potassium chlorides and potassium bromide. Experience gained with these salts will have a carry-over value for the analysis of other high purity materials as they become available.

The elements so far considered as the most likely impurities, due either to the nature of the salts or the treatments to which they have been subjected are: the cationic elements sodium, potassium, rubidium, lithium, cesium, calcium, strontium, barium, magnesium, copper, silver, lead, iron, aluminum, silicon, platinum, rhodium, zirconium and zinc; and the anionic elements bromine, chlorine, iodine, nitrogen, phosphorus, sulfur and oxygen (as oxygen or OH^-).

The general spectrum of analytical techniques and operations applicable to alkali halides would include such separation, purification or concentration operations as classical chemical wet methods, solvent extraction and ion-exchange. It would also include instrumental read-out techniques (with or without the concentration operations) such as emission spectroscopy, flame emission spectrophotometery, atomic absorption spectrophotometry, X-ray emission and fluorescence spectrometry, polarography, colorimetric spectrophotometry, solid state mass spectrography, neutron activation and radiochemical analysis, and optical analysis of the solids directly (absorption and luminescence spectra). It should be pointed out that while the same type

16

of separative operations, such as ion-exchange or solvent extraction, may be used either for analytical purposes or to obtain a purified product for crystal growth, requirements for the two purposes may be very different. An analytical separation which segregates an element for measurement is not concerned with any incidental contamination which does not interfere with the measurement. For purposes of purification, the same technique may be completely ruled out by the contamination factor.

The major factor limiting the application of all the techniques mentioned for our particular use has been the low concentrations of most of the impurities involved (less than 5 ppm or 5 micrograms per gram for most) and frequently the limited amount of sample available for a particular analysis, as, for example, for the purified ion-exchange specimens previously described. Only the most sensitive methods of analysis are capable of determining contaminants at these concentration levels. When instrumental read-out techniques are adequate, quantitative results are possible only when the instrument has been calibrated with a reference or standard material. Since salts of absolute purity are not available, highly purified salts must be prepared as base material for the preparation of synthetic standards by the addition of known impurity elements. The problem involving the necessity of ultra-high purity standards for analysis and guidance in attempts to produce those very same ultra-pure materials is obviously a circular one and necessitates much effort and cross-checking by varied analytical techniques before a quantitative analysis with any real validity is possible.

b. Classical Chemical Methods; Solvent Extraction; Ion-Exchange.

Two initial attempts were made to separate impurities from KCl by classical wet chemical methods. Potassium was precipitated as potassium perchlorate from a solution of the chloride. The recrystallized salt and the residual solution (after concentration) were analyzed for impurities as compared to the starting material. The results were indeterminate. Calcium was precipitated as calcium oxalate from a KCl solution, using added lanthanum as a carrier. The recovery of known amounts of added calcium was poor and indicated incomplete and variable co-precipitation of calcium at concentrations of less than 10 ppm. Comparison of analytical results indicated that the addition of impurity elements from reagents, manipulative operations, and the environment was of such magnitude that ultra-purification and analysis by these methods was not feasible. Further efforts at purification and pre-concentration were therefore limited to solvent extraction and ion-exchange procedures.

17

One acceptance test for the purchase of our solid state mass spectrograph, described later, was the detection of the 43 isotope of calcium in NaCl at approximately the 10 ppb level. This isotope was chosen because calcium is a common impurity in alkali halides and the isotopic abundance of calcium 43 is 0.13%, so that an analysis in the 5 to 10 ppm range for total calcium would provide a reliable analysis of the 43 isotope in the low ppb range. A major effort was therefore made to develop an analytical method for calcium in the low ppm range with the thought that this would in turn enable us to set up a reliable standard for calcium in the low ppb range on the mass spectrograph. Methods in the literature indicated an ultimate lower limit, with poor reliability, of 2 ppm, which was not adequate for our purposes. 8-hydroxy quinoline in chloroform was used as a solvent extractant to separate calcium from alkaline solutions of NaCl. Synthetic standards were prepared by addition of calcium in known amounts to purified samples from available natural and commercial salt. By using 10-gram samples and flame emission photometry as a read-out technique, cross-checking with emission spectroscopy, it was possible to analyze for calcium in the 1-10-ppm range with a ± 1 ppm variation. A number of available large single crystals of NaCl were analyzed for calcium, and an Optovac crystal with 5.5±1 ppm calcium was selected for the acceptance test. The limit of purity for calcium obtainable in NaCl was about 0.5 ppm. The problem of additive contamination and blanks from reagents and environment was a limiting factor. Among the other solvent extraction materials which have been obtained for future analytical work are TTA, dithizone, and dithiol carbamate.

Among ion-exchangers Dowex A-1 chelating resin is known for its removal of divalent and trivalent cations from alkali salts. A specially purified grade of this resin was obtained for analytical work (Chelex-100, Bio-Rad Laboratories). A lower limit of 2 ppm calcium has been reported for analyses using this resin. Experimental work with Chelex-100 was run concurrently with the solvent extraction work and on many of the same salts. This work indicated that calcium could be removed to a lower limit of 1 ppm from NaCl and KCl. While this shows some promise for purification, the problem of added impurities from the resin and eluting reagents limits its usefulness for analysis of ultra-pure materials. The separation factors for some of the trivalent and transition elements are better than for the alkaline earth elements, however, so experiments will be made using Chelex-100 to check the feasibility of pre-concentrating those elements for analysis. Some of the inorganic ion-ex-

changers such as ZP-1, have potential usefulness for separation of the alkalis from each other, particularly rubidium and cesium from the lighter alkalis. These exchangers may be useful for separation and preconcentration of these elements from sodium and potassium salts for determination by flame spectroscopy. Other exchangers have recently[17] been mentioned in the literature for separation of sodium from potassium halides.

c. Emission Spectroscopy

As previously described in the section on purification by zone-refining, emission spectroscopy of our standard reagent grade KBr showed the presence in some quantity of the cationic elements sodium, rubidium, calcium, magnesium, aluminum and silicon. Elements detected at the level just above the detection limit were copper, iron, manganese and nickel. Elements not detected were lithium, cesium, strontium, barium, silver, lead and chromium. The technique does not determine anions. After zone refining, however, lithium, barium, silver, lead and chromium were found in the tail portion of the refined ingot, apparently concentrated there by the zone-refining process. This indicates the probability that these elements were present in the starting material at concentrations too low for detection by emission spectroscopy. (The introduction of some of these impurities from the silica boat or the treatment atmosphere can not be entirely excluded.) These data emphasize the fact that detection limits can vary from 0.1 ppm to 10 ppm or even higher, and that considerable amounts of certain elements can be present without detection by emission spectroscopy. The effectiveness of the emission spectrograph in checking purification efficiency is thus subject to obvious limits. Further, the nominal concentration of 0.1-1 ppm assigned to "just-detectable" impurities is obviously not an absolute value, but differs for elements detectable with different sensitivities. In the absence of very careful calibration, using known standards for each impurity in each particular matrix of interest, the nominal figures used can serve only as a relative basis for comparison of a particular impurity in different samples of the same matrix material. As in the case cited, however, emission spectroscopy can be very useful in detecting either the introduction or the concentration of impurities during purification or manipulative procedures at levels above the sensitivity limits.

d. Flame Emission and Atomic Absorption Spectrometry

The ideal procedure for chemical analysis of ultra pure materials would be very sensitive and selective, have very few steps and require little or no chemical treatment, so that contamination possibilities would be kept to a minimum. Flame emission and atomic absorption spectrometry are

19

instrumental techniques which come close to meeting these requirements. Many procedures require only that the salt be dissolved in water and that the solution be analyzed without further treatment.

Most of the cationic impurities in alkali halide salts for which chemical analysis is required have great sensitivity to flame analysis by either emission or atomic absorption spectrophotometry. The alkali elements (Na, K, Cs, Rb, Li) are most sensitive to flame emission analysis; other elements (Ca, Mg, Sr, Zn, Ba, Pb, Ag, Au) are more sensitive to atomic absorption measurements. For this reason a versatile dual-purpose Flame-Emission/Atomic Absorption Spectrometer was acquired for use in the analytical program.

Much of the work during the past nine months has been centered on finding which impurity elements can be determined by use of this instrument without pre-concentration or separation. This encompasses the determination of which gases to use, operational parameters, matrix background toleration, detection sensitivity and effects of adding organic agents.

The work in this area shows that sodium can be determined at a concentration of 2 ppm in potassium bromide by flame emission spectrophotometry. An ultra pure sample of the salt could probably be given a analysis of 1 ppm sodium. Rubidium and cesium will require pre-concentration (by ion-exchange) if determinations of 10 ppm are to be made. Lithium is quite sensitive, and its determination will be investigated when a grating blazed for 7500A transmission can be ordered and adjusted to our instrument.

Calcium is more sensitive to flame emission analysis, but is better determined by atomic absorption techniques where matrix interferences are less bothersome when alkali halide salts are present. Calcium concentrations of 1 ppm ($1\mu g/gm$) in KCl, NaCl, and KBr are determinable.

Magnesium and zinc are very sensitive in atomic absorption spectrophotometry and it is believed that 1 ppm of these elements will be determinable when further experimentation has been completed. Other cationic elements have not as yet been investigated because their concentrations are generally <1 ppm and undetectable without separation or pre-concentration. When alkali halide salts of known higher purity become available, it may be possible to lower these limits of determinability since matrix effects could be more accurately determined and calibration curves obtained by the standard additive technique would be more accurate.

e. Mass Spectrography

Of all the analytical methods available for trace analyses in the low ppm and ppb concentrations for solids such as the alkali halides, the solid-state spark source mass spectrograph is in principle the most promising.

Its sensitivity, while varying for different elements, is very high, with detectability limits in the low ppb range for many elements. It will detect all the elements, including the halogens and other normally non-cationic species. A permanent record of a very wide spectrum of impurities is obtainable on a single photographic plate, and the mass range can be modified for better resolution of impurities by varying the magnetic field of the instrument. The method requires no preliminary separation of groups of impurities, such as is necessary with many other analytical procedures. The amount of sample needed is not large. Due to the complexities of sparking, of photographic recording of the data, and many other factors, however, reproducibility is at present poorer than with some other techniques. Certain practical difficulties, such as "memory" effects from previously run samples, can also occur, the severity of the problem depending on the nature of the materials previously run and the analyses being made.

A Consolidated Electrodynamics Corporation Type 21-110A Spark Source Mass Spectrometer has been purchased and installed in laboratory space designed and prepared specifically for the instrument. Two performance tests were specified. The first was detection of the 43-isotope of calcium in an NaCl matrix at the 10 ppb level, calcium being a typical impurity in alkali halides. The second was the detection, again at the 10 ppb level, of boron in a silicon matrix. Meeting the boron in silicon specification required the manufacturer to modify the source slits and apertures and to develop special techniques, because a reliable boron-doped silicon standard at the 10 ppb level was not available. The performance tests were met and the instrument was accepted in January 1965.

Since acceptance of the instrument, various samples have been run in order to become familiar with the operation and behavior of the instrument and the interpretation of the mass spectra obtained. Among the samples run have been: several samples of "spectroscopically pure carbon"; some nominally 99.9999% pure aluminum (Cominco Products, Spokane, Washington); a sample of floating-zone refined palladium; a very well characterized sample of pure iron analyzed and supplied to us by the Analytical Branch of the Metallurgy Division of NRL; and a variety of alkali halide samples. The latter, as anticipated, were somewhat difficult to ionize with the spark source, since they are insulators. In our initial work we used a counter-electrode of gold. The use of a metallic counter-electrode is a technique widely employed when sparking insulating materials, although it has the disadvantage of adding the

21

counter-electrode constituents to the mass spectrum obtained. Currently, however, we are sparking KBr using two electrodes of the alkali halide (8 mm. long, 2x2 mm. in cross-sectic ., cleaved from single crystal KBr) one in each jaw of the mechanical holder, corner tips nearly touching. A few minutes after application of the sparking voltage surface electrical breakdown of the electrodes takes place and arcing begins between the tips. We have no explanation at present for the relative ease with which this occurs, in contrast to the difficulties usually experienced with insulators.

Our first objective was to obtain reliable and reproducible mass identification data by accurate measurement of mass spectral line positions on the photographic plate. This is now done routinely by using a Jarrell-Ash comparator and a Vernac optical reader to determine position with a nominal accuracy of $\pm$ 2 microns. Concentrations are presently being estimated by the "visual method"[18] using the potassium 41 isotope as an internal standard for potassium salts. This method of concentration determination is only semi-quantitative since, as well as neglecting some other possible sources of error it assumes that the relative sensitivity of the source for ion production of different elements is similar and that the line areas of visually similar lines are the same. The estimate may be in error by a factor of 3. The analyses can be made more quantitative by the use of a microphotometric method. This will be done with a Joyce-Loebl microdensitometer as more accurate data are required.

The major difficulty we have thus far encountered in the use of the mass spectrograph has been a "memory" effect which has given spurious indications of the presence of previously run materials in later run samples. Careful cleaning of source parts by means of abrasive and acid cleaning has been successful in either diminishing or removing many of these. A false indication of about 500 to 1000 ppm of Na^+ and a slightly larger amount of Cl^+ apparently stemming from previously run NaCl has been much more difficult to remove. Other but less serious difficulties have been presented by the presence of oxygen, nitrogen, carbon and hydrocarbon lines due to small amounts of residual gases in the source vacuum, which interfere with the detection and quantitative estimation of lines due to the lower atomic weight impurities Mg, Al, Si and S. Work is currently under way to eliminate the alkali halide memory problem as well as to reduce interference caused by residuals from ambient gases and the hydrocarbon vacuum pumping oils. To minimize the memory problem, emphasis is temporarily being devoted exclusively to

22

KBr analysis. This will include specimens from the purification and crystal growth programs, standards, and KBr from any other source which may become of interest for comparison.

f. Other Analytical Methods

Neutron activation is a highly sensitive, specific, and often non-destructive method of analysis. The most useful applications have been made using thermalized reactor neutrons and comparing samples and standards simultaneously irradiated. The low flux of neutron generators limits their effective usefulness. We have procured gamma and beta counting equipment and some impurity elements found in alkali halide salts are currently being irradiated. When the sensitivities of these elements and the need for radiochemical separations have been determined, it will be possible to assess the feasibility of using this technique in the analytical program.

X-ray fluorescence procedures have been used to determine iodine in the form of iodide in potassium bromide. The iodide is preferentially precipitated and collected by classical chemical procedures and its amount is established by X-ray fluorescence measurement. As little as 5 ppm may be accurately determined. Possibilities of other applications exist but have not yet been investigated.

g. Analytical Prospect

The chemical characterization of ultra-pure alkali halide crystals requires that individual elemental impurities be determined at concentrations between a few ppm and the lowest possible detection limit. In most cases it will not be possible to reach these levels with flame analysis spectrophotometry without separation or pre-concentration. Emission spectroscopy can be useful for determining selected elements and for survey analysis to detect certain cationic contaminants introduced in the purification processes. Procedures involving the pre-concentration and separation techniques of solvent extraction and ion-exchange may be very useful if environmental contamination and reagent blanks can be kept sufficiently low. With the exception of emission spectroscopy, all these procedures involve the determination of one element at a time. When sample amounts are limited and several samples are to be analyzed, the time and effort necessary can become prohibitively large.

The solid state mass spectrograph has detection sensitivities for impurities down to the level of parts per billion atomic, except near the mass of the major constituents. In spite of the operational difficulties previously

described, it seems to offer the best general instrumental approach for the chemical characterization of ultra-pure materials.

The approach which presently appears most promising is to concentrate analytical efforts on the development of methods to provide an accurate chemical analysis of selected pure salts. The latter can then be used as standards for calibration of the mass spectrograph, which, because of its high sensitivity for most impurities and its capacity for simultaneously recording a wide spectrum of impurities on a single plate will be able to provide survey analyses of raw materials, processed intermediate materials, and the final products of purification and crystal growth. Selected samples can be referred for analysis by other methods as the need arises.

REFERENCES

1. C. T. Butler and J. R. Russell, ORNL Solid State Division Annual Reports ORNL-3480 (May 31, 1963) and ORNL-3676 (May 31, 1964).

2. H. Gründig, Z. Physik 158, 577 (1960).

3. R. W. Warren, Rev. Sci. Instr. 36, 731 (1965).

4. W. J. Fredericks and J. L. Hatchett, 1962 International Symposium on Color Centers in Alkali Halides, Stuttgart, Germany.

5. K. A. Kraus and H. O. Phillips, J. Am. Chem. Soc. 78, 694 (1956).

6. C. B. Amphlett, L. A. McDonald, J. S. Burgess and C. J. Maynard, J. Inorg. Nucl. Chem. 10, 69 (1959).

7. K. A. Kraus, H. O. Phillips, T. A. Carlson, J. S. Johnson, 2nd United Nations Conference on Peaceful Use of Atomic Energy, Geneva, 1958, paper 1832.

8. G. H. Morrison and H. Freiser, Solvent Extraction in Analytical Chemistry, J. Wiley and Sons, Inc., New York, 1957.

9. R. B. Quincy, Jr. and D. E. Lavalle, Oak Ridge National Laboratory Report ORNL-TM-1071, March 1965.

10. D. Patterson, Rev. Sci. Instr. 33, 831 (1962).

11. F. Pizzarello, J. Appl. Phys. 25, 804 (1952).

12. D. C. Reynolds and L. C. Greene, ibid, 29, 559 (1958).

13. P. D. Fochs, ibid, 31, 1733 (1960).

14. H. R. Leonhardt, J. Electrochem. Soc., 112, 237 (1965).

15. H. Gründig, Z. Physik, 182, 477 (1965).

16. Rept. NRL Prog., April 1964, pp. 18-20 and 32-34.

17. V. Nevoral and G. Hajkova, Chem. Listy, 59, 222 (1965).

18. R. D. Craig, G. A. Errock and J. D. Waldron, Determination of Impurities in Solids, Advances in Mass Spectrometry, Pergamon Press, NY-London 1959, edited by J. D. Waldron.
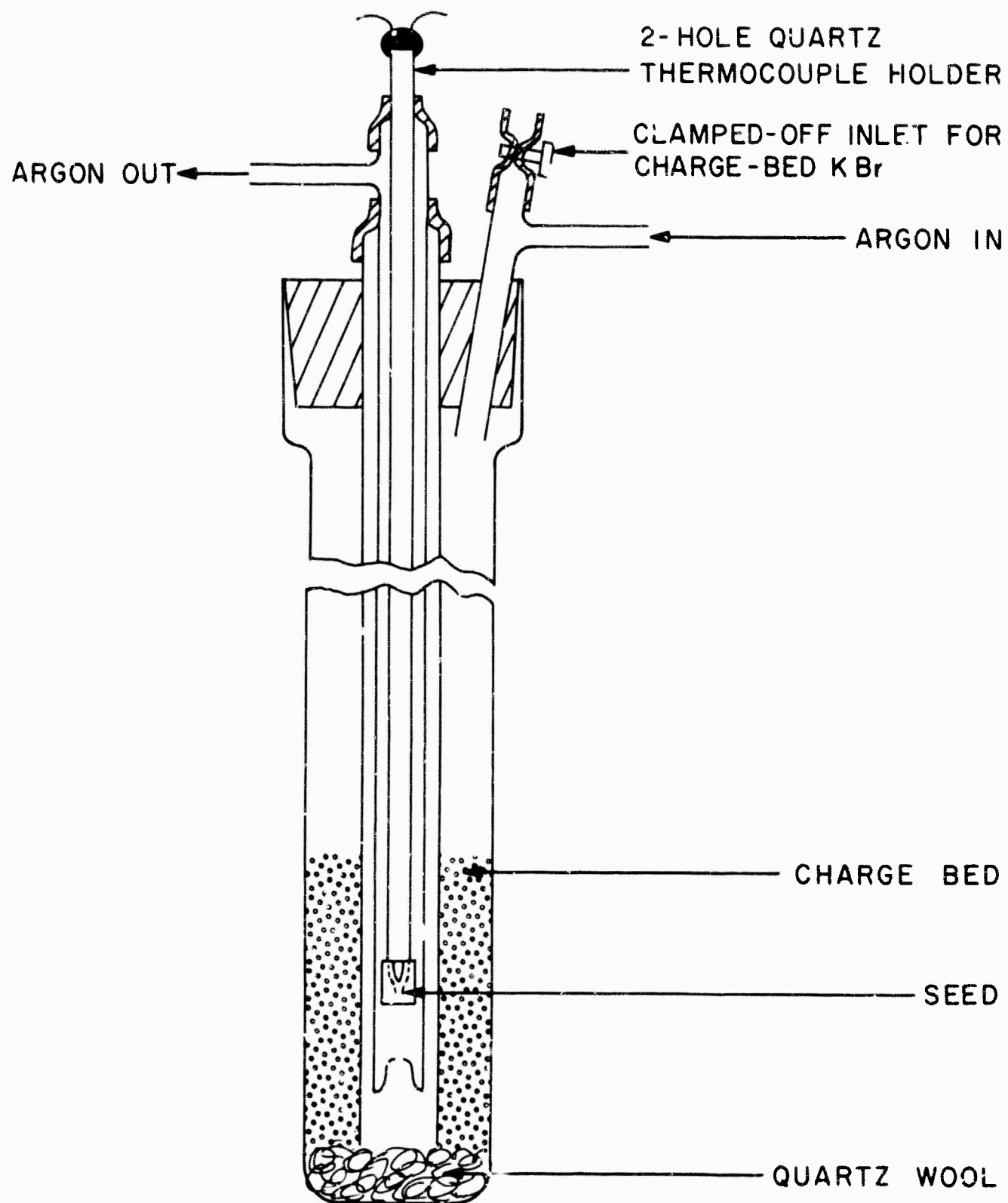
Fig. 1 - Apparatus for vapor deposition studies

REFRACTORY METAL CRYSTALS

Personnel Engaged in Program

Principal Investigator: M. R. Achter

        T. G. Digges, Jr.
        T. C. Reuther, Jr.
        R. G. Vardiman
        C. L. Vold
        1 Technician half time

BLANK PAGE

REFRACTORY METAL CRYSTALS

A. INTRODUCTION

The long term objective of this program is the preparation and study of highly perfect specimens of refractory metals in which the only structural feature is a grain boundary of controlled misorientation. To achieve this purpose it was necessary to develop techniques for the production of highly perfect single crystals and for joining them to make bicrystals. During the past year there has been activity in four areas:

1. Procedures have been developed for the growth of single crystals of niobium of high perfection by the strain-anneal technique and for the study of their structure by x-ray and metallographic methods.

2. Measurements have been made of the rate of sintering of porosity in the grain boundaries of niobium bicrystals.

3. Bicrystals have been prepared for the study of the interfacial energy as a function of misorientation.

4. Techniques have been developed for the measurement of intergranular diffusion in the bicrystals of niobium.

B. SINGLE CRYSTALS OF NIOBIUM

The investigation of the perfection of single crystals of niobium as a function of the process variables has been completed and a paper for publication is being prepared. The major findings of this investigation are summarized below.

So that the grain boundary in the bicrystals to be studied would be the only significant structural imperfection it was desired that the single crystals from which bicrystals were to be prepared would be as perfect as possible. Also, for ease of handling it was necessary that the crystals be of large diameter. To satisfy both of these requirements, techniques for the growth of single crystals of niobium by strain-anneal were developed and the crystals were compared to those grown by zone melting. It was found that by the use of the solid state technique it was possible to grow crystals as large as one inch in diameter[1]. Control of orientation of the single crystals was achieved by a procedure involving bending of a partially

29

grown crystal in which growth was then continued around the corner. The bending jig constructed for this purpose is shown in Fig. 1.

Two criteria of perfection were used in the evaluation of the growth methods. In one, the tilt angle of the sub-grain boundaries was measured by a modified Berg-Barrett technique called the Schulz method. By this means the tilt angle ϕ may be computed by use of the formula

$$ W = \frac{2\,\phi\,S}{\sin\,\phi} \cos \alpha + 2\,\phi\,S \sin \theta \sin \alpha $$

where S is the film to specimen distance, θ is the angle of incidence of the x-ray beam, a is the angle between the subgrain boundary and a line formed by the intersection of a plane perpendicular to the beam with the specimen surface and W is the width of the subboundary on the x-ray micrograph, corrected for magnification of reproduction. Tilt angles as small as 15 seconds may be measured by this method. For the second measure of structural perfection, the dislocation density, double crystal spectrometer rocking curves were used. Attempts to use etch pit counts for comparison were unsuccessful. As shown by other investigators, etch pits become increasingly difficult to produce with increasing temperature of anneal and the temperatures used for grain growth in this investigation are higher than the annealing temperatures used by the other investigators.

In addition to these quantitative criteria, the evaluation of the perfection was supplemented by visual inspection of the x-ray micrographs for two features — evidences of residual strain and subgrain size. A larger number of sub-boundaries is indicative of a greater overall dislocation density.

In Table 1 are contained the results of the structure studies on the crystals grown by strain-anneal and by zone melting. For each crystal there is entered in the table the dislocation density and the tilt angle in seconds of arc for the subboundary of the greatest misorientation in that crystal. In the as-grown condition it is clear, based on both of these criteria, that the best of the strain-anneal crystals, Fig. 2, are considerably more perfect than those grown from the melt, Fig. 3. The effect of each of the conditions of growth is discussed separately.

I. Recrystallization Temperature

It is important that the recrystallization temperature be high enough to ensure complete recrystallization with no

residual fiber texture remaining. Single crystals could not be grown if the recrystallization temperature was lower than 1545°C. Other than the requirement of complete recrystallization, the temperature in this step appeared to have no effect on the perfection of the crystal.

II. Amount of Strain

As long as full recrystallization was achieved, there was no effect of the amount of strain when it was varied between 1 and 2-1/2 percent. When, however, a low degree of strain, 1 percent for crystal No. 12, was combined with a low recrystallization temperature of 1545° a relative y imperfect crystal was produced. With 5 percent of strain, recrystallization took place and a single crystal was not produced.

III. Temperature of Growth

Considering both the dislocation density and the magnitude of the tilt angle, examination of Table 1 shows that the optimum in perfection was achieved with a growth temperature in the neighborhood of 2000°. At temperatures higher than this, creep of the rod under its own weight introduced imperfection. At lower temperatures, reduced mobility of the defects evidently contributed to an increase of crystal imperfection.

IV. Velocity of Growth

With the exception of the dislocation density of crystal No. 11, it would appear that a slower rate of growth is conducive to greater crystal perfection. In support of this conclusion, visual observation of the x-ray micrographs indicates a more strained appearance for the crystals No. 2 and 11 grown at the faster rate in comparison to crystals No. 1 and 10 grown at the slower rate.

V. Orientation Effects

Two orientation effects were found which are not at the present time completely understood. Both the dislocation density and the tilt angle measured on the (110) plane are lower than the same parameters measured on the (110) plane. Secondly, it was found that crystals oriented closer to the [111] direction tended to be more perfect than those farther from this direction. The possible significance of these orientation effects in terms of a dislocation model is discussed in the paper under preparation.

VI. Annealing Effects

Annealing of the crystals grown in the solid state
resulted in a significant reduction in the dislocation
density. This reduction, however, was not accompanied by
a reduction in the magnitude of the tilt angle of the sub-
boundaries. It is concluded that the substructure is
anchored by the impurities and can be significantly
modified only by a high angle interface being swept
through the structure. This conclusion is fortified
by the annealing results on zone melted crystals. These
crystals, in the as-melted condition, were strained and
then zone annealed. The degree of perfection obtained
by the two stage process is considerably below that which
can be obtained in the best crystals grown by strain-
annealing.

C. SINTERING OF INTERGRANULAR POROSITY IN BICRYSTALS

Under certain conditions a large amount of porosity may
be introduced during the welding of niobium bicrystals. A
study has been undertaken of the sintering out of this
porosity as a function of various parameters, such as
boundary misorientation.

I. Dislocation Model of the Grain Boundary

For such a study it is necessary to have bicrystals
with boundaries of various degrees of pure tilt and pure
twist. The classical one dislocation pure tilt boundary
in the body centered cubic lattice involves rotation of a
[111] plane about an axis in that plane. Unfortunately,
in the strain-anneal method for producing single crystals,
it is almost impossible to obtain a [111] normal near the
rod axis. One may, however, obtain a two-dislocation pure
tilt boundary by similar rotation of the [110] plane, and
orientations suitable for this are easily obtained. The
only disadvantage is that, depending on the axis of
rotation (which is fixed for a given specimen), the dis-
locations may be of mixed edge and screw type, rather
than pure edge.

To make a symmetrical pure tilt boundary, it is only
necessary to cut two slices from the same single crystal
and rotate one 180° with respect to the other. If the
(110) normal is, say, 5° from the axis of the rod, this
means that the resulting bicrystal has the (110) planes
tilted 10° with respect to each other. The symmetry of
the lattice under 180° rotation then assures us of having

32

a $10°$ pure tilt boundary. Crystals have been grown suitable for making boundaries of 6,11,16,20,34, and 46 degrees of tilt.

A pure twist boundary may exist only on a [110] plane, where a two dislocation network is formed. Since it is improbable that a crystal will be grown with the [110] normal exactly parallel to the rod axis, it is necessary to bend the rod to the necessary orientation by the technique described above.

II. Experimental Procedure

Bicrystals of niobium are made from half-inch diameter single crystals which have been grown by the strain anneal method. These are cut, polished, and pressure welded in a vacuum induction heating furnace at $1500°C$. The usual pressure is 500 psi, which is near the yield point of niobium at this temperature. The bicrystal is then sectioned longitudinally, electropolished, and etched lightly to sharply define the void structure in the boundary. In computing the void density, correction must be made for the enlargement of the voids by the etchant, which can be done by measuring the void width and extrapolating to zero etching time. This shows the true void width is about $5x10^{-5}$ in.

III. Results

In early experiments, the welding was accomplished by holding under pressure as above for one hour. It was observed that a $19°$ boundary showed only 6.5% porosity, (Fig. 4) while a zero degree boundary showed 27% porosity after this treatment (Fig. 5). A similar effect has been previously observed in other sintering experiments, where the presence of a grain boundary was necessary for the closing of a pore. This was attributed to the action of the boundary as a sink for vacancies.

It was felt that void coalescence should be studied during annealing at $1800°C$, after a short weld at $1500°C$ in order to separate effects due to the pressure during welding. The sintering rate should be useful in the analysis of data from bicrystals of various orientations. Fig. 6 shows the porosity change during annealing for a $42°$ tilt boundary, welded for 5 min. at $1500°C$ and 500 psi. The large decrease in porosity in the first half hour, followed by a much slower rate, suggests that something other than the boundary is affecting the sintering rate.

33

The welding process should introduce dislocations, particularly at the boundary where two slightly irregular surfaces must accommodate each other. At the annealing temperature, these dislocations can climb readily, thus providing a convenient sink for the excess vacancies coming from the boundary voids. Thus, the sintering rate would be initially high, and decrease as the dislocations climbed out of the vicinity of the boundary.

To check this, a zero angle bicrystal was welded at 1000 psi, twice the usual pressure. A back reflection Laue x-ray showed the spots spread over 5 to 6 degrees in the direction of the applied pressure (normally only small irregularities in the Laue spots can be observed). The porosity in this specimen decreased from 59% to 12% after 1/2 hour anneal at 1800°C. The Laue spots decreased to 4° and were less dense, indicating some polygonization. No bicrystal, even of large misorientation has shown a comparable decrease in porosity in this time.

Schulz x-ray micrographs (as described above) have been taken of a zero angle specimen welded in the usual manner, and of the same bicrystal after a three hour anneal at 1800°C (Figs. 7 and 8). The blurred and wavy effect from the as-welded picture is due to excessive strain and high dislocation density, and is strongly reduced in the annealed picture. This supports the previous hypothesis, that excess dislocations in the as-welded bicrystal contribute to high initial sintering rates.

Studies are in progress to clarify the annealing behavior, and to determine how the effect of orientation on sintering may best be isolated. These include sintering rate studies for various orientations and welding techniques, plus x-ray determinations of dislocation structure.

D. GRAIN BOUNDARY ENERGY

The relative grain boundary energy of niobium as a function of misorientation will be determined using the thermal groove technique. In this investigation sintered bicrystals of various misorientations of both the simple tilt and pure twist types will be sectioned, polished and annealed to produce a thermal groove. The equilibrium contact angle of the groove with the crystal surface will be measured interferometrically, and from this, the relative grain boundary energy computed.

34

To date, several bicrystals with pure tilt boundaries have been produced in the manner described in the section on sintering above. A furnace is now available for the 2000° to 2200°C anneals to produce the thermal grooves. It is expected that data from this study will be forthcoming in the next quarter.

E. GRAIN BOUNDARY DIFFUSION

A study of grain boundary diffusion in sintered bicrystals of niobium has been undertaken. Both self diffusion and alloy diffusion of titanium into boundaries of bicrystals of various misorientation of both the simple tilt and pure twist types will be studied. In tilt boundaries, measurements will be made both parallel to and perpendicular to the tilt axis.

Alloy diffusion will be followed with the electron-beam microprobe of the Metallurgy Division. Standards are available for the system niobium-titanium from earlier work on lattice diffusion in that system.

Analysis in the grain boundary self diffusion experiments will be a sectioning technique. Deposition of the niobium 95 tracer will be done by evaporation at the Oak Ridge National Laboratory. The newly developed micro-sectioning process utilizing a series of anodizing and stripping steps will be used. This technique makes possible the sectioning of layers as small as 100 angstroms and can reproduce layers of from 200 to 600 angstroms with ease. The highly polished scratch-free surface required for successful stripping is obtained by grinding through 3-0 paper and electropolishing from two to four hours at 10 volts in an electrolyte of 90 H_2SO_4:10 HF contained in a graphite cathode. Anodization is done in a dilute aqueous solution of either NaF or KF at voltages of from 30 to 90 volts D.C.

Calibration of this sectioning procedure by alternate masking and stripping is underway. Step height after the anodic film is stripped is measured interferometrically. Fig. 9 is an interference photograph showing such a calibration step. A preliminary calibration curve of thickness versus film resistance (voltage drop) is given in Fig. 10.

In future diffusion work, penetration along the "triple line" common to three crystals of a tricrystal may also be examined using sintered, oriented tricrystals. Some observations on the penetration of liquid metal coolant

35

through containment vessels as well as the failure of some grain boundary diffusion models under certain circumstances suggest that such triple lines may be very high transport paths and may actually make a significant contribution to penetration type mass transport.

Reference

1. T. G. Digges, Jr. and M. R. Achter: Growing Large Single Crystals of Niobium by the Strain-Anneal Method. Trans. AIME 230 (1964) 1737.

TABLE 1

Growth and X-Ray Data of Niobium Crystals
(110) reflections unless otherwise indicated

	T_x	$\varepsilon\%$	T_G	v	B_m	N_D	φ
1	1667	2.5	2300	.44	19.5	1.0×10^6	39
(110) reflection					17	6.0×10^5	68
2	1667	2.5	2300	1.25	23	2.1×10^6	None
After annealing at 2000°C for 10 hours					17	6.0×10^5	70
3	1667	2.5	2200	.48	24	2.6×10^6	38
4	1667	2.5	2100	.48	24	2.6×10^6	35
5	1637	2.5	2030	.46	19	1.0×10^6	180
6-A	1667	2.5	2300	.48	28	3.6×10^6	80
(Ī10) reflection					21	1.5×10^6	65
6-B	1667	2.5	2000	.48	22	1.8×10^6	25
(Ī10) reflection					18	8.0×10^5	35
6-C	1667	2.5	1700	.48	23	2.1×10^6	45
(Ī10) reflection					19.5	1.0×10^6	45
7-A	1667	2.5	2300	.49	21	1.5×10^6	85
(Ī10) reflection					17.5	6.9×10^6	45
7-B	1667	2.5	2000	.49	20	1.3×10^6	35
(Ī10) reflection					19	1.0×10^6	25
7-C	1667	2.5	1700	.49	21	1.5×10^6	80
(Ī10) reflection					18.5	9.1×10^5	38
8	1667	1.0	2050	.43	18.5	6.9×10^6	49
9	1667	1.0	2300	.42	17.5	5.7×10^6	60
10	1545	2.0	2315	.44	23	2.1×10^6	40
After annealing at 2000°C for 10 hours					18.5	9.1×10^5	42

No.	T_x	$\epsilon\%$	T_G	v	B_m	N_D	Φ	Notes
11	1545	2.0	2315	1.22	27.5	3.4×10^6	33	
					16	4.0×10^6	32	After annealing at 2000°C for 10 hours
12	1545	1.0	2300	.45	28	3.6×10^6	88	
					27.5	6.9×10^5	70	After annealing at 2000°C for 10 hours
13	1545	2.0	2040	.44	14.5	1.5×10^5	30	
14	1610	2.0	2400	.43	50	1.5×10^7	160	
15	1635	2.0	1935	.48	22.5	2.0×10^6	60	
1?	1635	2.0	1815	.49	18	8.0×10^5	170	
17	1510	2.0	1715	.50	15	2.4×10^5	94	
18	1610	2.0	1610	.51	36	7.0×10^6	125	
19					22	1.8×10^6	70	As grown electron-beam zone melted
20					26	2.9×10^6	63	As grown electron-beam zone melted
					17.5	6.9×10^5	36	(1̄10) reflection
21					20	1.3×10^6	104	Electron beam zone melted crystal annealed at 2300°C at 1/2"/hr
22					19	1.0×10^6	73	Electron beam zone melted crystal strained .75% and annealed at 2300°C at 1/2"/hr
23					32	5.2×10^6	56	Electron beam zone melted crystal strained 0.2% and annealed at 2300°C at 1/2"/hr
24					27	4.5×10^6	64	Electron beam zone melted crystal strained 2.6% and annealed at 2300°C at 1/2"/hr

T_x – Recrystallization Temperature (°C)

$\epsilon\%$ – Strain

T_G – Temperature of Crystal Growth (°C)

v – Rate of Movement of Rod (inches/hour)

B_m – Measured Half-Width B_m in Seconds

N_D – Number of Dislocations/cm^2

Φ – Approximate Magnitude of Largest Tilt Boundaries in Seconds
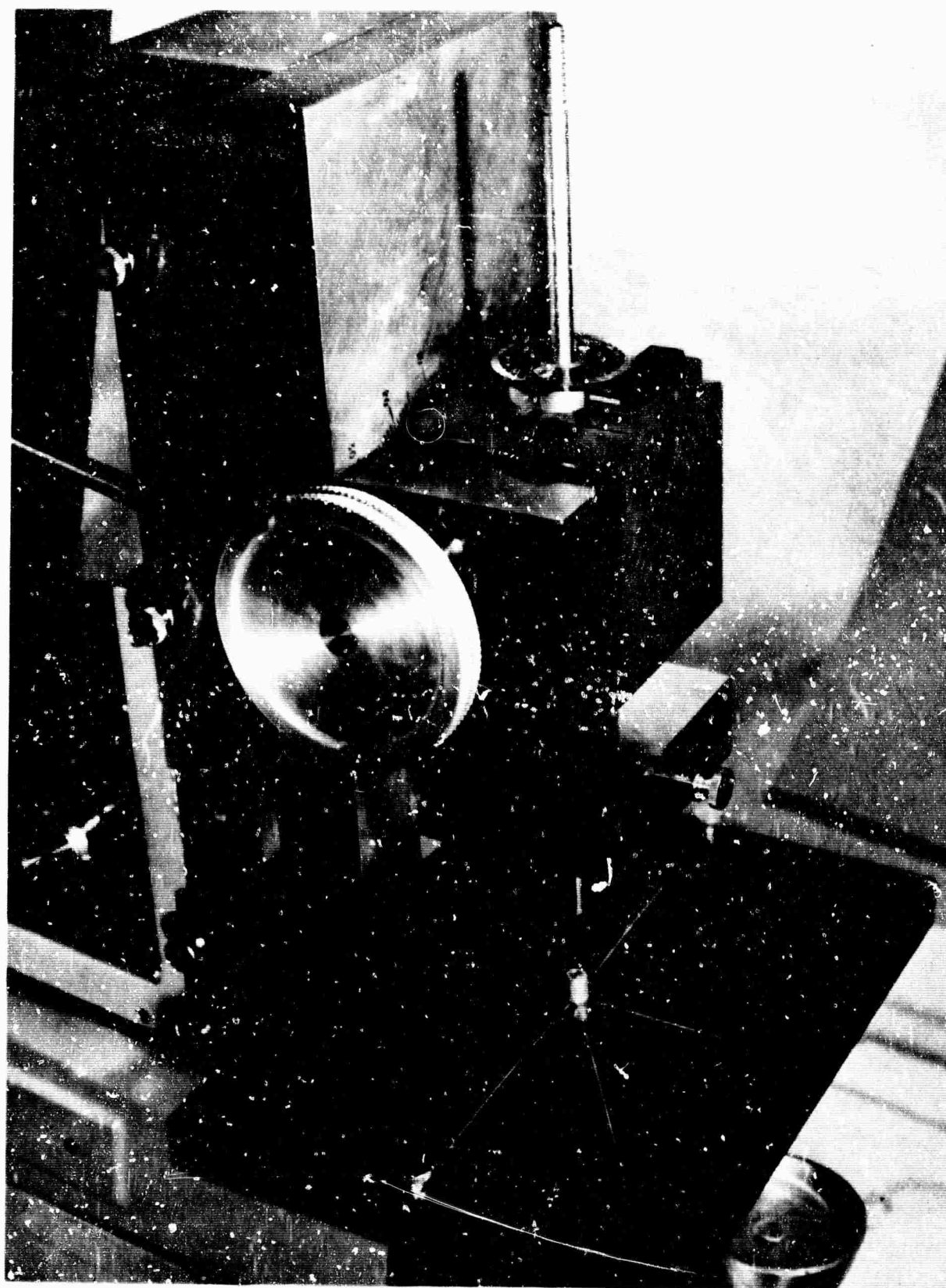
Fig. 1 - Bending apparatus for controlling the orientation
of single crystals grown by the strain-anneal technique
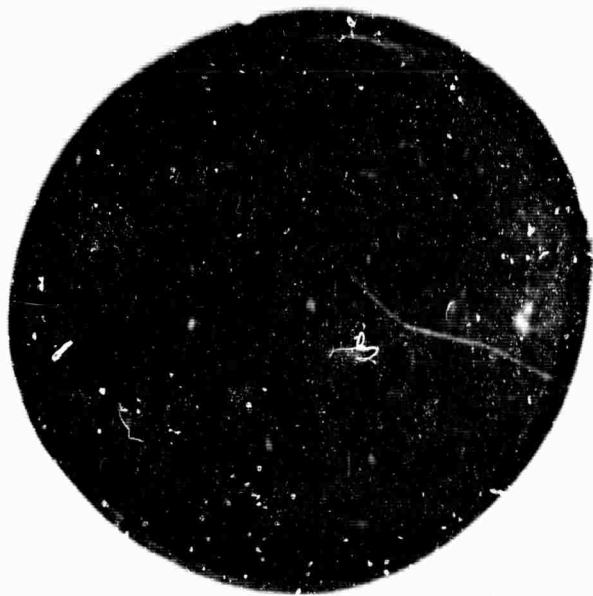
Fig. 2 - Schulz x-ray micrograph of crystal No. 1 (Table 1) grown by the strain-anneal technique.

Fig. 3 - Schulz x-ray micrograph of crystal No. 20 (Table 1) grown by the zone melting technique.
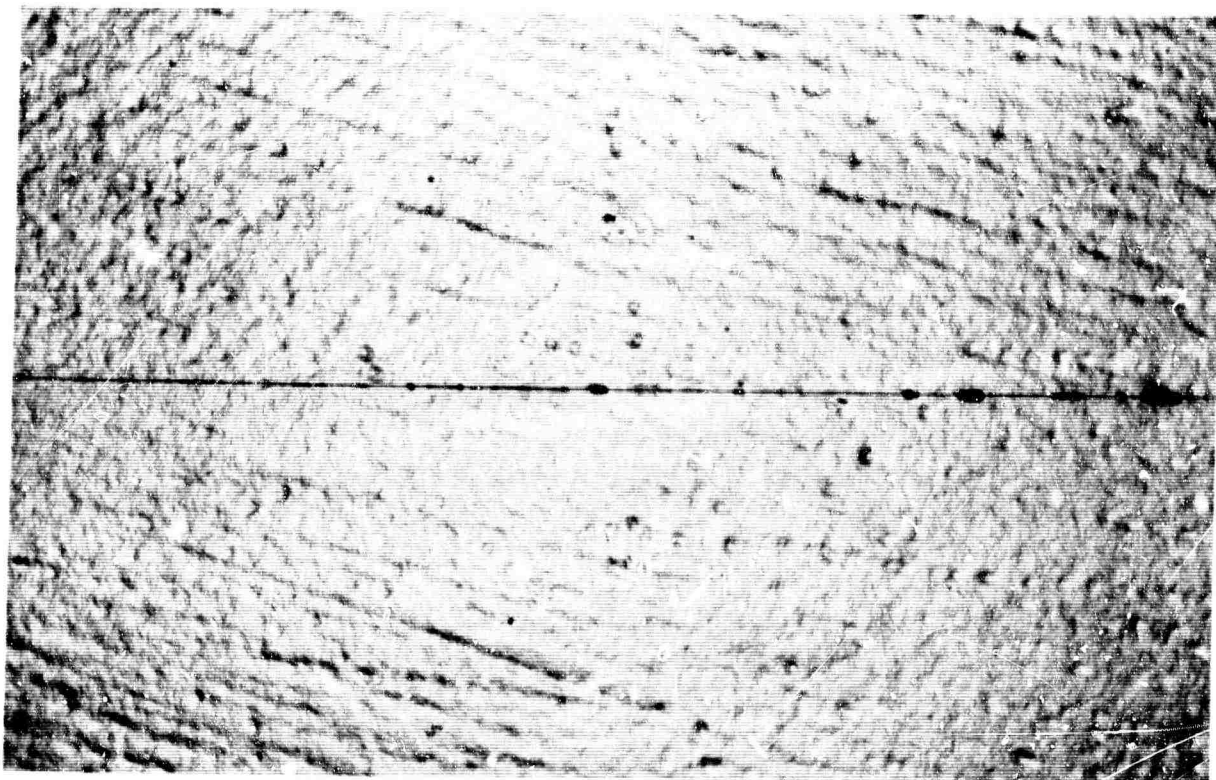
Fig. 4 - 19° bicrystal welded 1 hr. at 1500°C and 500 psi. 50X.
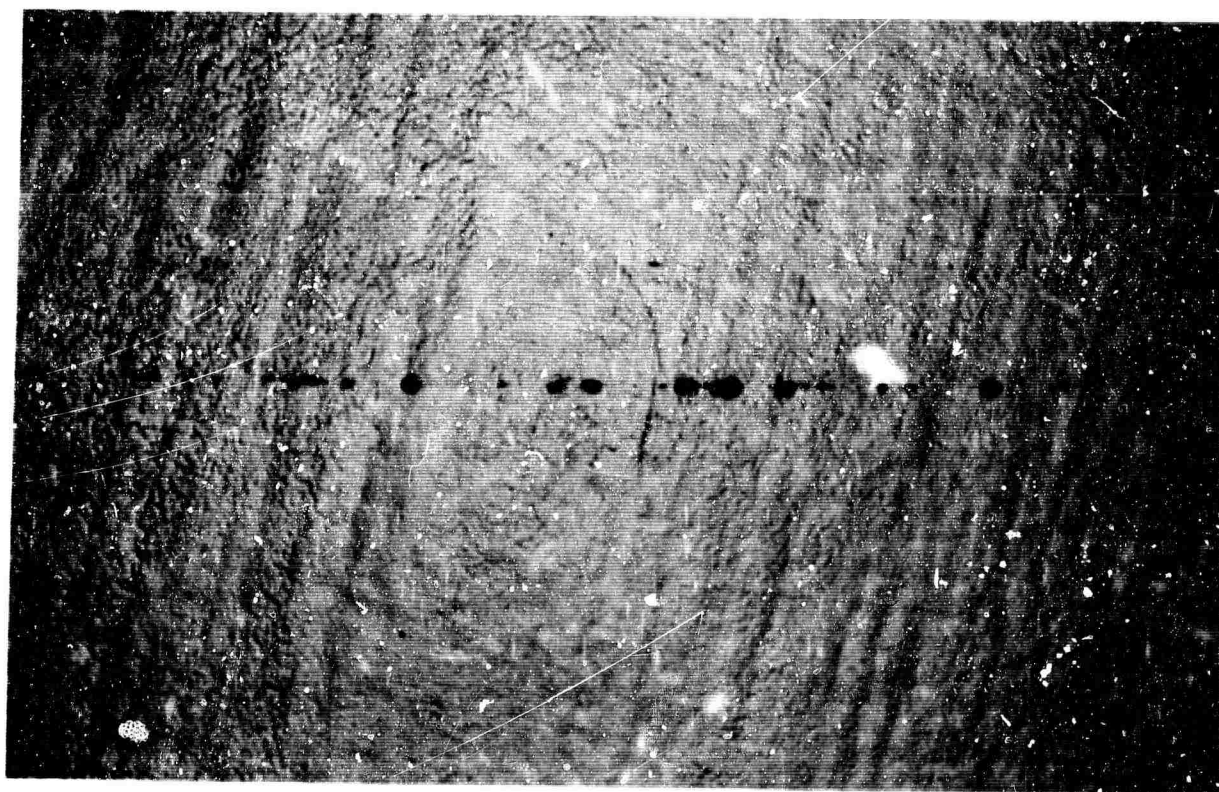
Fig. 5 - 0° bicrystal welded 1 hr. at 1500°C and 500 psi. 50X.

41
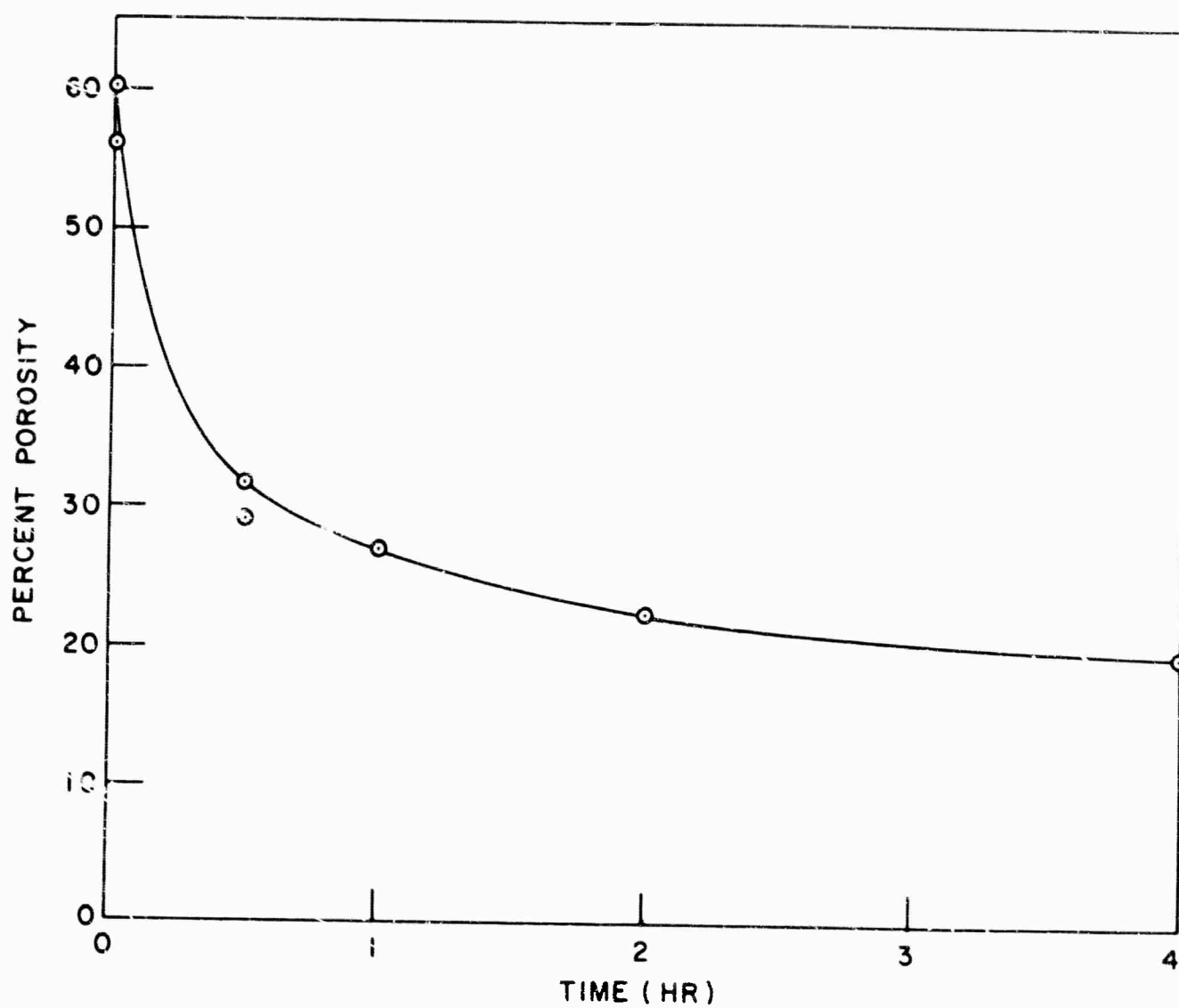
Fig. 6 - Void density in a 42° tilt boundary vs. annealing time at 1800°C.

42
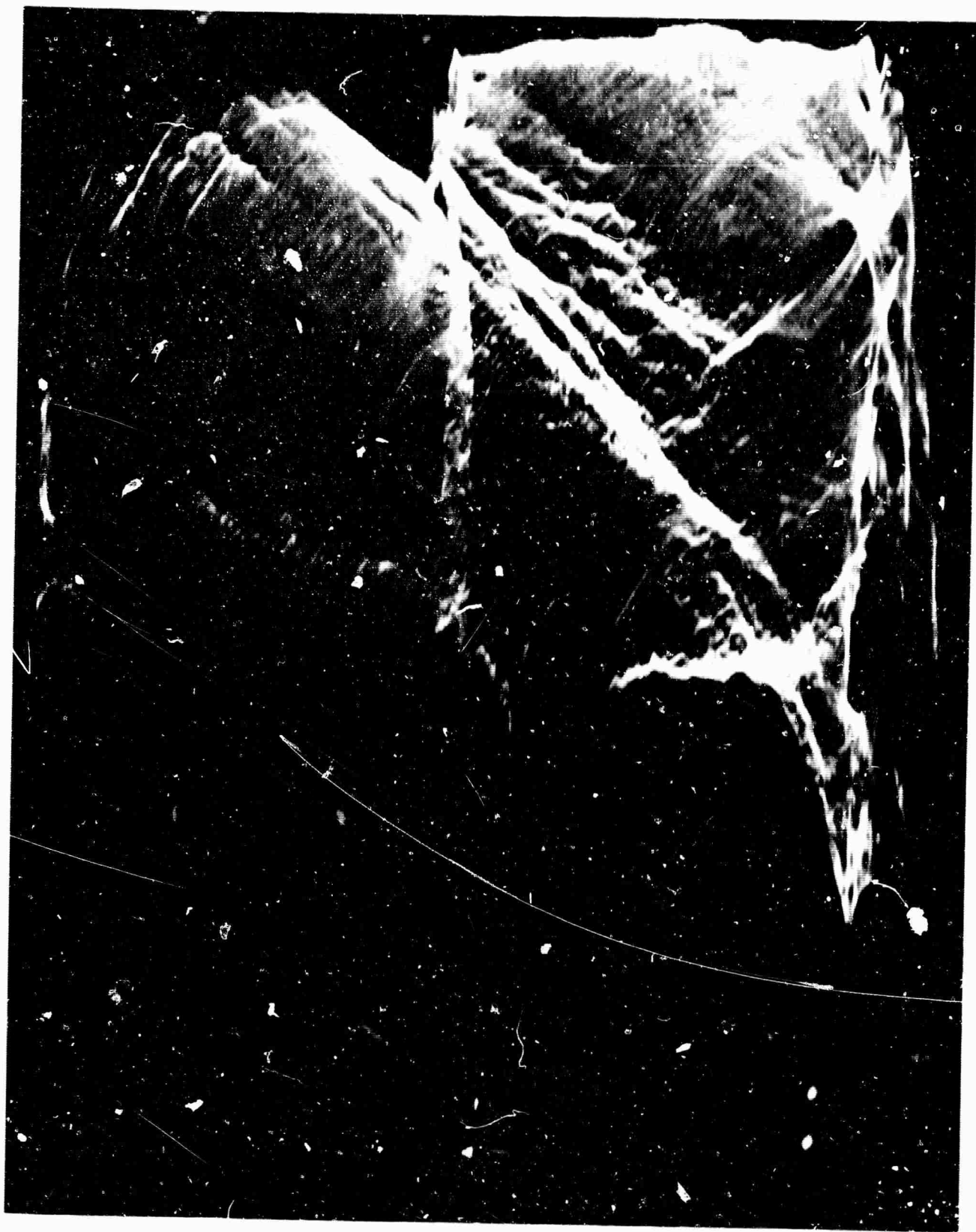
Fig. 7 - Schulz x-ray micrograph of a (100) plane of a zero
degree bicrystal, welded 5 min. at 1500° C and 500 psi

43

Fig. 8 - Schulz x-ray micrograph of a (110) plane of a zero
degree bicrystal, annealed 3 hr. at 1800°C.

44
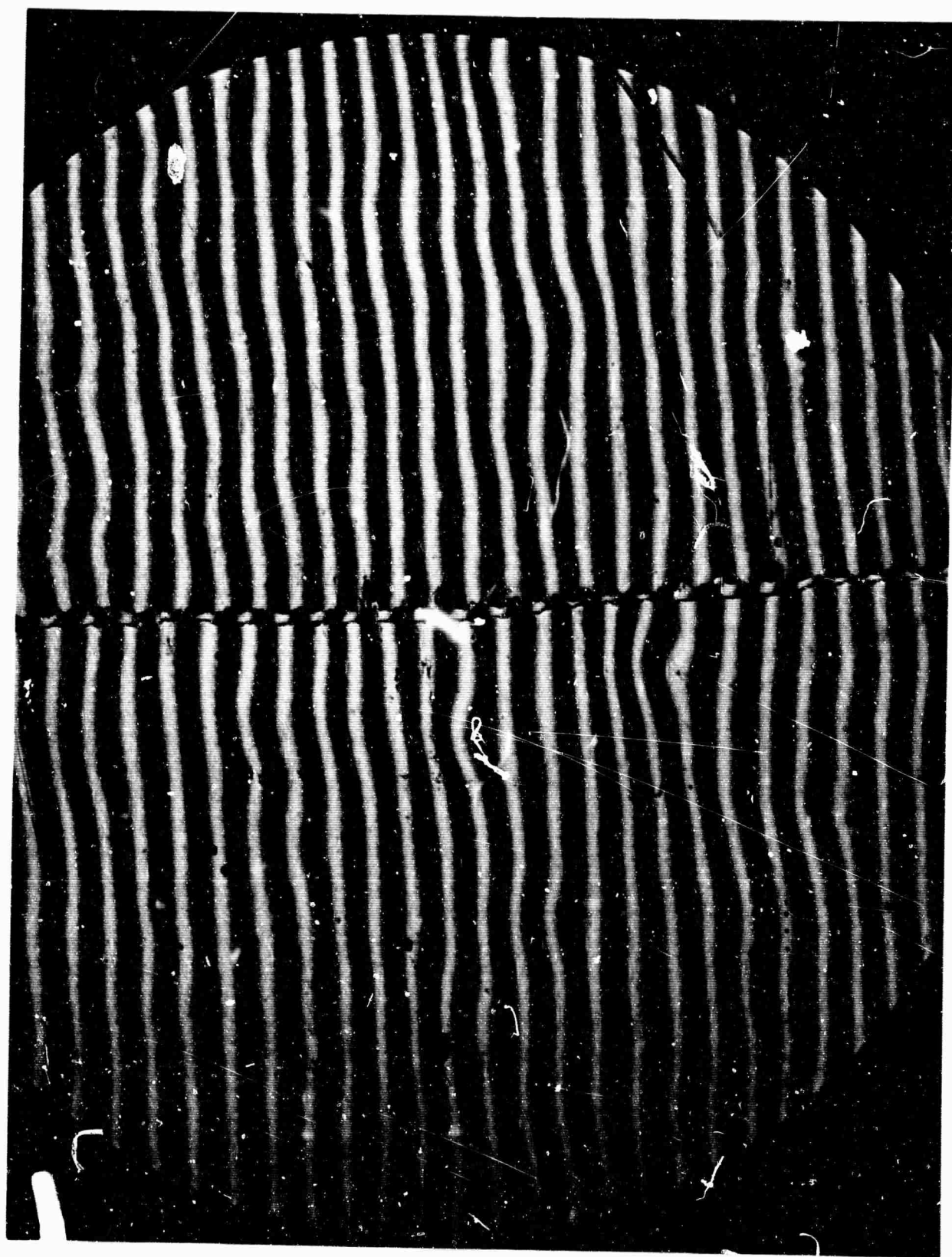
Fig. 9 - Interference photograph of an electropolished niobium surface. The fringe shift is at a 600 angstrom step on the surface which was produced by masking, anodizing to 90 v, and stripping. At the step there is a band of unstripped anodic film. (λ = 0.27 μ; X200.)
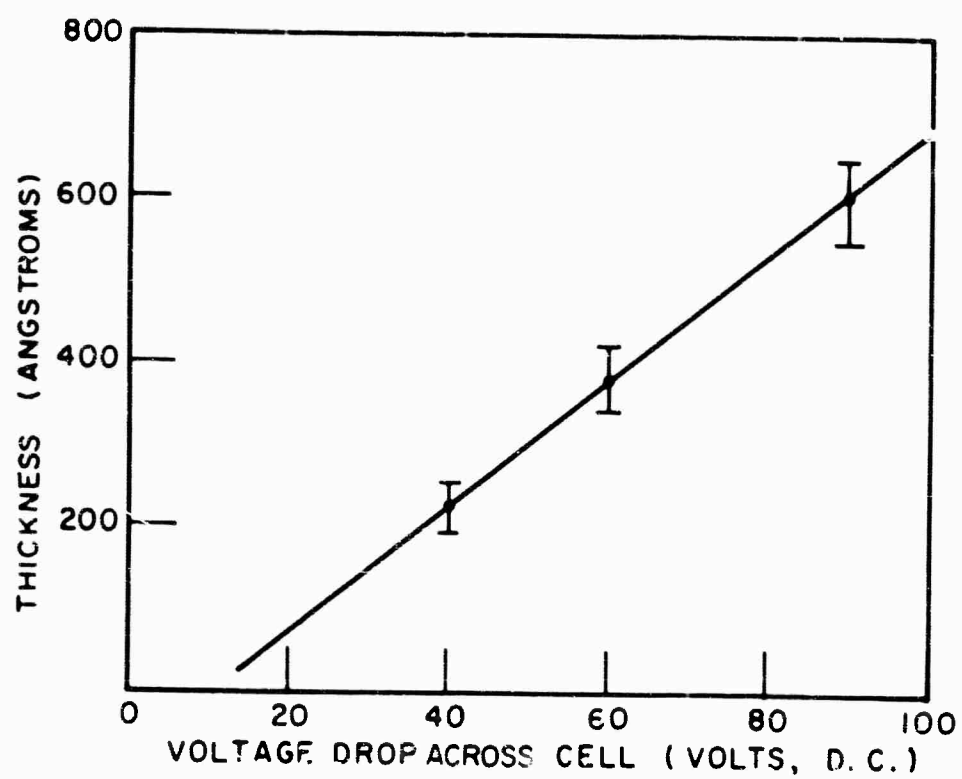
Fig. 10 - Preliminary calibration curve for the anodization of niobium in dilute aqueous NaF. Thickness in angstroms vs. voltage drop across the anodic cell.

TRANSITION METAL AND INTERMETALLIC COMPOUND SINGLE CRYSTALS

Personnel Engaged in Program

Principal Investigator: A. I. Schindler
M. E. Glicksman
G. N. Kamm
B. C. La Roy
R. J. Schaefer
T. J. Schriempf
C. L. Vold

1 Technician

BLANK PAGE

TRANSITION METAL AND INTERMETALLIC COMPOUND SINGLE CRYSTALS

A. CRYSTAL GROWTH KINETICS

I. Effects of an Electric Current on the Solidification of Metals

At a stationary solid-liquid interface, the temperature gradients in the solid and liquid phases normally attain values such that the heat flowing into the interface from the liquid is equal to the heat flowing out of the interface into the solid. The gradients necessary to maintain these heat flows will differ to the extent that the thermal conductivities of the solid and liquid differ. If the interface is freezing at a constant rate, the temperature gradients must change in such a manner that the heat of fusion is carried away. The temperature gradient in the liquid is an important factor in determining the substructure and distribution of impurities in a growing crystal. For example, a shallow temperature gradient may permit constitutional supercooling to develop during crystal growth, resulting in cell formation and lateral solute segregation (1).

Passing an electrical current through the interface can modify the temperature, the temperature gradients, and consequently the growth conditions of the resultant crystals through several effects:

a) Resistance heating, whose magnitude will in general differ in solid and liquid, will alter the temperature distribution during crystal growth;

b) Peltier heating or cooling, depending on the direction of electric current flow, will change the temperature gradient at the solid-liquid interface.

The relative importance of these effects will depend on the geometry of the system, the physical properties of the metal, and the current density. Peltier effects should be small in normal metals with typically low thermoelectric powers, but could be significant in a semi-metal such as bismuth. Note that since Peltier effects are proportional to the current, while resistance heating is proportional to the square of the current, their individual effects are, in principle, separable. Thus, passing an electric current of properly selected magnitude and direction through a crystal-melt interface can provide an extra degree of control over the crystal growth process.

To investigate the influence of electric currents on crystal growth, observations were made of the effects of these currents on (1) the temperature gradients in the vicinity of a liquid-solid interface in pure metals and (2) the resultant morphology of the solid-liquid interface in dilute alloys.

For both series of experiments, the metal crystals were solidified unidirectionally in forked boats of machin-able lava containing electrodes which permitted electric currents to pass up one side of the fork and down the other. See Fig. 1 and 2. The currents are therefore flowing from solid to liquid in one branch and from liquid to solid in the other.

For the temperature gradient measurements the apparatus in Fig. 1 was employed. Three thermocouples on each side of the fork, spaced at intervals of one centimeter, were inserted through the bottoms of these boats into the molten metal; these thermocouples were insulated electrically from the metal to prevent the pick-up of spurious potentials.

The boat was surrounded by a cylindrical furnace which moved at a controlled rate of 1 to 4 cm/hr along a track lying parallel to the specimen axis. As the boat emerged from the furnace, solidification proceeded down both branches of the fork and the temperatures of the thermocouples were measured by a multipoint recorder. The variation of tempera-ture with time of an individual thermocouple then gave an accurate representation of the variation of temperature with distance from the interface as the interface moved past the thermocouple at a uniform rate.

Measurements were made in this fashion on crystals of pure bismuth and pure tin. The bismuth crystals showed a much steeper gradient on the solid side than on the liquid side of the interface. In Fig. 3, curve (a) shows the tem-perature profile for the case in which no current flows along the specimen, while curves (b) and (c) show the temperature profiles when Peltier heating and cooling have been produced at the interface by electric currents flowing into and out of the solid, respectively. The curves have been shifted hori-zontally to bring the interface to a common origin. Joule heating, greater in the solid than in the liquid, makes the overall gradient shallower when current flows. It may be seen that Peltier cooling results in a relatively steeper gradient in the liquid adjacent to the interface, while Peltier heating produces a shallower gradient.

50

The dashed line in Fig. 3 shows the local equilibrium temperature of an impure melt, which is depressed near the interface by the solute accumulated in that region. In the regions where the melt temperatures lie below this equilibrium temperature, the liquid is constitutionally supercooled, and it is seen that the extent of the supercooled region is affected by Peltier heating or cooling.

Measurements of temperature gradients in tin showed very little discontinuity in gradient at the interface, and no perceptible effect of Peltier heating. The lattice observation was expected because the Peltier coefficient between solid and liquid in tin is an order of magnitude smaller than that in bismuth. The effect of currents on the overall gradient in tin has yet to be determined.

For the studies of the influence of electric currents on growth morphology, the forked boat was made of two pieces of lava, one of which could slide in a steel runway. The extended region C in Fig. 2 contains a seed crystal of the desired orientation, which propagates down both branches of the boat producing a forked single crystal. During solidification, current can be lead in through graphite plugs under the regions A. When the crystal has grown to the junction of the two crucible sections at B, a catchment mechanism is released, and the spring jerks the crystal away from the liquid, exposing to view the solid-liquid interface as it was during solidification. Direct comparison can then be made between the two interface morphologies resulting when direct current flows into and out of the solid, all other conditions being equal.

It is found that tin-doped bismuth crystals growing into the melt are generally bounded by facets lying in crystallographic planes of the type {100}. When the mean orientation of the interface differs from {100}, these facets form parallel ridges or pyramids whose sides are bounded by {100} facets (Fig. 4). Segregated impurities tend to build up to high concentrations in the valleys between ridges, so that even in these crystals containing only 1/2-wt % tin, eutectic material (43-wt % tin) is deposited locally. Metallographic examination revealed that the eutectic material is confined to plate-like regions primarily lying parallel to the {100} planes of the bismuth matrix. Crystals have been grown at several different current densities, and preliminary results indicate that the distance between the faceted ridges is smaller at the interface where Peltier cooling occurs than at the interface where Peltier heating occurs.

The precise influence of growth rate, current density, and solute content on interface morphology and substructure have not yet been determined.

II. Dendrite Tip Temperature Measurements

It is generally accepted that the temperature of a solid-liquid interface must depart from the thermodynamic equilibrium temperature if either solidification or melting occurs at the interface. Fig. 5 illustrates a typical temperature distribution to be found along the axis of a pure metal dendrite growing from the melt with a constant tip velocity, v_i. As shown, the steady-state temperature of the advancing tip is T_i; moreover, the interface may be considered as supercooled an amount ΔT_i with respect to the equilibrium temperature, T_e, and superheated an amount ΔT_d with respect to the melt's temperature, T_ℓ, at a large distance from the dendrite. The equilibrium temperature is, of course, established some distance back from the tip along the stationary portions of the dendrite body.

The significance of separating the overall supercooling, ΔT, into the terms ΔT_i and ΔT_d is that these temperature differences determine two distinct, but coupled, rate processes, viz., ΔT_i determines the kinetic rate of the crystallization process at the active solid-liquid interface while ΔT_d determines the rate of thermal diffusion from the advancing dendrite tip to the surrounding, cooler melt. Since we expect that the crystallization velocity of a particular metal growing in a specific crystallographic direction is governed solely by the overall melt supercooling, ΔT, it then follows that there must also be some unique division of ΔT between ΔT_i and ΔT_d for stable, steady-state crystal growth, such that the release of latent heat during growth is just balanced by the specific heat flow away from the crystal.

Because of the rapid growth kinetics which exist in most metal systems, and the fine, fragile nature of metallic dendrites, no experimental methods have been developed, heretofore, for measuring the apportioning of ΔT between ΔT_i and ΔT_d at various growth velocities; furthermore, only few data exist for a limited number of systems on the relationship between dendrite velocity and the easily measured overall supercooling.

We have devised a method which permits measuring the velocity of crystal growth along with the corresponding values of ΔT_i and ΔT_d. Fig. 6 shows the apparatus employed

52

and displays the operation of the method. A horizontal,
pyrex chamber, 1 cm. in diameter and about 30 cm. long, is
partially filled with the molten metal under study. In
this case, bismuth was used. Two tungsten pins, which
serve as electrodes, are immersed in the molten metal and
connect the specimen to the external circuitry. The speci-
ment chamber is allowed to cool slowly into the supercool
temperature range below the normal (272°C) freezing point
of bismuth until crystallization commences. If we assume
that nucleation occurs at the right end of the melt, then
the crystallization front, advancing toward the left,
passes the right and left electrodes, in turn. Because
the advancing dendritic crystals differ from the liquid
in their thermoelectric properties, a potential is developed
in the specimen which is detected in the external circuit
during passage of the solid-liquid interface between the
electrodes. Fig. 7 shows some typical waveforms obtained
by this method. Each waveform is composed of two pulses
of opposite polarity; moreover, these pulses occur when
the crystallization front enters and leaves the zone
between the electrodes. The time separation of the two
pulses provides a convenient measure of the transit time
of the crystals between the electrodes, and, knowing the
electrode spacing, can be used to calculate the average
crystal growth velocity. Also, the pulse height has been
shown to be proportional to ΔT_d; details of this analysis
will be given elsewhere. Fig. 8 shows the correlation
existing between ΔT_d (pulse height) and the growth velocity
(inverse pulse separation). Because a thermocouple was not
provided for measuring the melt's temperature, T_ℓ, at the
time of freezing, the ΔT_d values must remain in arbitrry
units. Nonetheless, these data show an interesting linear
relationship between the growth velocity and ΔT_d over the
range of velocity observed.

III. Transformation Rates During Dendritic Solidification

In describing the kinetics of a phase transformation,
it is usually sufficient to specify the transformation rate
for a unit of interphase boundary. For instance, when
dealing with solidification processes it is convenient to
determine only the average rate of advance of a crystal
growing into the surrounding melt, i.e., the growth velocity.
While the growth velocity often remains constant during the
rapid dendritic solidification of a uniformly supercooled
melt, the overall transformation--defined as the product of
the growth velocity and the instantaneous area of the active
solid-liquid interface--exhibits a complex behavior. More-
over, while the measurement of growth velocity (specific

53

rate of transformation) in solidifying systems is straight-
forward, measurement of the overall rate is difficult.

Because a difference in mass density exists between
the solid and liquid phases which are present during solidi-
fication, mass convection will accompany the freezing process.
Furthermore, the mass convection will occur at a rate which
is exactly proportional to the overall rate of solidification.
It has been shown (2) that a transfer of mass during crystal
growth results in an acceleration of the center of mass of
the solidifying system which can be monitored with externally
coupled accelerometers. As will be shown here, the accel-
eration-time profiles obtained during solidification from
an accelerometer provide a means of judging the overall rate
of transformation occurring within the specimen.

Fig. 9 shows an idealization of one type of solidifying
system which has been investigated both theoretically and
experimentally. Shown in the figure is a cross-section
through a cylindrically configured mass of uniformly super-
cooled molten metal through which a spherical solidification
front is advancing. It must be borne in mind that the solidi-
fication front depicted is not the true solid-liquid interface,
but is a surface which denotes the instantaneous, average
spatial positions of the tips of the dendritic crystals which
are advancing into the cooler melt. It is further assumed
that crystallization was initiated (nucleated) on axis at
the base of the cylinder, and that this base is rigidly
fastened to a massive foundation. As indicated in the
figure, the radial velocity of the front is constant; this
feature of the model has been experimentally verified with
high speed cinematography for bismuth and nickel. Note also,
that the material behind the solidification front is a
mixture of dendritic crystals and melt--all at the equilib-
rium temperature--while the material ahead of the front is
untransformed, supercooled melt.

The overall transformation rate, derived for the
expanding-front solidification model just given, is shown
plotted against the dimensionless radius of the front, r/R,
in Fig. 10. For comparison, the transformation rate for a
planar front with a circular cross section of radius R has
been chosen for reference and appears in this figure with
the arbitrarily assigned value of unity. Here we assume
that both the spherical front and the planar front have
the same surface density of dendrite tips, i.e., the same
fraction of active, solid-liquid interface.

54

Fig. 11 shows the dimensionless accelerations of the center of mass as a function of reduced radius, r/R, expected for the expanding-front solidification system. Curves have been calculated for systems having various aspect ratios (h/R). The most notable features in the predicted acceleration curves are the sharp rise to a maximum, followed by a sudden reversal in sign, and a minimum followed by a decay of the acceleration to an almost constant value for the remainder of the solidification. Fig. 12 shows experimentally determined acceleration-time data obtained from the output of an accelerometer attached to a solidifying supercooled specimen of bismuth having an aspect ratio, h/R=15. Although the experimentally determined acceleration data (Fig. 12) are plotted with time as the abscissa, while the theoretical curves (Fig. 11) have dimensionless distance as the abscissa, the qualitative features of these figures should be comparable if the solidification model fits the experimental situation. Indeed, Figs. 11 and 12 show good correlation between theory and experiment.

The immediate conclusion reached here is that the transformation-induced accelerations are predictable from a knowledge of the overall transformation rates. It now also seems feasible to reverse this procedure, i.e., measure the accelerations and indirectly calculate the transformation rates. Finally, an interesting possibility that is suggested by this method would be to study the solidification process during the transition period between the nucleation event, which starts the transformation, and the period of steady-state dendrite growth.

B. GROWTH AND PERFECTION OF CRYSTALS

I. Hafnium

As part of the examination of the effects of an ultra-high vacuum environment upon the degree of purification obtained during zone refining, a hafnium rod has been subjected to floating zone melting in the 10^{-9} torr electron beam zone refiner. A total of four melted passes was made on an 18 cm. long hafnium specimen. The pass speed was 2.8 cm/hr and the characteristic pressure while melting was 5×10^{-8} torr. Room temperature to liquid helium temperature resistance ratio measurements were made on the starting material, and then in several increments along the specimen after the first and fourth melted pass. The results of these measurements are illustrated in Fig. 13. The resistance ratio (impurity) profile obtained after pass number one is characteristic for zone refining of a

long specimen containing an impurity with a segregation coefficient greater than one. After the fourth pass, the entire zone melted portion of the specimen exhibited a resistance ratio of 11.7. No profile was evident.

A quantitative x-ray fluorescence analysis of the unmelted portion of the specimen and a portion which had been melted four times indicated the presence of 2.7% zirconium in both. Although this unexpectedly high zirconium content detracts greatly from the utility of the specimen for experimental purposes, it does allow some interesting interpretation of the resistance ratio data.

Little is known of the exact form of the low temperature resistance of metals as a function of impurity content. However, it may be said with relative certainty that residual resistance is quite insensitive to small variations about an impurity content as large as a few percent.

The resolution of a resistance ratio profile along the specimen after the first melted pass, in spite of this insensitivity, indicates that a certain amount of impurity was swept out by the zone refining process. The increase in the resistance ratio of the central part of the specimen after one pass over the ratio of the starting material indicates that preferential volatilization was also active in the removal of impurities. After the fourth melted pass, the resistance ratio has increased to a value of 11.7 and the profile has been obliterated. This is most plausibly explained by the assumption that the same impurities which were moved by the zone refining process during the first pass were removed by volatilization during the next three.

Even though the zone refining process is most efficient when large concentrations of impurity are present, no difference in zirconium content between unmelted and four times melted hafnium was indicated by x-ray fluorescence. This and the absence of a resistance ratio profile after four passes leads one to conclude that little or no zirconium has been removed from the specimen. In that case we may say that the observed increase in resistance ratio was due to the removal of measurable (and probably large) amounts of other impurities.

II. Ruthenium

Electron beam zone refining of ruthenium has been initiated in order to obtain high purity single crystals

56

for use in low temperature thermal conductivity experiments. Such specimens are required in order to minimize the effects of impurities and lattice defects on electron scattering. Single crystal ruthenium has been prepared by electron beam zone refining (3), but very little data is available concerning the purity of these specimens. In particular there seem to be no data at all on the variation in purity along the zone-refined rod, none on the effectiveness of the technique as a function of purity of starting material, and also none on the degree of purification per pass. Although the details of such data are probably valid only for a particular apparatus, the general features of the results to be described below are of interest in the study of the techniques of purification of metals.

The starting materials for this study were ruthenium powders obtained from two sources: Engelhard Industries, Inc. furnished powder of nominally 99.9% purity, and United Mineral and Chemical Corporation supplied a powder of nominal purity of 99.999%. This was formed into bars roughly 1/4" square by 1-1/2" long by compressing at 40 ksi, sintering one hour at 1200°C in a hydrogen atmosphere, and sintering one hour at 2100°C in a vacuum of 5×10^{-5} torr (4). Final densities varied from 92 to 96% of theoretical density. These bars were then ground into cylinders by conventional grinding techniques.

The welding of the bars into longer rods and subsequent zone melting was carried out in a vacuum of about 1×10^{-6} torr. The initial melting was accompanied by severe bubbling, presumably caused by gases trapped in the compacted material. It was found necessary to remove the sides of the molybdenum "pillbox" which normally surrounds the molten portion of the rod and provides focusing of the electron beam. This resulted in a somewhat longer molten zone, but apparently permitted the pumps to remove the evolved gases and vapor at a much greater rate and reduce the rate of deposition of ruthenium on the tungsten filament. Even with this arrangement it was found necessary to replace the filament after each melting pass along the rod. The difficulty of maintaining a molten zone in the severely sputtering ruthenium, complicated by the low surface tension and high vapor pressure of the molten material and the high thermal conductivity of the solid, gave rise to rods of quite irregular cross section. Fortunately this geometry can be adapted to anticipated low temperature thermal conductivity studies.

The degrees of purification obtained were evaluated by measuring the ratio of the electrical resistance along

57

the rod at "room temperature" (from 28°C to 32°C) to that at 4.2°K. This ratio (RRR) is very sensitive to small amounts of dissolved impurities and probably varies approximately inversely with their concentration (5). However the value of RRR is not sensitive to impurities in the form of oxides and, in addition, suffers from the disadvantage that it is sensitive to strains in the sample. Nevertheless at present these ratios provide the only convenient way of determining relative degrees of purity for the very low impurity levels encountered in this work.

The ratios were determined by passing current (1 amp at room temperature and 10 amps at 4.2°K) through the specimens and measuring the potential drops between adjacent pairs of copper leads fastened along the rods. The copper leads were held to the specimen simply by the use of pressure sensitive tape. The contact was improved by wrapping wax-impregnated nylon tape around the junction and tying it securely. Although this method of applying potential leads gives little trouble in the form of electrical noise, it has been found that the position of the contacts sometimes changes slightly with cooling to 4.2°K and subsequent warming to room temperature. By repeating measurements, however, this effect can easily be detected. The influence of strain was checked after 4 passes by repeating the measurements before and after annealing the sample. No differences in RRR were found. The values reported herein are repeatable with differences of less than 5%.

The results obtained with a sample prepared from 99.9% pure powder are shown in Fig. 14. Values of RRR obtained after 3, 4, and 6 passes are indicated. The RRR of the material, after compressing and sintering but before melting, is about 100, as indicated in the figure by the straight line. The overall upward trend of the curves with increasing number of passes shows that evaporative purification is taking place. However, it is also apparent from the increased purity at the beginning of the pass and the relative decrease in purity at the end that the ruthenium is undergoing purification by zone-refining. The only significant departure from typical zone-refining profiles is the center value of RRR obtained after 6 passes. As this coincides with a rather thick portion of the sample, the metal probably was not melted completely at this point. Although more zone melting did, indeed, bring this value into agreement with the other profiles, no further significant increases in RRR were obtained.

At this point the rod was placed in a zone-refining apparatus with a vacuum capability of 10^{-9} torr. One pass in this device, during which the residual pressure was 10^{-7} torr, did not improve the specimen, and gave only a slightly changed profile. The slight differences are probably due to the increased difficulty of maintaining a molten zone, for at this stage the rod had become quite irregular. The results are shown in Fig. 14 as UHV; the value of 785 represents the average RRR over a larger portion of the rod than was obtained prior to the UHV pass, but is consistent with a profile unchanged from that at 6 passes. The value of 710 in the center of the rod shows that proper melting brings the low value obtained following 6 passes into agreement with the other profiles. Thus it is apparent that 6 melting passes at 1×10^{-6} torr yield the full degree of purification available by zoning the 99.9% pure material.

The effect of evaporative purification can be roughly separated from the zone-refining effect. Assuming that RRR is inversely proportional to the impurity concentration, C, one has

$$\frac{C}{C_O} = \frac{RRR_O}{RRR}$$

where the subscript o refers to values at that point of the rod where only evaporative purification took place. By drawing smooth curves through the bars in Fig. 14, approximate profiles were obtained for 3, 4 and 6 passes. The curves were arbitrarily forced to be parallel to the abscissa between 5 and 6 cm, and the values here were taken as RRR_O. The low point in the center of the 6-pass results was ignored. The results, shown in Fig. 15, indicate that zone-refining per se stopped after four passes. It also appears that evaporative purification did not take place uniformly along the rod, for, at both ends, RRR_O/RRR decreases with increasing number of passes. (In simple zone refining the impurities removed from one end accumulate at the other.) By comparing only that part of the profile in Fig. 15 near the beginning of the pass with the zone refining profiles calculated by Pfann (6), one finds an effective distribution coefficient between 0.7 and 0.8.

X-ray diffraction measurements made on the rod after all melting had been completed show that it is a single crystal for about 8 cm from the beginning of the pass, and that the c axis of the hcp structure is approximately perpendicular to the axis of the rod. Thus the values of RRR reported here are representative of the electrical resistance parallel to the basal plane.

59

Two passes at about 1×10^{-6} torr have been accomplished at present on the 99.999% material. The results, shown in Fig. 16, indicate a purification trend similar to that obtained with the less pure powder. The low value at the beginning is probably due to incomplete melting. Visual inspection of the rod indicates that it is probably not yet in single crystal form. The relatively high value of RRR (a significant portion of the rod has an RRR>1000) obtained with the more pure starting material are encouraging, and it is hoped that further zoning will yield a specimen of even higher purity.

It should be noted that the highest published value of RRR for ruthenium is about 500 (7). (A value of 720 has apparently been obtained elsewhere.)(8). Thus the work outlined here indicates a substantial improvement in the purity level of this material.

III. Copper

We have successfully grown a high purity single crystal of copper by the electron beam melted, floating zone technique. To our knowledge this is the first single crystal of copper which has been grown by this method. To determine the crystalline perfection of this crystal, x-ray micrography, double crystal spectrometer rocking curves and etch pit studies were made.

The crystal was grown from 1/4-inch diameter rod having an initial purity of 99.999%. Three outgassing passes followed by four molten passes were made in the electron beam zone refiner. The resultant single crystal was about 2 inches long. Some difficulty was encountered in maintaining a uniform molten zone, and frequent manual adjustment of the beam current was required. At no time did the pressure during melting exceed 1×10^{-6} torr.

A (111) surface was prepared using spark erosion planing, followed by electropolishing in a solution of 60% orthophosphoric acid and 40% water. X-ray diffraction micrographs did not yield well defined sub-boundaries, indicating that the substructure had very small sub-grain size. Rocking curve half widths were measured with an x-ray double crystal diffractometer, and the dislocation density was computed from the equation (9)

$$\beta_C^2 = 4b^2 N_D$$

where β_C is the half width of the rocking curve, as modified by the dislocations, b is Burgers vector, and N_D is the

60

number of random dislocations per sq cm. In practice, one
measures a quantity β_m, the measured half width of the
rocking curve, which is related to β_C by the relation

$$\beta_C^2 = \beta_m^2 - \beta_{1N}^2 - \beta_{2N}^2.$$

Here β_{1N} and β_{2N} are the natural half widths of the first
and second crystals, respectively. The actual values of
β_{1N} and β_{2N} are approximately an order of magnitude less
than the measured quantity β_m; therefore, in the case of
the measurements on the copper crystals, β_{1N} and β_{2N} can
be safely neglected. The dislocation densities so computed
ranged from 1×10^8 to 7×10^8 lines/cm^2 depending on their
location on the specimen surface.

A more direct procedure in determining dislocation
densities is the measurement of etch pit densities. Using
appropriate reagents, etch pits occur where dislocation
lines emerge from the specimen surface. A two second etch
in the reagent developed by Livingston yielded well defined
etch pits, as is shown in Fig. 17. The lower limit of the
dislocation density, as determined by direct etch pit
counting, was 2.5×10^7 lines/cm^2 and the upper limit was
estimated to be approximately an order of magnitude greater.
Thus, the dislocation densities, as determined by etch
pit counting and rocking curve measurements, are consistent.

C. PURITY CHARACTERIZATION STUDIES

I. Purity Determinations for Ferromagnetic Metals

An important facet of the production and utilization
of high purity metals is the method of purity determination.
For most metals, a very sensitive measure of purity is the
residual resistance ratio; $RRR = R_{30°C}/R_{4.2°K}$. However this
method is not directly applicable to ferromagnetic materials
because the value of $R_{4.2°K}$ contains magnetoresistive con-
tributions, even in zero applied field, which are comparable
to those of impurity scattering.

Two mechanisms, both based upon the orientation of
Weiss domains, have been postulated to explain the domination
of $R_{4.2°K}$ by some factor other than impurity scattering.
Sudovtsov and Semenenko (10) have proposed diffuse scattering
from domain walls while Berger and de Vroomen (11) suggest
a magnetoresistance effect due to the magnetization within
the individual domains. Either of these mechanisms can
result in a magnetoresistance contribution at zero applied
magnetic field. This contribution can be varied by applied

61

fields smaller than that required to magnetically saturate the specimen. Above the saturation field, variation in resistance with field can, in both cases, be attributed to "normal" magnetoresistance such as is exhibited by non-ferromagnetic metals.

The mechanism proposed by Berger and de Vroomen (11) considers the magnetoresistance resulting from the intrinsic Weiss field. The field acting on a conduction electron in a ferromagnetic metal is B, the magnetic induction. In the absence of an applied field, B within a domain is equal to the spontaneous magnetization $4\pi M_S$ (22 Kgauss for iron). At fields above technical magnetic saturation, the total field acting on the conduction electrons is $H_{app}+4\pi M_S$. To obtain the true zero field resistance for iron samples, it is necessary to extrapolate the resistance behavior beyond saturation to the resistance value corresponding to $B=0$. Using this value of resistance a $RRR \big|_{B=0}$ can be obtained which should be comparable to RRR values for metals having no intrinsic magnetization.

To test this notion, the resistance of three iron specimens was measured at room and liquid helium temperatures using standard potentiometric procedures. At liquid helium temperature, data were taken as a function of applied longitudinal magnetic fields up to 5K Oe and of specimen currents of 10 amperes and lower. The specimens are described in Table 1.

In order to differentiate between the mechanisms mentioned above, it was necessary to apply a magnetic field exactly transverse to the direction of electric current flow in the specimen. Due to the cylindrical form of the specimens, a slight deviation from the perpendicular will result in a component of H along the rod axis which, because of the high permeability of iron, will cause magnetization of the specimen in the longitudinal direction.

Since exact alignment would have been extremely difficult for all specimens and impossible for irregular specimen Fe 1, the magnetic field induced by electric current flowing in the specimen was used to study transverse magnetoresistive behavior. At room temperature, no variation of resistance was observed to result from a variation in specimen current. Fig. 18 shows that magnetoresistance was observed at $4.2°K$. Specimen resistance increased as electric current was increased. Other observers (10) have noted an initial decrease in

the resistance of iron as an external transverse magnetic field is applied. Although the induced field applied here was non-uniform over the specimen cross section and not of the same form as used by these observers, it would seem probable that the initial decrease which they observed was due to mis-alignment of the specimen as mentioned above.

The direct relationship between measuring current and resistance does not appear to be correctly predicted by the domain wall scattering concept. An increase in the induced transverse magnetic field should increase the proportion of Weiss domains aligned in transverse directions. According to the domain wall scattering model, the consequent decrease in the number of domain walls encountered by conduction electrons should result in a decrease in resistance, in conflict with our observations.

On the other hand, our data does appear to agree with the model of Berger and de Vroomen. Without precise knowledge of the collision integral, the magnitude of neither transverse nor longitudinal magnetoresistance in small applied magnetic fields can be calculated. However, it is observed that the longitudinal magnetoresistance is, in general, smaller in magnitude than the transverse magnetoresistance. Therefore, we would expect that changing the random distribution of Weiss domains present in a demagnetized sample to one in which transverse alignment is preponderant, would increase specimen resistance in a manner similar to that seen in Fig. 18. It appears that magnetoresistance due to the internal fields of the domain is at least the dominant factor in the low temperature resistivity.

Fig. 19 is a plot showing normalized resistivity change $(\rho_{H_{\parallel}} - \rho_0)/\rho_0 = \Delta\rho/\rho_0$ vs. applied longitudinal magnetic field, $H_{\parallel}$, at 4.2°K. As $H_{\parallel}$ is increased to small values above H=0, $\Delta\rho/\rho_0$ decreases rapidly. After the initial decrease, $\Delta\rho/\rho_0$ varies only slightly with applied field for values of H=800 Oe or higher. This initial behavior may also be explained on the basis of Berger and de Vroomen's picture. As H is increased from zero, the normal distribution of Weiss domains is changed in favor of longitudinal alignment. The resulting decrease in resistance due to the decrease in number of those domains whose internal field is perpendicular to the current is not compensated by the resistance increase due to the increased number of domains whose internal field is parallel to the current. The net result is a resistance decrease.

The slight increase in resistivity with applied field in the region where the specimen is ferromagnetically

63

saturated is probably "normal" longitudinal magnetoresistance due directly to the total field. Although marked differences (probably due to crystal texture) are noted between specimens Fe 1 and Fe 3 below saturation, their behavior above saturation is quite similar. The magnitude of the initial resistivity change is very dependent upon purity. $[\Delta\rho/\rho_0]_{min}$ for purified specimens Fe 1 and Fe 3 is 20 times smaller than that for non-purified specimen Fe 2 and also much lower than the values noted by other investigators (9). Further study may show that the magnitude of $[\Delta\rho/\rho_0]_{min}$ is a satisfactory indication of purity, however it is felt that, for the present, the more fundamental method of extrapolation to zero induction and calculation of $RRR|_0$ should be used.

Figs. 20 and 21 show the variation of $[\rho_{H_{\#}} - \rho_0]/\rho_0 = [\rho_B - \rho_{22\ KOe}]/\rho_{22\ KOe}$ with B for applied fields greater than those necessary to saturate the specimen (H $\overset{\sim}{>}$ 1 K Oe). The results of a linear extrapolation of these data have been used to obtain $R_{B=0}$, $T=4^\circ K$. From these values true RRR's have been calculated and are given in Table II and compared with the RRR values obtained in the normal manner with the applied field equal to zero (H=0) Uncertainty in extrapolation is mainly responsible for the large uncertainties in the $RRR|_{B=0}$ values.

It is felt that the values of $RRR|_{B=0}$ provide an indication of purity superior to the normal RRR which gives values of 300 or less even for iron specimens of known high purity (10). The values of $RRR|_{B=0}$ obtained for the purified specimens are more compatible with the values of RRR obtained for similar, but non-ferromagnetic metals.

II. A Study of Impurity Distributions in Single Crystals Using Resistivity Ratio Measurements

An increasing number of metals are becoming available in "ultra high purity" or "superpure" grades rated as "99.999" or "99.9999", the latter having nominally one part per million or less total of analyzed, usually metallic, impurities. It is of interest to analyze some of these metals and single crystals carefully grown from them. The resistivity ratio method is employed which, although non-specific for particular impurities, gives a measure of the total impurity as it affects the electronic conduction. If high purity specimens are being selected for Fermi surface studies, the electron mean free path is the significant factor, and the residual resistance or resistivity ratio is the appropriate measure of purity. The handling and growing of crystals from these metals clearly require

64

special care because a surface oxide or sulfide layer or a finger print represents a serious contamination. The crucible material chosen and the atmosphere present during growth are particularly critical.

Apparatus developed for resistivity ratio determinations by the eddy current decay method has been applied to the analysis of impurity distribution in single crystals of gold, silver, copper, aluminum, zinc, and cadmium. Except where noted, these crystals were grown under the supervision of Dr. James Kirn at Virginia Institute of Scientific Research using the Czochralski method. After etching to remove any surface contamination, the pure metal was melted by induction in a high purity graphite (Stackpole) crucible, then oriented seed crystal was dipped into the melt and steadily withdrawn with a rotating motion. The diameter of the crystal pulled was controlled manually by adjustment of the r-f induction power. All of these crystals were melted and pulled in an inert atmosphere of purified argon. The variable of the growth studied was the pulling rate. Pairs of crystals were grown with all other conditions held as nearly alike as possible. Table III summarizes for each crystal the source and grade of metal, the orientation of the seed, the speed and condition of growth, and the resistivity ratio profile obtained.

Most impurities have a greater solubility in the liquid than in the solid phase so that crystallization results in a purification of the first portion of the crystal to solidify. If there is no addition or subtraction of impurities, the first portion would be more pure and the last portion to solidify would be less pure than the starting material. Crystals Nos. 1, 4, 5, 9, 12 and 13 show this characteristic decrease of purity from the seed region towards the end. Tests were made of starting materials Nos. 6 and 10 which were similar to those used for growing the copper and aluminum single crystals, and at least the first portions of these crystals are appreciably purer than the samples examined. The copper crystal No. 8 was an exception and apparently had become contaminated. The silver crystals Nos. 2 and 3 have a profile opposite to the usual rule in that the regions near the seed showed a lower purity than the latter part of the crystals. This is suggestive that impurities were present having a greater affinity for the solid than the liquid.

The principal variable under investigation was the effect of growth rate on crystal purity. It was found

65

in each case that a slower rate was associated with a higher resistivity ratio, at least near the seed end. In each case the more slowly grown crystal was the second to be grown from the particular crucible. It is conceivable that its higher purity could be associated with a leaching of impurities by the first melt. The rotation of the crystals during pulling, while applied principally to achieve a straight crystal of uniform circular cross section, apparently had a beneficial effect on purity by mixing the molten metal. Nearly all the pulled crystals showed a strong profile, while the copper crystal (No. 7), grown in a fixed graphite crucible using a slowly moving induction coil, showed essentially none. Unexpectedly, the copper crystal grown by the electron beam floating zone method showed a resistivity in the single crystal portion lower than in the starting material and lower than in the ummelted portion of the rod. The purified argon atmosphere in which the crystals were pulled appeared to have been slightly contaminated with oxygen, since crystals expose for a longer time because of a slower growth rate showed, in general, a greater surface contamination. That the presence of oxygen does not always have an adverse effect on the resistivity ratio was shown by Young and Savage (12). They found that their Bridgman-grown copper crystals, initially having a resistivity ratio of 500, showed a resistivity ratio of about 3500 after internal oxidation. Internal oxidation can precipitate the iron known to be present along with a number of other dissolved metals.

REFERENCES

1. J.W. Rutter and B. Chalmers, Can. J. Phys. 31, 15 (1953).

2. M.E. Glicksman, "Dynamic Effects Arising from High-Speed Solidification," Acta. Met., In Press.

3. D.W. Rhys, J. Less Common Metals, 1, 269 (1959).

4. We are indebted to B.C. Allen of the Battelle Memorial Institute for kindly preparing these compacts.

5. See, for example, J. E. Kunzler and J.H. Wernick, Trans. AIME 212, 85 (1958).

6. W.F. Pfann, Zone Melting, Wiley, New York, 1959.

7. G.K. White and S.B. Woods, Phil. Trans. Roy. Soc., A 251, 273 (1959).

8. R.F. Vines, International Nickel Co., Inc. (private communication).

9. L. Kaufman and S.A. Kulin, Trans. AIME, 215, 273 (1959).

10. A.M. Sudovtsov and E.E. Semenenko, JETP, 8, 211 (1959).

11. L. Berger and A.R. de Vroomen, Bull. Am. Phys. Soc., Series II, 10, 16 (1965).

12. F.W. Young and J.R. Savage, Research Materials Information Center, Oak Ridge National Laboratory, ORNL - RMIC-2, p. 3.

Papers published under this contract:

(1) J.T. Schriempf, "The Electron Beam Zone Refining of Ruthenium," J. of the Less-Common Metals, 9, 35 (1965).

(2) M.E. Glicksman, "Dynamic Effects Arising from High-Speed Solidification," accepted for publication in Acta Metallurgica.

Table I

Iron Specimens Used in Magnetoresistance Measurements

Specimen	Preparation	Diameter	Length Between Potential Leads
Fe 1	U.H.V. zone refining	Irregular approx. 4 mm	4 cm
Fe 2 *	Annealed, but not refined. From same stock as Fe 1.	5 mm	3.5 cm
Fe 3	Single crystal prepared by Materials Research Corp.	2 mm	1.5 cm

*For specimen 2, two "runs" were made. Run two used a new set of contacts placed approximately, but not exactly, in the same places as those used in run 1.

Table II

Comparison of Residual Resistance Ratio Obtained by the Extrapolated Method $RRR|_0$ and in the Regular Manner RRR

Specimen	$RRR|_0$	RRR
Fe 1	630 ± 50	231 ± 5
Fe 2		
contact set 1	32 ± 5	30.5 ± 0.5
contact set 2	40 ± 5	37.9 ± 0.5
Fe 3	specimen too small to allow sufficient resolution for extrapolation	242 ± 5

Table III

Summary of Crystal Growth Conditions and Resistivity Ratios

No.	Crystal	Source	Grade	Seed Orienta- tion	Crystal Size	Growth Rate (in./hr.)	Surface	Resistance Ratio Profile
1	Gold	Cominco* (spatters)	99.9999	(111)	0.7 to 1.0 cm. dia.	2	small amount of contamination	816 at seed decreasing to 240 at end
2	Silver	Cominco (rod)	99.9999	111	0.7 to 1.0 cm. dia.	1-1/4	clean	830 near seed increasing to 1120 near the end
3	Silver	Cominco (rod)	99.9999	111	0.7 to 1.0 cm. dia.	3-1/8	clean	Abt. 800 near seed increasing to 890 near end
4	Copper	ASARCO+ (rod)	99.999	111	1 to 1.4 cm. dia.	1-1/4	some oxide formation on surface	?370 near seed decreasing to 1310 at end
5	Copper	ASARCO (rod)	99.999	111	1 to 1.4 cm. dia.	3-1/8	clean	1160 near seed decreasing to 800 at end
6	Copper	ASARCO (rod)	99.999	polycrystalline rod 3/8" dia.			vacuum annealed	nearly uniform at 2160
7	Copper	ASARCO (rod)	99.999	Bridgman grown 1/2" dia. at NRL in high vacuum		1-1/4	clean	nearly uniform at 1640
8	Copper	ASARCO (rod)	99.999	Electron-beam zone refined at NRL			clean	1970 at the single crystal end rising to 2210 3 cm. distant
9	Aluminum	Cominco (ingot)	99.9999	110	1 to 1.3 cm. dia.	1-1/4	dirty with oxide	3440 near seed. 3640 in mid-region, and 3110 at end
10	Aluminum	Cominco (ingot)	99.9999	110	1.3 cm. dia.	3-1/8	clean	nearly uniform at 3130
11	Aluminum	Cominco (ingot)	99.9999	---	1.4 cm. dia.		spark cut single crystal from original ingot	fairly uniform at 2420
12	Zinc	Cominco (rod)	99.9999	0001	1.2 cm. dia.	1	contained oxide	6300 near seed decreasing to 5000 at end
13	Zinc	Cominco (rod)	99.9999	0001	1.2 cm. dia.	2	contained oxide	5960 near seed decreasing to 5170 at end
14	Cadmium	Cominco (rod)	99.9999	0001	1.2 cm. dia.	3-1/8	clean	8 cm. distance about 7500 near seed, about 9000 in mid-section about 8200 at 8 cm. from seed
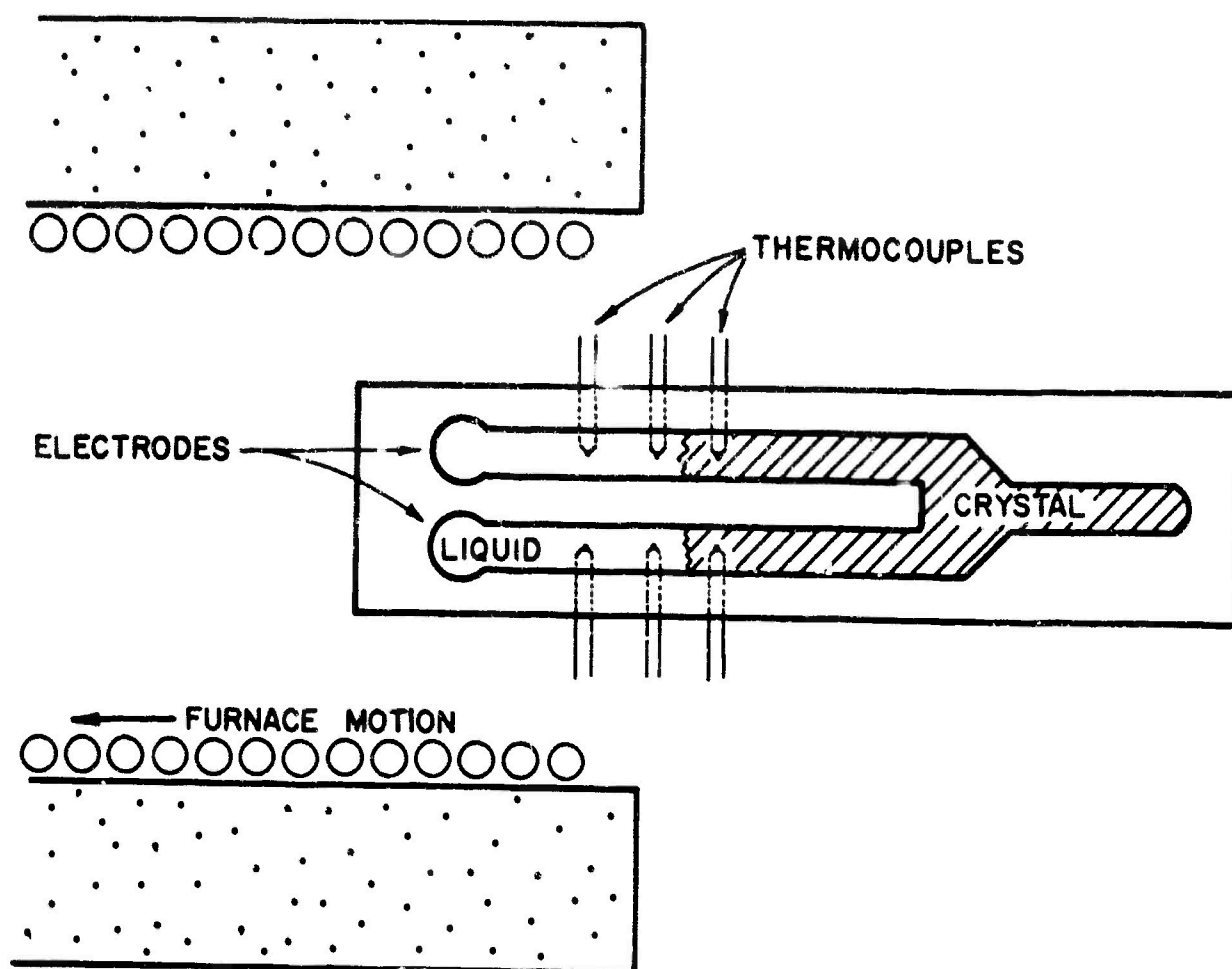
Fig. 1 - Forked crystal growing in lava boat, showing positions of thermocouples and direction of furnace motion.
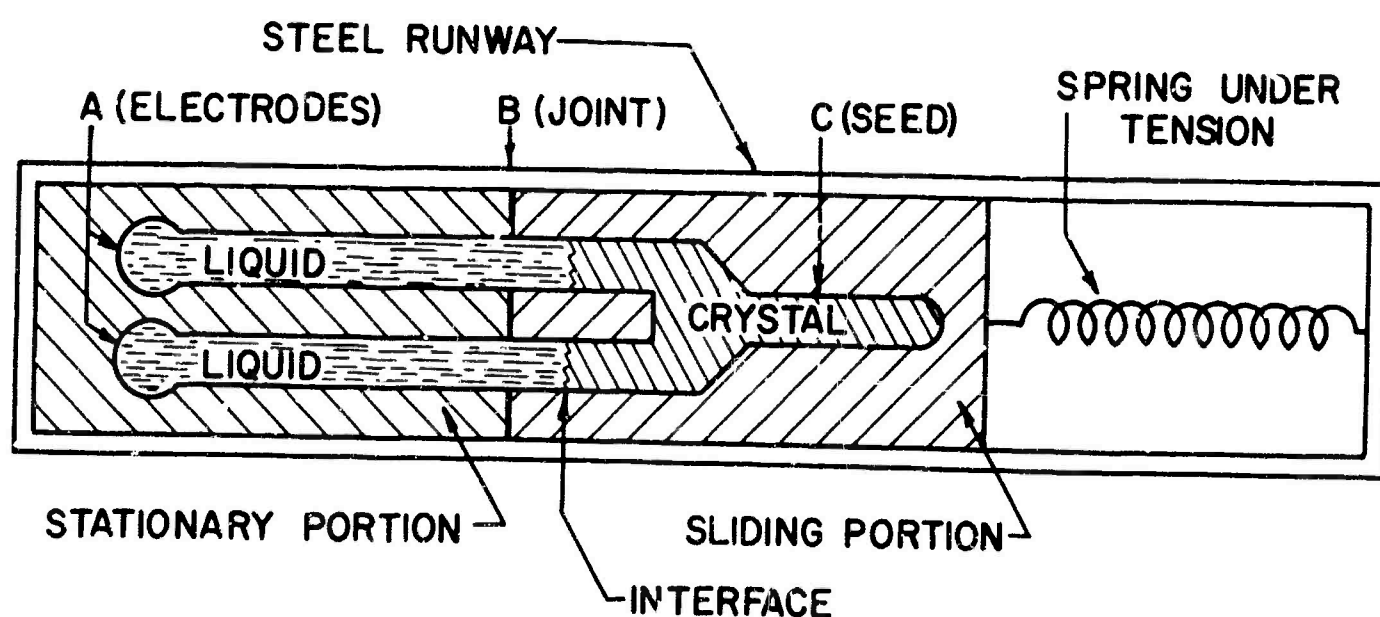
Fig. 2 - Boat for observing effects of electric current solid-liquid interface morphology; spring mechanism can be released when interface reaches joint at B.
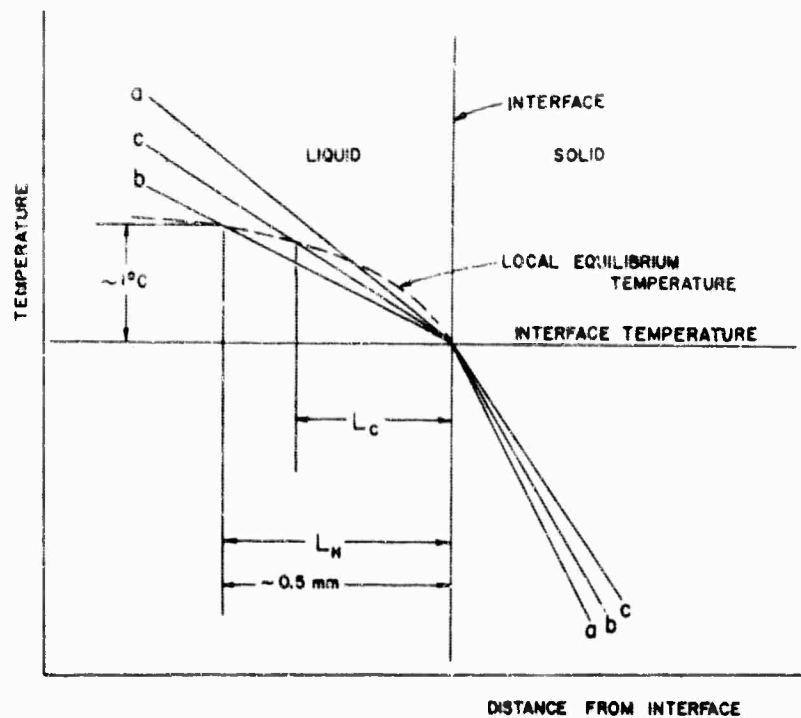
Fig. 3 - Temperature profiles of growing bismuth crystals, (a) with zero current, (b) with Peltier heating, and (c) with Peltier cooling. L_H and L_C are the regions of constitutional supercooling of impure melts with Peltier heating and cooling, respectively.

Fig. 4 - Schematic representation of a faceted interface between solid and liquid Bi-1/2 wt % Sn.

73
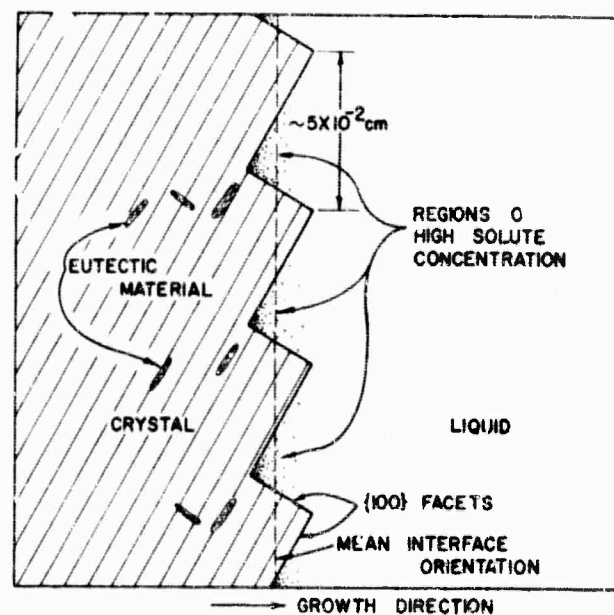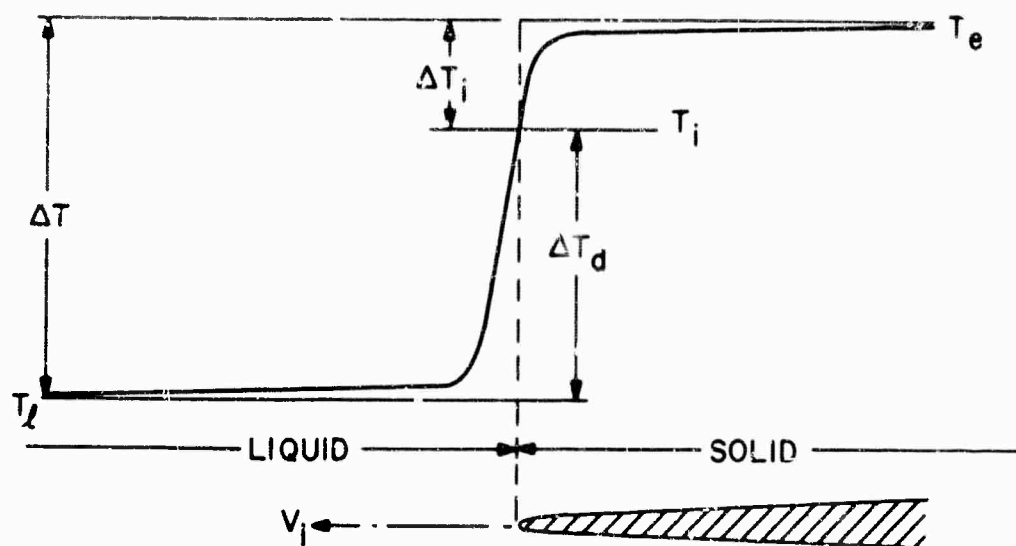
Fig. 5 - Axial temperature distribution for a dendrite advancing at a velocity v_i.
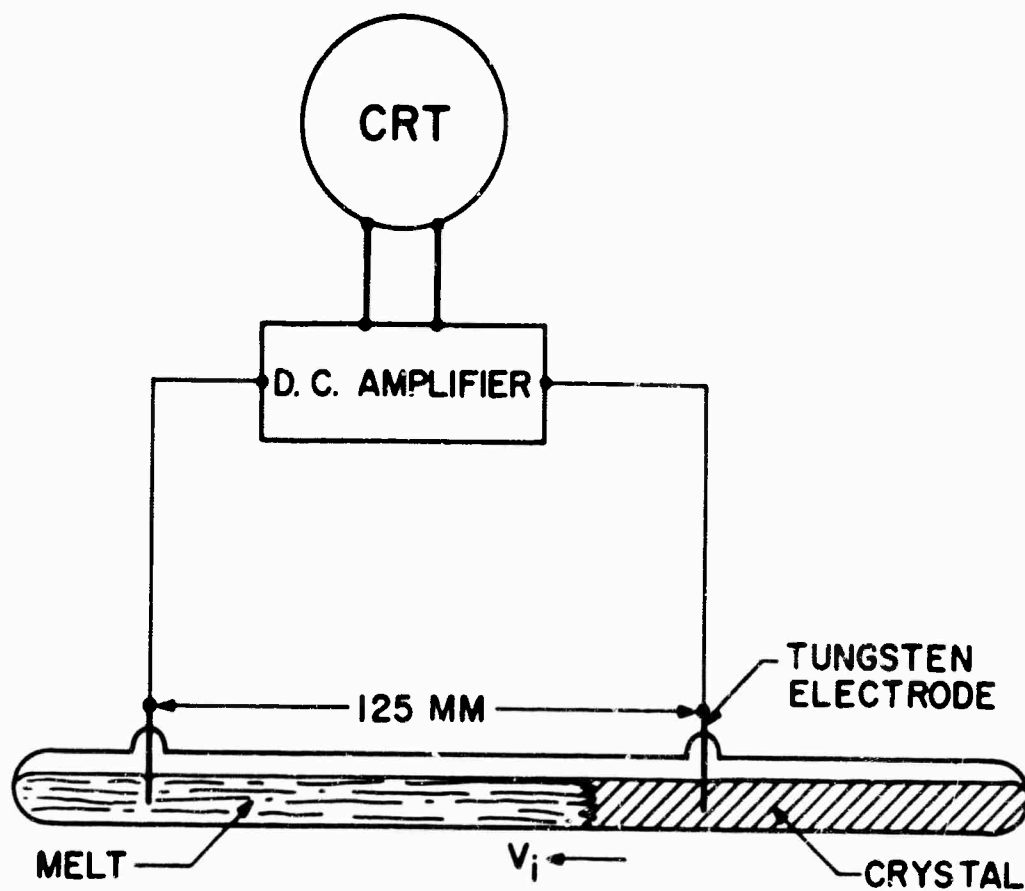
Fig. 6 - Thermoelectric apparatus for measuring dendrite velocities and temperatures.

a. $v_i = 210$ cm/sec
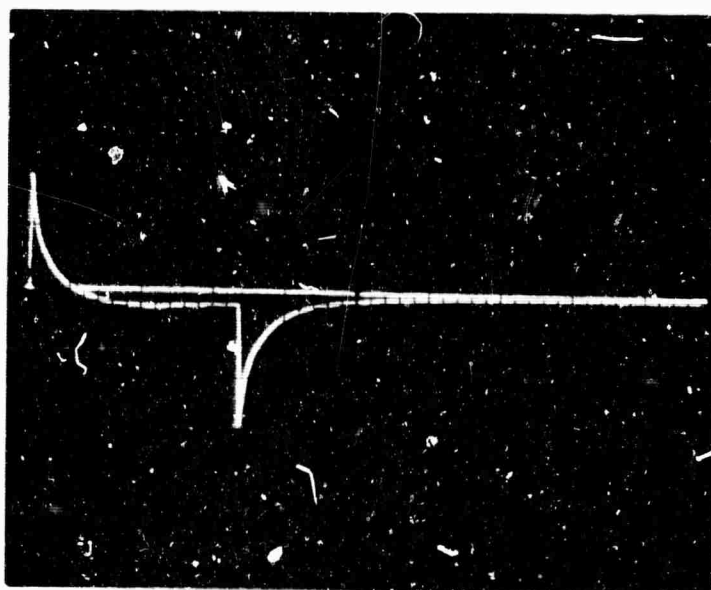
b. $v_i = 450$ cm/sec

Fig. 7 - Oscilloscope traces of the thermoelectric signal generated during crystal growth. Vertical deflection sensitivity: 2 mv/div; horizontal sweep rate: 10 msec/div.

75
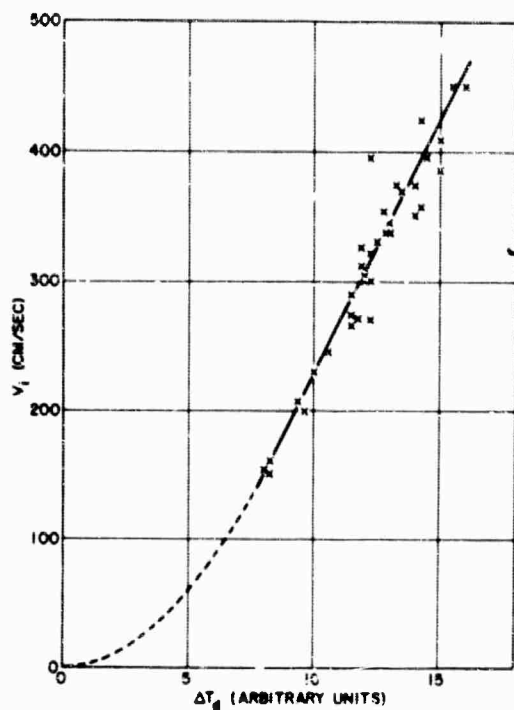
Fig. 8 - Velocity of bismuth dendrites, v_i, against supercooling, ΔT_d, (for thermal diffusion). Region below 150 cm/sec, as indicated by dashes, not investigated; note, however, curve must pass through origin.

Fig. 9 - Idealized solidification model. After nucleation occurred on the base of the system, the solid-liquid transformation proceeds by expanding dendritic growth upward through the cylindrical volume. Dashed curves behind solidification front indicate earlier front positions at equal time intervals.
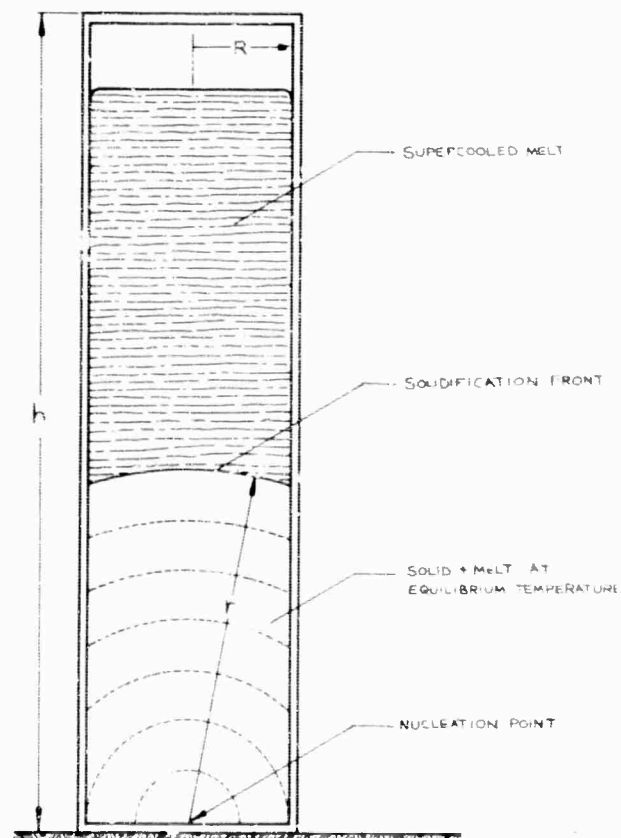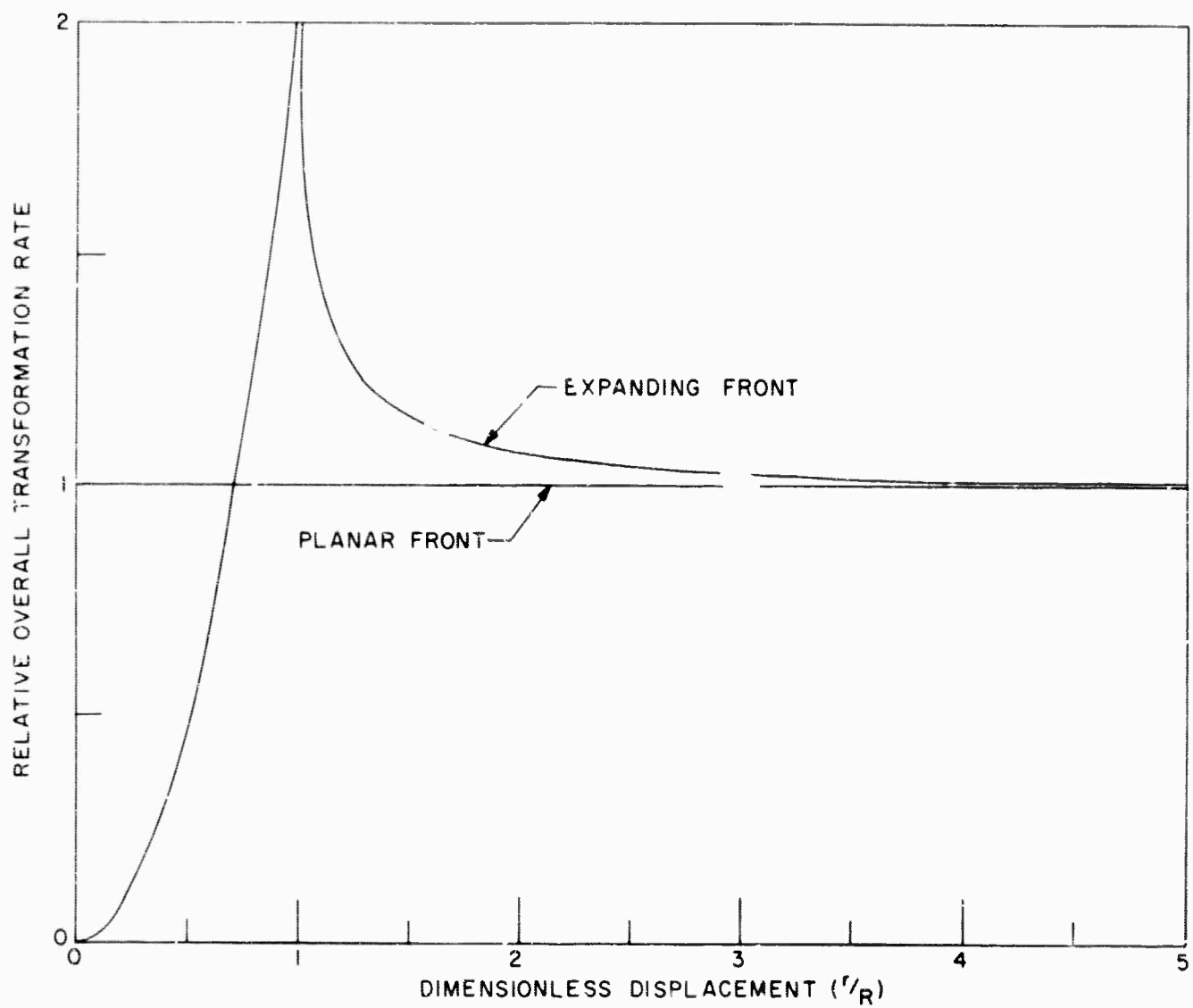
Fig. 10 - Overall transformation rate of an expanding-front solidification model (relative to a planar-front model) plotted against dimensionless displacement of the front from the point of nucleation.

77
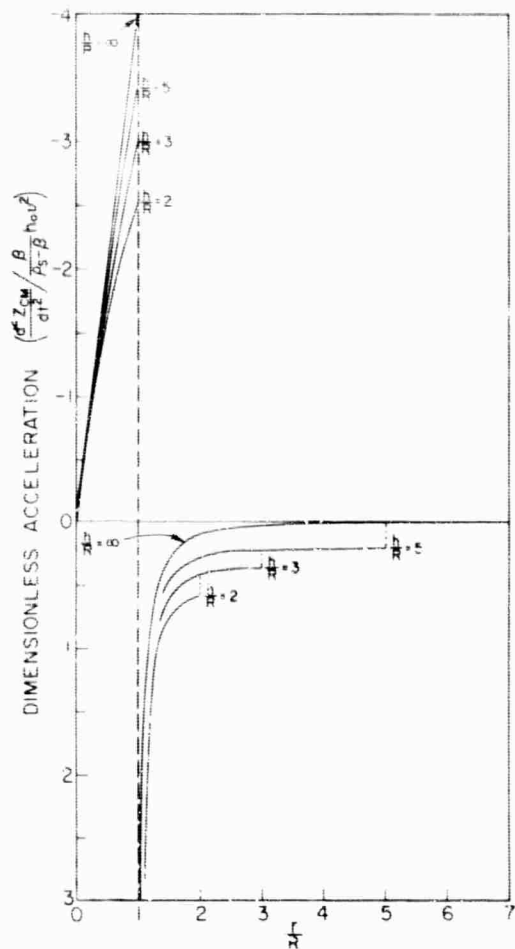
Fig. 11 - Theoretically derived variation of dimensionless, transformation-induced accelerations of the center of mass with dimensionles displacement of the front from the point of nucleation. (Expanding-front model).
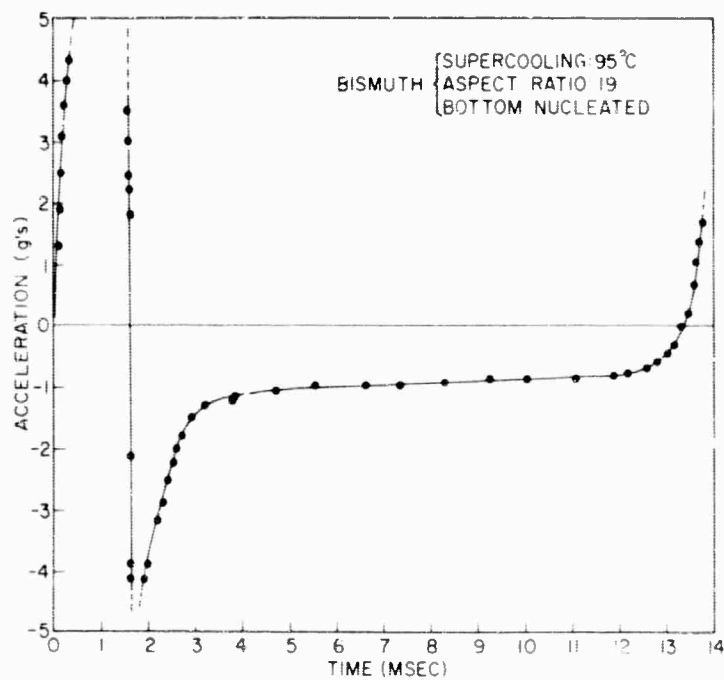
Fig. 12 - Experimental acceleration-time data for a cylindrical bismuth specimen. The specimen was supercooled approximately 95°C below its equilibrium melting point when solidification started.

Fig. 13 - Room temperature to liquid helium temperature resistance ratios for hafnium.
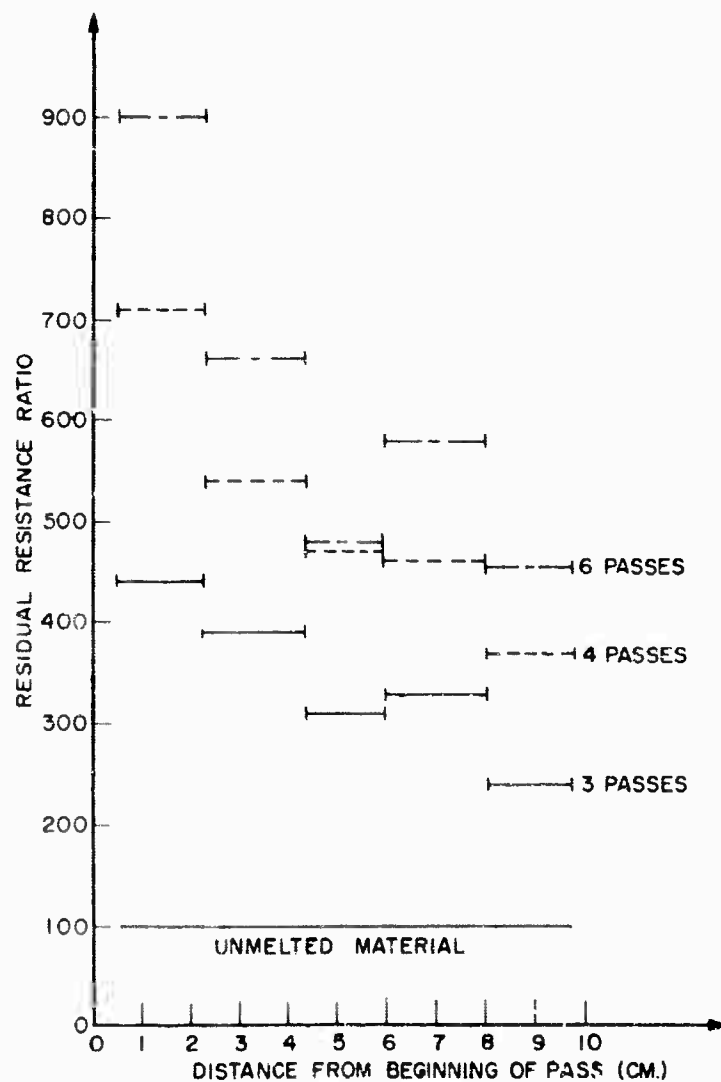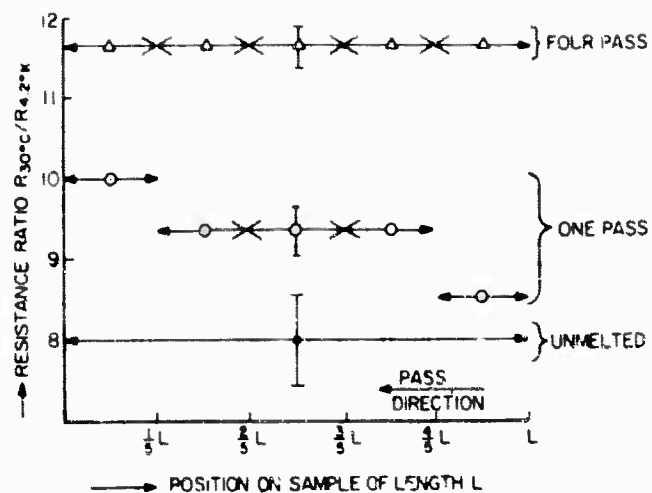
Fig. 14 - RRR profiles for zone-melted ruthenium. Starting material was nominally 99.9% pure.

79
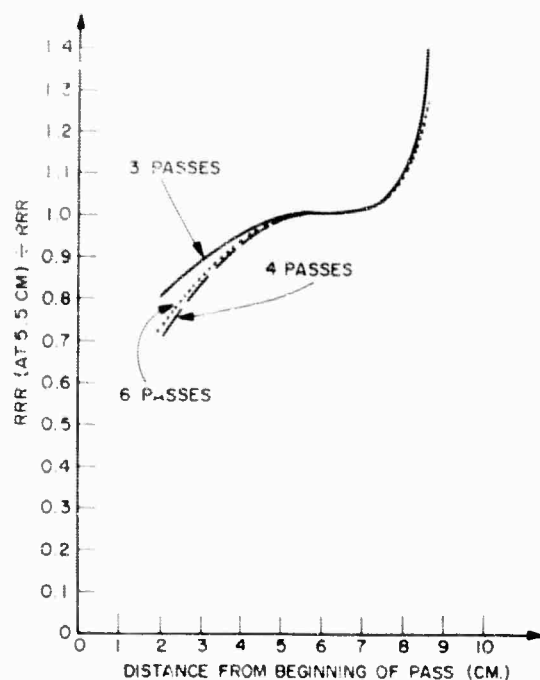
Fig. 15 - Concentration profiles (derived from Fig. 14) for zone-melted ruthenium. The effect of evaporative purification has been approximately removed by assuming that only evaporative purification takes place between 5 and 6 cm.
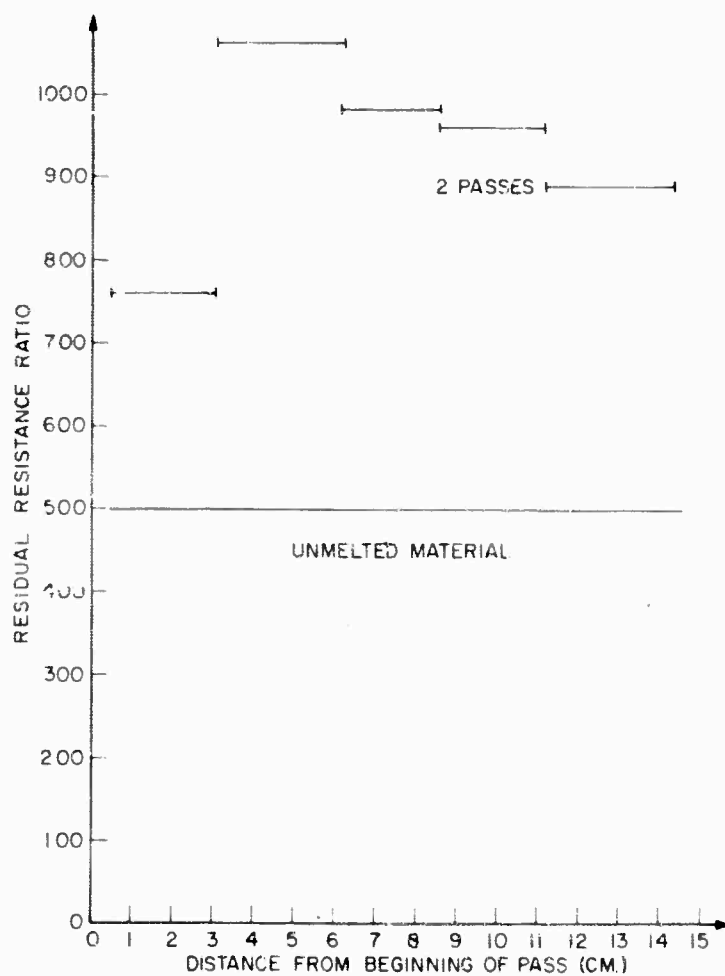
Fig. 16 - RRR profile for zone-melted ruthenium. Starting mater. was nominally 99.999% pure.

Fig. 17 - Dislocation etch pits on a copper
single crystal. X1500.

81
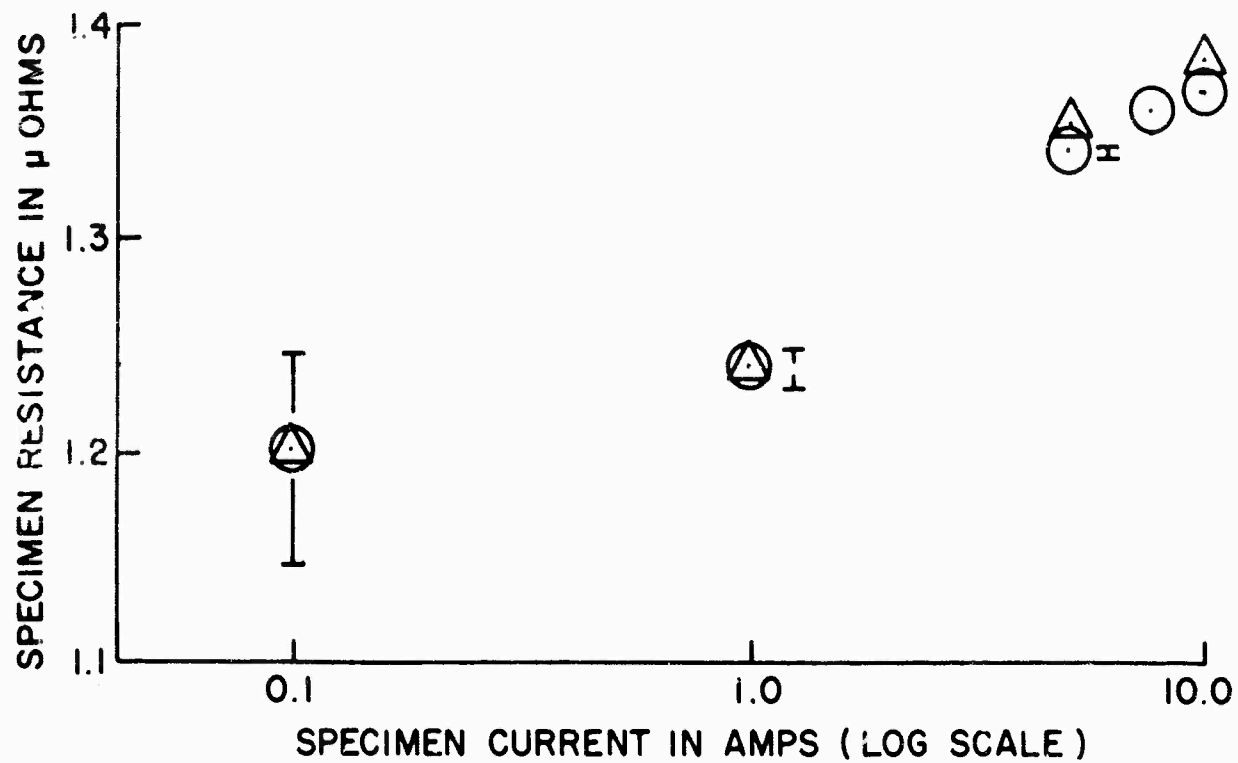
Fig. 18 - Variation of resistance with axial electric current
in specimen Fe 1.
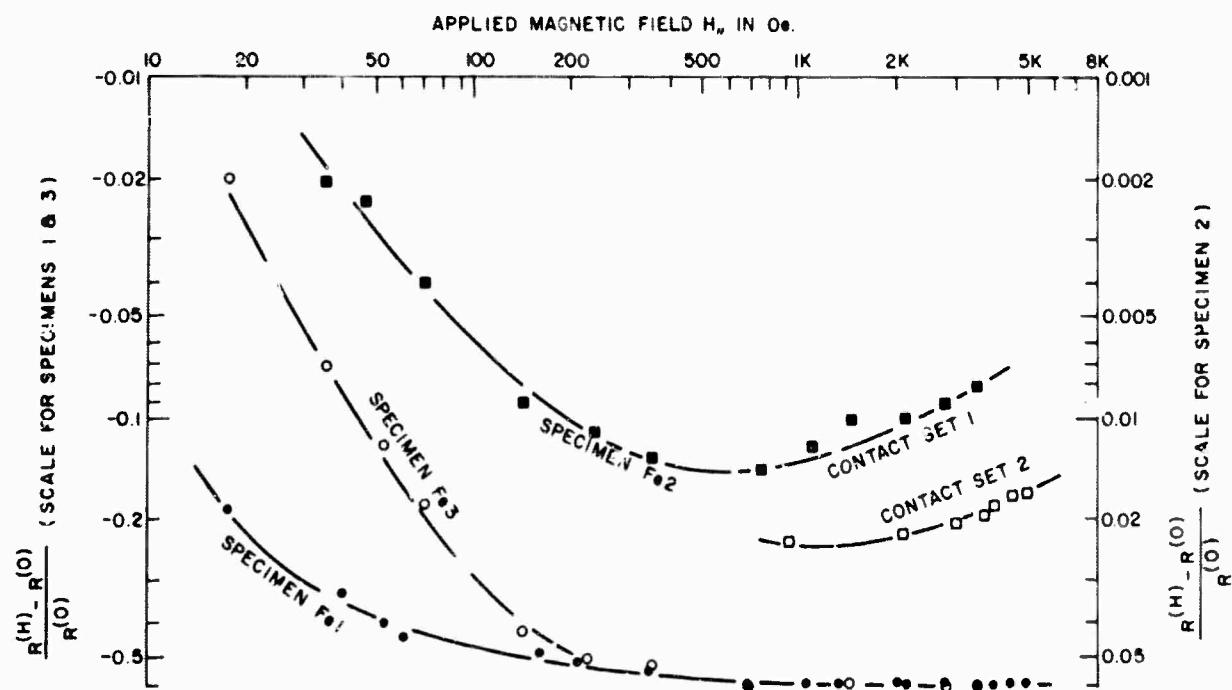
Fig. 19 - Behavior of the resistance of iron specimens in an
external applied field H .
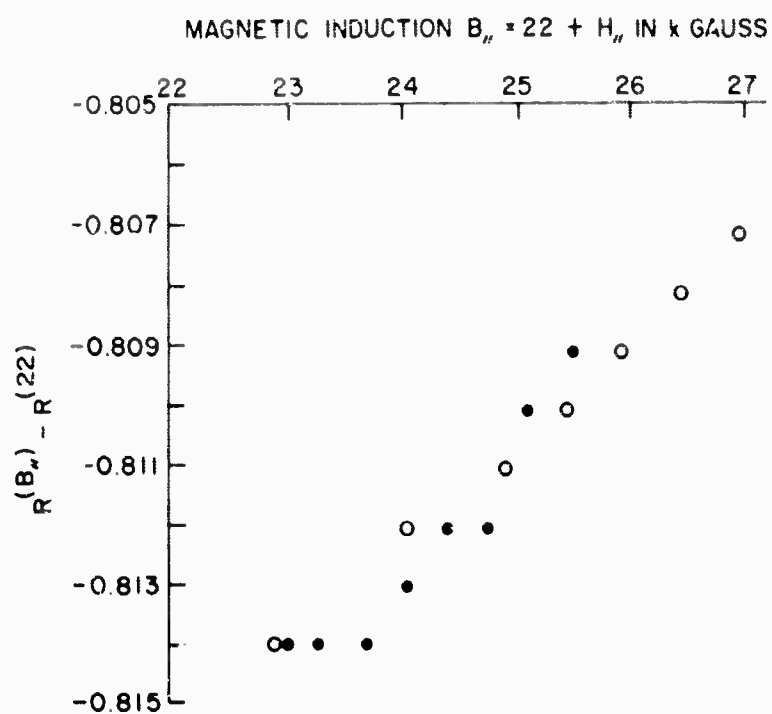
Fig. 20 - Variation in resistance with
magnetic induction for specimen Fe 1.
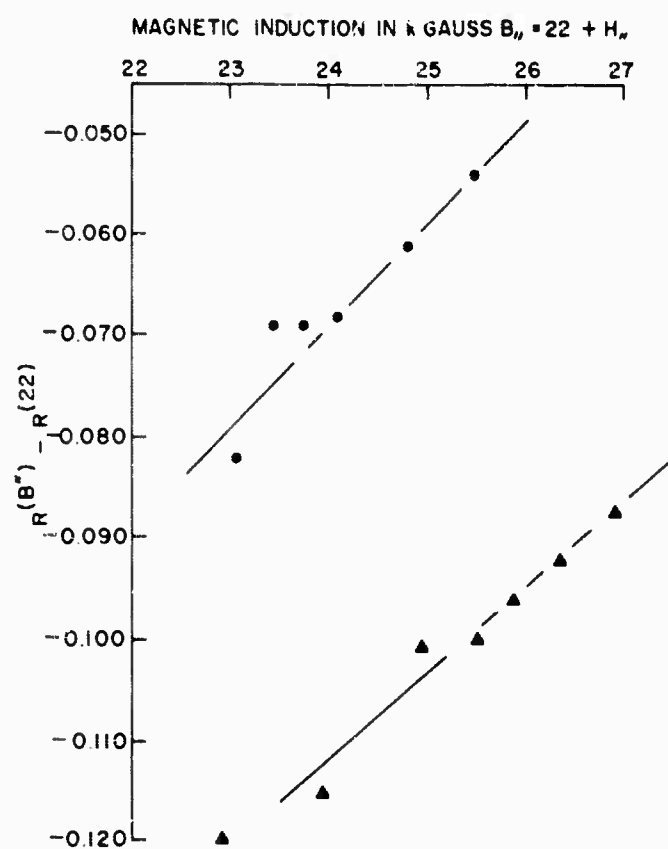
Fig. 21 - Variation in resistance with
magnetic induction for specimen Fe 2.

MAGNETIC MATERIALS

Personnel Engaged in Program
Principal Investigator: G. T. Rado
V. Folen

MAGNETIC MATERIALS

A. INTRODUCTION

The work being carried out on this project is directed toward the synthesis of single crystals having interesting magnetic properties, the main emphasis being on materials which provide basic information on ferro-, ferri-, antiferro-, and paramagnetism. The production of such single crystals by the Magnetism Branch at NRL is necessary because most crystals obtained elsewhere have been found unsatisfactory both in variety and quality.

The report of June, 1964, contains a list of single crystals synthesized by means of the flux method during the earlier phases of this project. Also included in the report of June, 1964, is a list of significant results obtained with the use of these crystals.

B. PROGRESS IN FY 1965

In order to improve the size and quality of $Ga_{2-x}Fe_xO_3$ single crystals, a number of syntheses were performed utilizing various fluxes ($BaO-B_2O_3$, $Bi_2O_3-BiF_3$, and $Bi_2O_3-B_2O_3$) and variations in the growth parameters (soak times, soak temperatures, and cooling rates). Since the initial results involving the $BaO-B_2O_3$ and $Bi_2O_3-BiF_3$ fluxes were unsuccessful, most of the synthesis attempts were made with the $Bi_2O_3-B_2O_3$ flux. The method finally adopted involved a mixture of 30.6g Ga_2O_3 and 21.4g Fe_2O_3 (initial value of x = 0.9) which was blended in a mortar and then added to a similarly prepared mixture of 16g B_2O_3 and 140g Bi_2O_3. The resulting mixture was further blended in the same manner, packed in a 100cc Pt crucible and covered securely. Three such crucibles were placed in a top-opening, glowbar-type furnace and heated slowly to 1175°C. The temperature was held at this point for one hour, then lowered at a rate of two degrees per hour to 500°C. The power was turned off and the furnace allowed to cool to room temperature. The crystals were recovered by dissolving away the flux in hot, dilute HNO_3.

Although a major difficulty with the use of this flux is a pre-dominance of twinned crystals, single crystals having dimensions 2mm x 2mm x 7mm have been synthesized. These crystals are now sufficiently large for measurements of the magnetoelectric effect, magnetic anisotropy, magnetization, and optical absorption.

Additional Al_2O_3 single crystals containing various dopants have been synthesized with the use of $PbO-PbF_2$ fluxes. For this synthesis, 10.0g Al_2O_3 and 0.01g metal (Mn^{2+}, Fe^{3+}) oxide were mixed in a mortar and added to the previously blended flux mixture (43.7g PbO, 47.8g PbF_2). All four materials were blended once more in the mortar. The mixture was packed in a 40cc Pt-Rh-Pt crucible which was then covered tightly and placed in a horizontal, front-loading, glow-bar type furnace. The furnace was heated to 900°C, held at this temperature overnight, and then heated further to 1290°C. After four hours the temperature was lowered at a rate of 1.5° per hour to 950°C and the power turned off. The crystals were allowed to cool to room temperature in the furnace and then recovered by leaching out the flux in hot, dilute HNO_3.

Undoped Al_2O_3 single crystals grown in this way were subsequently doped with Cu^{3+} by means of a diffusion process. The Al_2O_3 crystals were imbedded in powdered CuO in a Pt crucible. The crucible was heated to 950°C, held at that temperature for 164 hours, heated to 1290°C over a period of 4 hours, held at that temperature for 20 hours, and then allowed to cool to room temperature in the furnace. The crystals were recovered by leaching away the CuO with hot, dilute HNO_3.

An Al_2O_3 single crystal containing Ni^{2+} as a dopant was produced by high temperature diffusion for electron spin resonance (ESR) studies. The ESR linewidth measurements on this crystal provide a sensitive measurement of the crystalline perfection since the Ni^{2+} ion in Al_2O_3 possesses a large D-parameter in its spin Hamiltonian. The presence of the Ni^{2+} ion in the Al_2O_3 single crystal was verified by measure-

ments of the optical absorption spectrum. This previously unreported
spectrum has been found to be in accord with crystal field theory
predictions.

The far infrared magnetic resonance absorption spectra of spin-
ordered crystals can provide useful information on the magnetic structure
of these systems. A program has been initiated for such a study on
$Ga_{2-x}Fe_xO_3$ using facilities which have recently become available at
this Laboratory.

C. SIGNIFICANT RESULTS DURING FY 1965

Results of particular significance, made possible by the high quality
single crystals synthesized on this project, include the following:

$Al_2O_3:Cu^{3+}$

First observation of the effects of an applied electric field on the
paramagnetic resonance of a $3d^8$ ion (Cu^{3+}). The high degree of perfection
of the crystals used in this measurement was responsible for the relatively
narrow paramagnetic resonance linewidths (about 24 Oe at 9400 Mc/sec
and room temperature) that were observed. Such narrow linewidths are
necessary for the success of this experiment because the splitting
resulting from the applied electric fields are small.

$Al_2O_3:Mn^{2+}$

Determination of the hyperfine and nuclear electric quadrupole
spin Hamiltonian parameters of Mn^{2+} in Al_2O_3 by the use of the ENDOR
technique at liquid helium temperatures.

In earlier measurements on Mn^{2+} in Al_2O_3 reported by other
workers certain hyperfine paramagnetic resonance lines were not
observed, making it impossible to determine the electric quadrupole
parameter. However, these hyperfine lines were easily resolved in
the Al_2O_3 single crystals obtained in the present ARPA project.

89

β-Ga_2O_3:Mn^{2+}
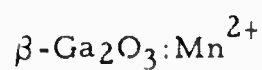
First observation of the Mn^{2+} nuclear electric quadrupole inter-
action (Q') in a rhombic crystal field. The fine and hyperfine structure
in a rhombic crystal field was also observed in these unusually perfect
crystals which have possible Maser application. These results on Q'
and the fine structure, combined with earlier results on Al_2O_3:Mn^{2+},
show that pure crystal field theory does not explain the behavior of
Mn^{2+} in these oxide materials and that one must invoke overlap and/or
covalent effects for a possible explanation of certain spin Hamiltonian
parameters. (See Appendix).

D. PROPOSED PROGRAM FOR FY 1966

During the next fiscal year, the preparation and characterization
of new and improved magnetic single crystals will be continued. Some
of these studies will include piezoelectric Q determinations of $Ga_{2-x}Fe_xO_3$
as a function of growth conditions, optical absorption analysis, far infrared
resonance spectrum, x-ray analysis, and appropriate magnetic measure-
ments on the new and/or improved materials. Attempts will be made to
obtain improved gallium i n oxide single crystals.

APPENDIX

ELECTRON SPIN RESONANCE OF Mn^{2+} IN β-Ga_2O_3

V.J. Folen

(Preprint of paper to appear in The Physical Review)

BLANK PAGE

Electron Spin Resonance Spectrum of Mn^{2+} in β-Ga_2O_3

V. J. Folen
U. S. Naval Research Laboratory, Washington, D. C. 20390

ABSTRACT

The electron spin resonance spectrum of Mn^{2+} has been
investigated in monoclinic β-Ga_2O_3 at 24 kMc/sec. It was found
that the spectrum consists of a set of lines corresponding to a
single type of environm nt. This spectrum (including the fine and
$\Delta m = 0$ hyperfine structure) is satisfactorily described by the spin
Hamiltonian for Mn^{2+} in a rhombic crystal field with the following
derived constants: $A_z = -87.7 \pm 0.2$ gauss; $A_y = -85.6 \pm 0.2$ gauss;
$g_z = 2.002$; $g_y = 2.007$; $D = 545.0$ gauss; $E = 124.3$ gauss. The y
crystal field axis is along the monoclinic axis (b) and the z crystal
field axis makes an angle of 18° with the c crystal axis (a > c).
Forbidden $\Delta m = \pm 1, \pm 2$ hyperfine transitions were also observed.
From the separations between the $\Delta m = \pm 1$ doublets, a value of
$Q' = +0.9 \pm 0.2$ gauss was obtained. On the basis of the axial crystal
fields inferred from the measured values of Q' in β-Ga_2O_3 and in
other oxide materials, it appears that the calculated crystal field
contribution to the D parameter of Mn^{2+} does not explain the experi-
mental results.

INTRODUCTION

The origin of the ground state splitting of the $3d^5 - {}^6S_{5/2}$ ions (Mn^{2+} and Fe^{3+}) has been the object of a considerable number of theoretical and experimental investigations. Such investigations have indicated that these splittings may arise from the combined action of the spin-orbit interaction (W_{so}) and the crystal field,[1-5] or from the intra-ionic spin-spin interaction (W_{ss}) and the crystal field,[2,4,5,6] or from overlap and covalency between the S-state cation and its ligands combined with the W_{so} or W_{ss} terms.[7] However, the degree to which these various mechanisms or their combinations apply and thus the origins of the various crystal field terms in the spin Hamiltonian have not been determined.

Additional information on the origin of the axial crystal field parameter (D) in the Mn^{2+} spin Hamiltonian may be obtained from measurements of both D and the nuclear electric quadrupole interaction parameter (Q') in a series of materials. Such measurements of Q' provide information on the axial crystal fields that are utilized in crystal field calculations of D.

In the present paper, the electron spin resonance (ESR) spectrum of Mn^{2+} in β-Ga_2O_3 is investigated. Values of D and Q' as well as other spin Hamiltonian parameters are obtained from the measurements and an analysis is given of the crystal field contribution to the D parameter on the basis of the axial crystal fields inferred from the measured values of Q' in β-Ga_2O_3, Al_2O_3[8], ZnO[9] and $CaWO_4$.[10] β-Ga_2O_3 possesses a monoclinic crystal structure (the most probable space group being $C_{2h}^3 - C2/m$)[11,12] and, among other things, is of interest

94

because the cation sites have large distortions from cubic symmetry making possible the observation of a nuclear electric quadrupole interaction.

THEORY

The ESR measurements on β-Ga_2O_3 were analyzed using the spin Hamiltonian appropriate for Mn^{2+} in a rhombic crystalline electric field[13]

$$\mathcal{K} = \beta(g_x H_x S_x + g_y H_y S_y + g_z H_z S_z) + D[S_z^2 - \frac{1}{3} S(S + 1)]$$

$$+ E(S_x^2 - S_y^2) + \text{Quartic Terms (a, F)} \qquad (1)$$

$$+ A_x S_x I_x + A_y S_y I_y + A_z S_z I_z - g_N\beta_N\, H\cdot I$$

$$+ Q' [I_z^2 - \frac{1}{3} I(I + 1)] + Q'' (I_x^2 - I_y^2)$$

where $Q' = \dfrac{3\,e\,q\,Q}{4I(2I-1)}$ and $Q'' = \dfrac{e\,q\,\eta\,Q}{4I(2I-1)}$ $\qquad (2)$

are the axial and rhombic part of the nuclear quadrupole interaction, respectively, Q is the nuclear electric quadrupole moment and η is the asymmetry parameter in the field gradient tensor. The quantity q in Eqs. (2) is related to the quadratic axial crystal electric potential coefficient A_2^0 by the equation

$$q = (1 - \gamma_\infty) (5/\pi)^{\frac{1}{2}} A_2^0 \qquad (3)$$

where γ_∞ is the Sternheimer antishielding factor.

For meas rements with H parallel to z, the eigenvalues (to second order) of Eq. (1) are given by:

$$F_{M,m} = g_z \beta HM + D[M^2 - \frac{1}{3} S(S+1)] + A_z Mm$$

$$+ Q'[m^2 - \frac{1}{3} I(I+1)] - g_N \beta_N Hm \tag{4}$$

$$+ \frac{A^2}{4} \left[\frac{[R'-m(m+1)][R-M(M-1)]}{H+D(2M-1) + A(m-M+1)} - \frac{[R'-m(m-1)][R-M(M+1)]}{H+D(2M+1) + A(m-M-1)} \right]$$

$$+ \frac{E^2}{8} \left[\frac{[R-M(M-1)][R-(M-1)(M-2)]}{H+2D(M-1) + Am} - \frac{[R-M(M+1)][R-(M+1)(M+2)]}{H+2D(M+1) + Am} \right]$$

+ Quartic terms

where $R' = I(I+1)$ and $R = S(S+1)$. Here the hyperfine constant A is assumed isotropic for the second order terms. The eigenvalues for H parallel to the y crystal field axis are obtained by replacing in Eq. (4) the quantities g_z, A_z, Q', D and E by g_y, A_y, $\frac{1}{2}(-Q'-3Q'')$, $\frac{1}{2}(-D-3E)$ and $\frac{1}{2}(D-E)$, respectively. Using Eq. (4) with appropriate expansions of the second order terms, one obtains the following relation for the resonant values of H corr(sponding to M, m $\rightarrow$ M-1, m transitions:

$$H_{M,m} = H_0 - (2M-1) D - A_z m - (A^2/2H) [I(I+1) - m^2 + (2M-1)m]$$

$$+ (A^2 D/2H^2)\{3[I(I+1) - m^2] (2M-1) - m[2S(S+1)+3(-2M^2+2M-1)]\}$$

$$-(A^3/2H^2)\left\{[2I(I+1)-3m^2](2M-1)+m[-S(S+1)-I(I+1)+3M^2-3M+m^2+2]\right\}$$

$$-(E^2/2H)\,[2S(S+1)-6M^2+6M-3] \tag{5}$$

$$+(E^2D/H^2)\left\{(2M-1)[3S(S+1)-5M^2+5M-6]\right\}$$

$$+(E^2Am/2H^2)\,[2S(S+1)-6M^2+6M-3]$$

where $H_0 = h\nu/g\beta$ and the spin Hamiltonian parameters are now divided by $g\beta$. In regard to the third order terms in Eq. (5), the A^2D and A^3 are in agreement with those obtained by Schneider and Sircar.[14] The E^2D and E^2A terms have been calculated in the present work.

On the basis of pure crystal field theory, Watanabe[2] has shown that the D-parameter for Mn^{2+} is related to the A_2^0 coefficient as follows:

$$D = -9.90\,\Delta^2 \times 10^{-10} + 3.62\,M'\,\Delta \times 10^{-5}\ cm^{-1} \tag{6}$$

where $\Delta = \frac{1}{4}(5/\pi)^{\frac{1}{2}} < r^2 > A_2^0$ and $M' \approx 0.2$.

The first term in Eq. (6) is due to a fourth order process quadratic in the axial crystal potential ($V_{ax} = A_2^0\,r^2\,Y_2^0\,(\theta,\varphi)$) and quadratic in W_{so} and the second term results from a second order process linear in V_{ax} and linear in W_{ss}. The quantity M' represents the radial part of a matrix element of W_{ss} between the ground state and the $3d^4 4s$ excited state in Mn^{2+}. The two terms in Eq. (6) have been recalculated by Germanier, et al[4] who obtained two additional terms,

one being due to a process linear in V_{ax} and cubic in W_{so} and a
second process linear in V_{ax}, W_{ss} and W_{so}. Recently, Leushin[5]
has performed another crystal field calculation of the W_{ss} and W_{so}
contributions to D. Using a procedure in which the strong cubic
field and electron electrostatic interactions are taken into account
in the same order of perturbation, he found that the ground state
splitting of the $^6S_{5/2}$ multiplet when calculated this way is almost
the same as that obtained by Watanabe's procedure. In all these
calculations, D is linearly and/or quadratically dependent on A_2^0.
From Eqs. (2) and (3), it is seen that Q' is linearly dependent on
A_2^0. Thus, one may obtain the value of A_2^0 from Q' measurements
on a particular material and use this value to predict the crystal
field contribution to D in the same material.

The Q' parameter can be readily obtained from measurements
of the separations of the forbidden $\Delta m = \pm 1$ doublets which occur
between the $M = \frac{1}{2} \leftrightarrow -\frac{1}{2}$, $\Delta m = 0$ transitions as was done previously
for Mn^{2+} in Al_2O_3[8] and ZnO.[9] The separation between these
doublets is given by

$$\Delta H_d = H_{M = \frac{1}{2},\ m+1 \to M = -\frac{1}{2},\ m} - H_{M = \frac{1}{2},\ m \to M = -\frac{1}{2},\ m+1}$$

$$= 17A^2/2H + (2g_N\beta_N/g\beta)\ H - \left\{ (Q'-4A^2D/H^2)(3\cos^2\theta - 1) \right.$$

$$\left. + 3(Q''-4A^2E/H^2)\sin^2\theta \cos 2\varphi + 25A^3/2H^2 \right\} (2m+1) \tag{7}$$

where θ is the angle that the z crystal field axis makes with H and
φ is the angle between the x crystal field axis and the projection of
H on the x-y plane.

CRYSTALLOGRAPHY AND EXPERIMENTAL METHODS

Geller[12] has shown the unit cell of β-Ga_2O_3 contains 4 molecules of Ga_2O_3 and that the ions are located in five sets of special positions 4i: (000, $\frac{1}{2}\frac{1}{2}$0) ± (xoz), each site having an m point symmetry. This mirror plane is perpendicular to the monoclinic b axis. According to Geller, the cation sites are either tetrahedrally or octahedrally coordinated, the former sites having considerably smaller dimensions than the latter. The a and c crystal axes are perpendicular to the monoclinic axis and the angle (β) between the a and c axes is 103.7°.

The ESR measurements were made on β-Ga_2O_3 single crystals containing about 0.05 wt. % Mn. These crystals were synthesized using the flux method.[15] A combined PbO and PbF_2 flux and a lowering rate of 1.5° C per hour from 1250° C were used in the crystal synthesis. Although many of the crystals were twinned, several untwinned crystals were found and these were used for the ESR measurements.

A 24 kMc spectrometer described earlier[8] was used in ESR measurements. Except for the forbidden hyperfine doublet spacings which were measured at 77°K, all the ESR data were obtained at room temperature.

RESULTS AND DISCUSSION

Measurements of the angular dependence of the $\Delta M = 1$, $\Delta m = 0$, ± 1, ± 2 ESR transitions in Mn^{2+} showed that the spectrum consists of a single set of lines corresponding to one type of environment. Since the octahedral sites are considerably larger than the tetrahedral sites in β-Ga_2O_3, it is probable that this spectrum is due to Mn^{2+} ions

in octahedral sites. The earlier measurements[16,17] on β-Ga_2O_3 doped with Cr^{3+} indicate that the Cr^{3+} ions reside in the octahedral sites. In contrast with the results on Mn^{2+} and Cr^{3+}, our measurements on the Fe^{3+} in β-Ga_2O_3 (to be published) show that two types of sites are occupied by the Fe^{3+}.

From measurements of the Mn^{2+} spectra with H in the a-c, b-c and b-a crystal planes, it was found that the y crystal field axis is along the b crystal axis (i.e., the monoclinic axis) and that the z crystal field axis makes an angle of 18° with respect to the c crystal axis as shown in Fig. 1. The spectrum for H along the z crystal field axis is shown in Fig. 2. The transitions in this spectrum are the allowed $\Delta M = 1$, $\Delta m = 0$ transitions. From a comparison of the relative intensities of the transitions in the five hyperfine sextets shown in this figure, it was found that the inhomogeneous broadening in the $M = \pm\frac{5}{2} \leftrightarrow \pm\frac{3}{2}$ and $M = \pm\frac{3}{2} \leftrightarrow \pm\frac{1}{2}$ sextets was not significantly larger than in the central $M = \frac{1}{2} \leftrightarrow -\frac{1}{2}$ transitions, indicating high crystalline perfection. The extra lines shown in the vicinity of the $M = \frac{5}{2} \leftrightarrow \frac{3}{2}$, $M = \frac{1}{2} \leftrightarrow -\frac{1}{2}$ and $M = -\frac{3}{2} \leftrightarrow -\frac{5}{2}$ sextets are due to a trace of Fe^{3+} in the crystals.

Measurements of the spectra with H along the z and y crystal field axes yielded (with the aid of Eq. (5)) the following values of the spin Hamiltonian parameters:

$A_z = -87.7 \pm 0.2$ gauss; $A_y = -85.6 \pm 0.2$ gauss; $g_z = 2.002$

$g_y = 2.007$; $D = 545.0$ gauss; $E = 124.3$ gauss.

Here the A parameters are assumed to be negative because in all materials where the sign has been determined, the A's were found to be negative.

From measurements of the unequal separations between the forbidden $\Delta m = \pm 1$ doublets (those occurring between the $M = \frac{1}{2} \rightarrow -\frac{1}{2}$, $\Delta m = 0$ transitions), a value of $Q' = +0.9 \pm 0.2$ gauss was obtained using Eq. (7). For this measurement H was directed in the z-y plane at an angle of 7 degrees from the z axis. It was necessary to make measurements at this small angle in order that the perturbation calculations used to obtain Eq. (7) are sufficiently convergent. When H was oriented at large angles with respect to z, it was necessary to take into account the large deviation of the orientation of the nuclear magnetic moment from that of the applied magnetic field in order to obtain agreement with the experimental line positions. For example, when H was applied 45° from the z direction, the nuclear moment was calculated to be oriented at an angle of approximately 30° with respect to H. Bir and Sochava[18] found that the large deviation of the direction of the nuclear moment from H had to be included in their intensity calculations also in order to obtain good agreement with the ESR experimental results on Mn^{2+} in $SrCl_2$.

A comparison of the values of A, D, Q' and $\frac{D}{Q'}$ for Mn^{2+} in $CaWO_4$, β-Ga_2O_3, Al_2O_3 and ZnO is given in Table I. The materials are listed in the order of increasing covalency which is indicated[19] by the values of A shown in the second column. From a crystal field calculation of the form of Eq. (6), it is seen with the use of Eqs. (2) and (3) that $\frac{D}{Q'}$ is linearly related to Q'. However, it appears from Fig. 3 that such a relationship is not consistent with the experimental results. A possible explanation of these results may be obtained from overlap and/or covalent mechanisms. Kondo[7] has calculated overlap and covalent contributions to D resulting from W_{so} and W_{ss}. His results show that D should be of the form: $D \propto (S^2 - \lambda^2)$, where S is

the overlap integral between the Mn^{2+} 3d orbital and the ligand orbital and λ is the degree of covalency. Since the axial crystal field is not involved explicitly in this model, such a model could explain the experimental results on the D parameter.

ACKNOWLEDGEMENT

REFERENCES

[1] J. H. Van Vleck and W. G. Penny, Phil. Mag. 17, 961 (1934).

[2] H. Watanabe, Progr. Theoret. Phys. (Kyoto) 18, 405 (1957).

[3] J. R. Gabriel, D. F. Johnson and M. J. D. Powell, Proc. Roy. Soc. A264, 503 (1961).

[4] A. M. Germanier, D. Gainon and R. Lacroix, Phys. Letters 2, 105 (1962).

[5] A. M. Leushin, Soviet Physics-Solid State 5, 1711 (1964).

[6] M. H. L. Pryce, Phys. Rev. 80, 1107 (1950).

[7] J. Kondo, Progr. Theoret. Phys. (Kyoto) 23, 106 (1960).

[8] V. J. Folen, Phys. Rev. 125, 1581 (1962).

[9] J. Schneider and S. R. Sircar, Z. Naturforsch 17a, 651 (1962).

[10] R. W. Kedzie (private communication); Phys. Rev. (to be published).

[11] J. A. Kohn, G. Katz and J. D. Broder, Am. Mineral 42, 398 (1957).

[12] S. Geller, J. Chem. Phys. 33, 676 (1960).

[13] W. Low, Paramagnetic Resonance in Solids (Academic Press, Inc., New York, 1960), p. 46.

[14] J. Schneider and S. R. Sircar, Z. Naturforsch 17a, 570 (1962).

[15] J. W. Nielsen and E. F. Dearborn, J. Phys. Chem. Solid $\underline{5}$, 202 (1958).

[16] M. Peter and A. L. Shawlow, Bull. Am. Phys. Soc. Ser. II $\underline{5}$, 158 (1960).

[17] H. H. Tippins, Phys. Rev. $\underline{137}$, A865 (1965).

[18] G. L. Bir and L. S. Sochava, Soviet Physics-Solid State $\underline{5}$, 2637 (1964).

[19] J. S. Van Wieringen, Discussions Faraday Soc. $\underline{19}$, 118 ('955).

[20] On the basis of Messbauer and ESR measurements, W. J. Nicholson and G. Burns (Phys. Rev. $\underline{129}$, 2490 (1963)) pointed out that there is a considerable scatter of the data points in a plot of D versus Q for Fe^{3+} (which also has a $^{6}S_{5/2}$ ground state) in various host materials.

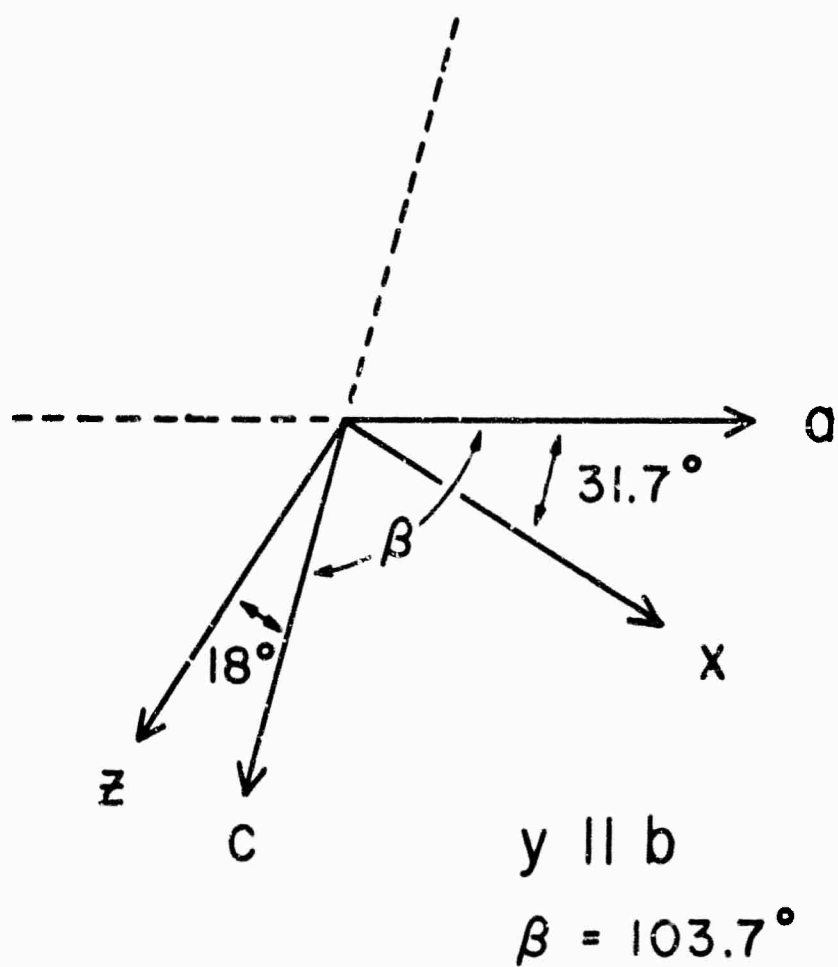Fig. 1 - Orientation of the crystal field axes (x, y, z) with respect to the crystallographic axes (a, b, c) for Mn^{2+} in β-Ga_2O_3. The b and y axes are perpendicular to the plane of the figure and β is the angle between the a and c axes.
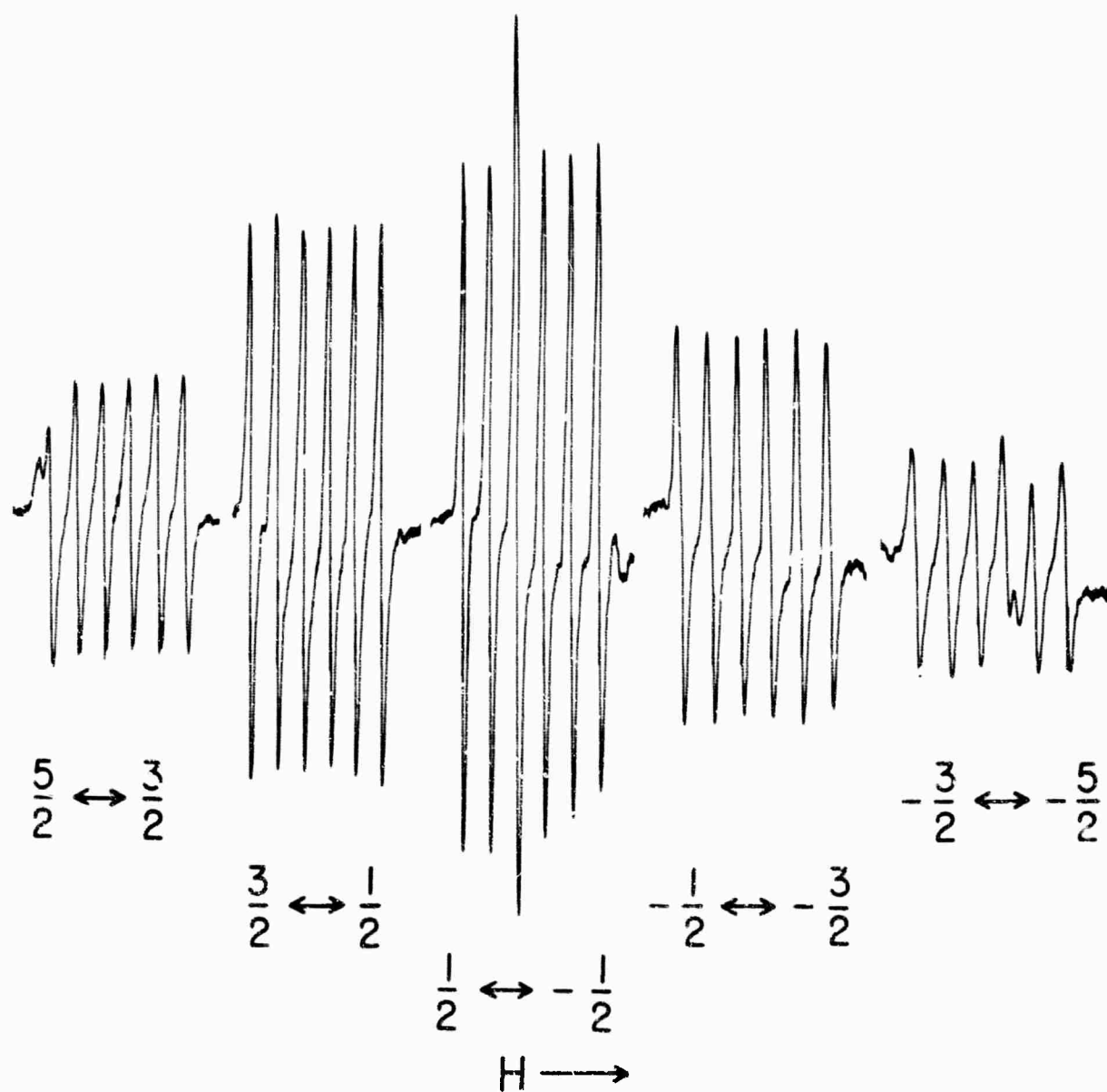
Fig. 2 - Electron spin resonance spectrum at $300°K$ of Mn^{2+} in β-Ga_2O_3 with the magnetic field H parallel to the z crystal field axis. Values of M are given for the initial and final states.
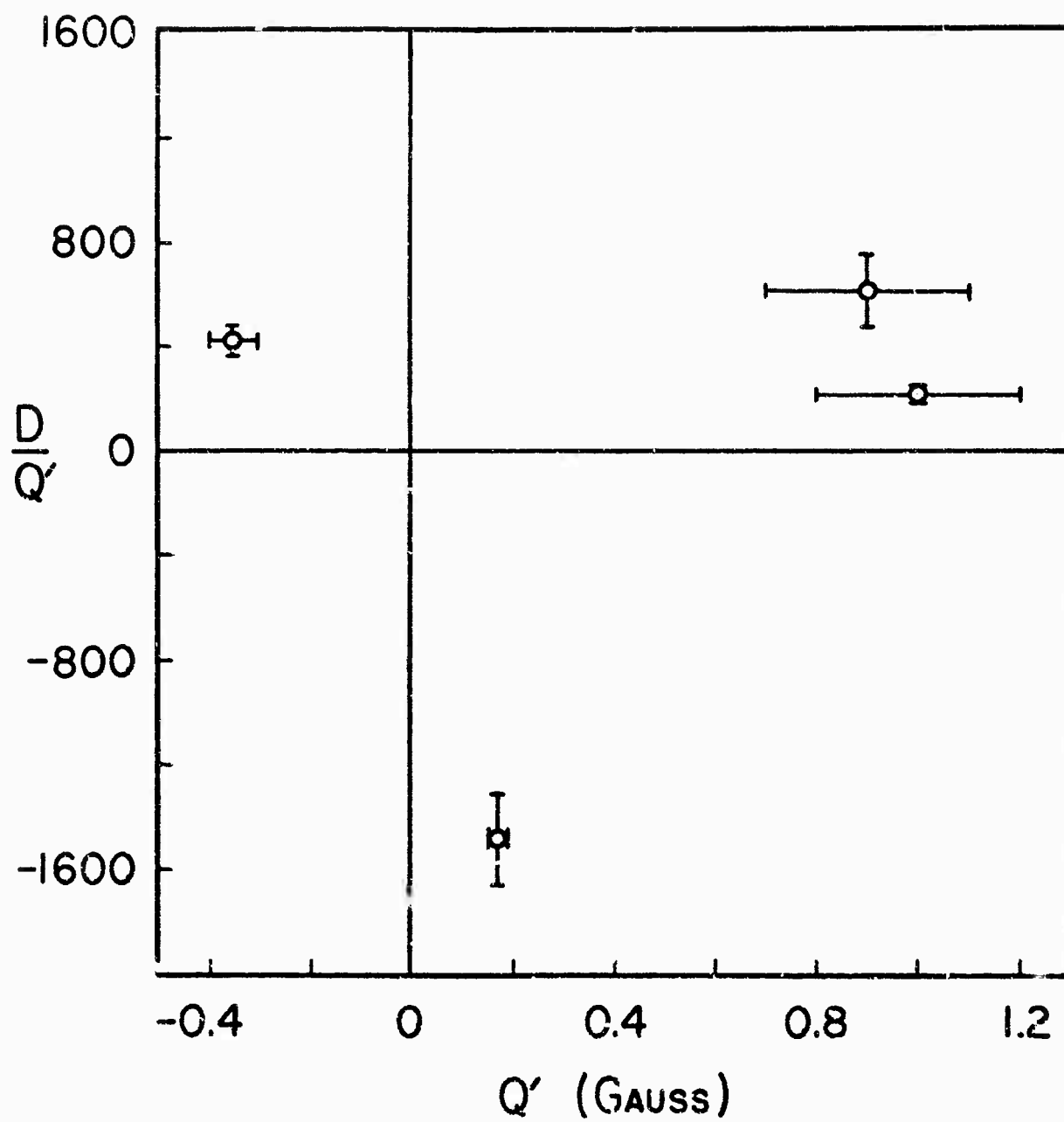
Fig. 3 - Absence of linear dependence of D/Q' on Q'.

TABLE I

Comparison of Experimental Values
of A, D, Q' and $\frac{D}{Q'}$ for Mn^{2+} in Various Host Lattices

Host Lattice	A(gauss)	D(gauss)	Q'(gauss)	$\frac{D}{Q'}$
$CaWO_4$	- 95.24[a]	- 147.4[a, b]	- 0.35 ± 0.05[b]	+ 421 ± 60
β-Ga_2O_3	- 87.7[c]	+ 545[c]	+ 0.9 ± 0.2[c]	+ 606 ± 135
Al_2O_3	- 85.2[d, e]	+ 207[d, e]	+ 1.0 ± 0.2[e]	+ 207 ± 41
ZnO	- 79.3[f]	- 252.7[f]	+ 0.17 ± 0.02[f]	- 1486 ± 175

[a] C. F. Hempstead and K. D. Bowers, Phys. Rev. 118, 131 (1960).

[b] See Ref. 10

[c] Present work

[d] W. Low and J. T. Suss, Phys. Rev. 119, 132 (1960).

[e] See Ref. 8

[f] See Ref. 9

DOCUMENT CONTROL DATA - R&D

(Security classification of title, body of abstract and indexing annotation must be entered when the overall report is classified)

1 ORIGINATING ACTIVITY (Corporate author)	2a. REPORT SECURITY CLASSIFICATION
U.S. Naval Research Laboratory Washington, D.C. 20390	UNCLASSIFIED
	2b GROUP

3 REPORT TITLE

PREPARATION AND CHARACTERIZATION OF ULTRA-PURE SOLIDS

4 DESCRIPTIVE NOTES *(Type of report and inclusive dates)*

Annual Report July 1, 1964 – June 30, 1965

5 AUTHOR(S) *(Last name, first name, initial)*

Schulman, J.H., Rado, G.T., Achter, M.R., and Schindler, A.I.

6. REPORT DATE	7a. TOTAL NO OF PAGES	7b. NO. OF REFS
August 1965	114	31

8a CONTRACT OR GRANT NO.	9a. ORIGINATOR'S REPORT NUMBER(S)
NRL Problems P03-07, P02-02, M01-09, and M01-10	
b. PROJECT NO	Memorandum Report 1640
ARPA Order 418	
c	9b. OTHER REPORT NO(S) *(Any other numbers that may be assigned this report)*
d	

10 AVAILABILITY/LIMITATION NOTICES

Unlimited distribution

11 SUPPLEMENTARY NOTES	12. SPONSORING MILITARY ACTIVITY
	ARPA

13 ABSTRACT

The research program on the preparation of ultra-pure alkali halide single crystals incorporates three interrelated steps: purification, single crystal growth, and characterization and analysis. Both physical and chemical purification methods are in use, and Kyropoulos techniques as well as zone-refining have been under study for single crystal production. Several other groups working on alkali halide purification are already devoting most of their efforts to KCl. KBr, on which much of our earliest work was done, is a material whose optical and physical properties are of great interest to solid-state physicists at NRL and at many other laboratories in this country and abroad. Since experience with solid state mass spectrometry here has emphasized the seriousness of cross-contamination which can result when the same apparatus is used for the processing or analysis of different alkali halides, efforts at NRL are being concentrated exclusively on KBr for the present. Results obtained in the purification, crystal growth, and analysis of KBr and other alkali halides are presented and some proposed lines of further investigation are discussed. In the preparation and study of highly perfect specimens of refractory metals, accomplishments have been made in four areas: (a) procedures have been developed for the growth of single crystals of niobium by the strain-anneal technique and for the study of their structure by x-ray and metallographic methods, (b) measurements have been made of the rate of sintering of porosity in the grain boundaries of niobium bicrystals, (c) bicrystals have been prepared for the study of the interfacial energy as a function of misorientation, (d) techniques have been developed for the measurement of intergranular diffusion in the bicrystals of niobium. Studies on transition metal and intermetallic compound single crystals have been concentrated in four main areas: (a) crystal growth kinetics, (b) transition metal crystal preparation, (c) crystal perfection, and (d) purity evaluation. These efforts constitute a broad approach toward growing and evaluating transition metal and intermetallic compound single crystals in states of extreme purity and perfection, and toward formulating and verifying improvements to current theories governing such crystal formation. Significant achievements in these areas are discussed in detail. It is anticipated that, in the coming year, each of the four areas outlined above will be further developed. Interactions between these areas will also be emphasized. The work on the preparation and characterization of magnetic materials has been primarily directed toward the improvement of the quality and size of flux-grown $Ga_{2-x}Fe_xO_3$ single crystals and toward the characterization of flux-grown Al_2O_3 and β-Ga_2O_3 single crystals by resonance (ESR and ENDOR) techniques. A considerable improvement was obtained in the size of $Ga_{2-x}Fe_xO_3$ single crystals. The high quality of the Al_2O_3 and β-Ga_2O_3 single crystals was confirmed by the practicability of successful ENDOR and applied electric field ESR measurements on Al_2O_3 and forbidden hyperfine ESR measurements on β-Ga_2O_3.

DD FORM 1 JAN 64 **1473**

109

14 KEY WORDS	LINK A		LINK B		LINK C	
	ROLE	WT	ROLE	WT	ROLE	WT
Solids Ultra-pure solids Alkali halides Single crystals Magnetic materials Electron spin resonance Refractory metal crystals Transition metal crystals Intermetallic compound single crystals						

INSTRUCTIONS

1. ORIGINATING ACTIVITY: Enter the name and address of the contractor, subcontractor, grantee, Department of Defense activity or other organization (*corporate author*) issuing the report.

2a. REPORT SECURITY CLASSIFICATION: Enter the overall security classification of the report. Indicate whether "Restricted Data" is included. Marking is to be in accordance with appropriate security regulations.

2b. GROUP: Automatic downgrading is specified in DoD Directive 5200.10 and Armed Forces Industrial Manual. Enter the group number. Also, when applicable, show that optional markings have been used for Group 3 and Group 4 as authorized.

3. REPORT TITLE: Enter the complete report title in all capital letters. Titles in all cases should be unclassified. If a meaningful title cannot be selected without classification, show title classification in all capitals in parenthesis immediately following the title.

4. DESCRIPTIVE NOTES: If appropriate, enter the type of report, e.g., interim, progress, summary, annual, or final. Give the inclusive dates when a specific reporting period is covered.

5. AUTHOR(S): Enter the name(s) of author(s) as shown on or in the report. Enter last name, first name, middle initial. If military, show rank and branch of service. The name of the principal author is an absolute minimum requirement.

6. REPORT DATE. Enter the date of the report as day, month, year; or month, year. If more than one date appears on the report, use date of publication.

7a. TOTAL NUMBER OF PAGES: The total page count should follow normal pagination procedures, i.e., enter the number of pages containing information.

7b. NUMBER OF REFERENCES: Enter the total number of references cited in the report.

8a. CONTRACT OR GRANT NUMBER: If appropriate, enter the applicable number of the contract or grant under which the report was written.

8b, 8c, & 8d. PROJECT NUMBER: Enter the appropriate military department identification, such as project number, subproject number, system numbers, task number, etc.

9a. ORIGINATOR'S REPORT NUMBER(S): Enter the official report number by which the document will be identified and controlled by the originating activity. This number must be unique to this report.

9b. OTHER REPORT NUMBER(S): If the report has been assigned any other report numbers (*either by the originator or by the sponsor*), also enter this number(s).

10. AVAILABILITY/LIMITATION NOTICES: Enter any limitations on further dissemination of the report, other than those imposed by security classification, using standard statements such as:

(1) "Qualified requesters may obtain copies of this report from DDC."

(2) "Foreign announcement and dissemination of this report by DDC is not authorized."

(3) "U. S. Government agencies may obtain copies of this report directly from DDC. Other qualified DDC users shall request through

_____ ."

(4) "U. S. military agencies may obtain copies of this report directly from DDC. Other qualified users shall request through

_____ ."

(5) "All distribution of this report is controlled. Qualified DDC users shall request through

_____ ."

If the report has been furnished to the Office of Technical Services, Department of Commerce, for sale to the public, indicate this fact and enter the price, if known.

11. SUPPLEMENTARY NOTES: Use for additional explanatory notes.

12. SPONSORING MILITARY ACTIVITY: Enter the name of the departmental project office or laboratory sponsoring (*paying for*) the research and development. Include address.

13. ABSTRACT: Enter an abstract giving a brief and factual summary of the document indicative of the report, even though it may also appear elsewhere in the body of the technical report. If additional space is required, a continuation sheet shall be attached.

It is highly desirable that the abstract of classified reports be unclassified. Each paragraph of the abstract shall end with an indication of the military security classification of the information in the paragraph, represented as (TS), (S), (C) or (U).

There is no limitation on the length of the abstract. However, the suggested length is from 150 to 225 words.

14. KEY WORDS: Key words are technically meaningful terms or short phrases that characterize a report and may be used as index entries for cataloging the report. Key words must be selected so that no security classification is required. Identifiers such as equipment model designation, trade name, military project code name, geographic location, may be used as key words but will be followed by an indication of technical context. The assignment of links, roles, and weights is optional.